

# **Design, Fabrication and Characterisation of a Fully Elastomeric Soft Sensor**

By

Xingtian Zhang

Submitted in accordance with the requirements for the degree of  
Doctor of Philosophy

The University of Leeds

Institute of Design, Robotic and Optimisation  
School of Mechanical Engineering

March 2022

The candidate confirms that the work submitted is his own, except where work formed part of jointly authored publications has been included. The contribution of the candidate and the other authors to this work has been explicitly indicated below. The candidate confirms that appropriate credit has been given within the thesis where reference has been made to the work of others.

The work presented here includes the papers below, and is partly used in Chapters 1-7:

- Zhang X, Kow J *et al.* **Adjustable compliance soft tactile sensor via an elastically inflatable fluidic dome**, *Sensors* 2021, 21(6), pp1970.
- Zhang X, Culmer P, Alazmani A. **Fully elastomeric and transparent soft strain sensor**. [Under Preparation. Plan to submit to *Sensors and Actuators A* by September, 2022]

For the papers above, I was responsible for the technical work carried out in the listed papers above, and the co-authors were responsible for reviewing the papers.

This copy has been supplied on the understanding that it is copyright material and that no quotation from the thesis may be published without proper acknowledgement. The right of Xingtian Zhang to be identified as the author of this work has been asserted by him in accordance with the Copyright, Designs and Patents Act 1988.

# Acknowledgement

I would like to express my special thanks to my two honoured supervisors, Dr Ali Alazmani and Dr Peter Culmer, who have devoted their inexhaustible passion to supporting and guiding me in my research. Their outstanding academic talents and incredible dedication to their research work have always enlightened me to break the edge of innovation. I would also like to thank the Surgical Technologies research group at the University of Leeds. All the excellent cooperation in our team has tremendously contributed to my research. The colleges are also my sincere friends, supporting me to pass my most brilliant period of life in Leeds. A special thanks to Jun Wai Kow and Dushyant Goordyal for your true friendship that bring me the most positive emotion, just like sunshine on a windy winter day.

Thank you to my precious wife Zhuoqian for walking through the path of PhD study together in Leeds. Your love, wisdom, comprehension and tolerance in our marriage build the strongest sense of security for me to overcome all the difficulties in work and life. Our competition of first obtaining a PhD degree seems to be going to the final episode, but best wishes to yours. And thank you to my family for supporting me all over this journey. The distance has never stopped you from caring and missing me; you are always by my side whenever and wherever I am.

# Abstract

Soft sensing refers to the technology for interaction and perception within the constantly growing field of soft robotics. It has been developed in response to the need for safe, precise and adaptive interaction with its environment. Soft sensing has advanced beyond the scope of industrial applications, spanning into dynamic applications such as surgery, drug delivery and health care. Research in developing soft sensors is becoming a rising focus in soft robotics due to the importance of interactions between humans and their environment in a robotic system. Active feedback is needed for soft robots to achieve accurate controls and safe interactions. However, there are still gaps in current research on soft sensors, for example, the lack of comprehensive study on the properties of soft materials and adaptive design of soft sensors.

This thesis examines the developments of soft robotics and soft sensors. A comprehensive review of state-of-the-art soft sensor research highlights the fundamentals of soft sensors in terms of materials, fabrication and applications. The literature review summary suggests that a fully elastomeric soft sensor may be a potential candidate to fill the gap in the adaptivity and stretchability of soft sensors.

A highly stretchable and electrically conductive soft material is studied to fabricate the target soft sensor. A new design is applied to propose a conductive polyacrylamide hydrogel, and a new experimental approach is conducted to

---

characterise the proposed hydrogel. Both the mechanical and electrical properties of the conductive hydrogel are studied simultaneously.

A fully elastomeric soft sensor is designed, fabricated, evaluated, and demonstrated based on the proposed soft material. The fully elastomeric soft sensor is then extended in application to two case studies. The thesis presents a complete design procedure, fabrication and characterisation of new soft material and a complete methodology of design, fabrication, testing and application of a fully elastomeric soft sensor.

---

# Contents

<b>Acknowledgement</b> .....	<b>III</b>
<b>Abstract</b> .....	<b>IV</b>
<b>Contents</b> .....	<b>VI</b>
<b>List of Tables</b> .....	<b>IX</b>
<b>List of Figures</b> .....	<b>X</b>
<b>Chapter 1 Introduction</b> .....	<b>1</b>
1.1 Soft Robotics and Soft Sensors .....	2
1.2 Research Motivation .....	2
1.3 Objectives.....	4
1.4 Thesis Structure.....	4
<b>Chapter 2 Literature Review</b> .....	<b>6</b>
2.1 Soft Robotics .....	7
2.2 Soft Sensors.....	13
2.3 Soft Materials for Soft Sensors .....	19
2.3.1 Conductive soft materials .....	19
2.3.2 Dielectric elastomer .....	24
2.3.3 Conductive hydrogels .....	25
2.4 Process of Soft Materials.....	29
2.4.1 Polymerisation of soft materials .....	30
2.4.2 Bond between different soft materials .....	34
2.5 Key findings and summary .....	37
<b>Chapter 3 Requirements, Concept and Approach</b> .....	<b>39</b>
3.1 Requirements.....	40
3.2 Concept .....	41
3.3 Approach .....	42
3.4 Summary .....	44
<b>Chapter 4 Ultraviolet Cross-link Hydrogels for Soft Sensors: Fabrication and Characterisation</b> .....	<b>45</b>

---

4.1 Fabrication Method .....	46
4.1.1 Fabrication of hydrogels .....	46
4.1.2 Variation of formulations .....	47
4.2 Characterisation .....	48
4.2.1 Tensile test and data acquisition configuration .....	49
4.2.2 Results of tensile test on electrical and mechanical properties of conductive hydrogels .....	51
4.2.3 Compression test on the electrical and mechanical properties of conductive hydrogels .....	63
4.3 Discussion and Summary .....	75
4.3.1 Fabrication .....	75
4.3.2 Tensile and compression test for the conductive hydrogels .....	76
4.3.3 Summary of ultraviolet cross-link hydrogels .....	77
<b>Chapter 5 Fully Elastomeric Soft Strain Sensor .....</b>	<b>79</b>
5.1 Design and Fabrication .....	80
5.1.1 Sensor design .....	80
5.1.2 PDMS encapsulation and anti-dehydration .....	80
5.1.3 Sensor fabrication .....	83
5.2 Modelling and Characterisation .....	85
5.2.1 Cyclic test on hydrogels .....	86
5.2.2 Peel test of the soft sensor .....	87
5.2.3 Electrical properties test on the soft sensor .....	89
5.3 Application of soft strain sensor .....	91
5.3.1 Monitoring finger joint movement .....	91
5.3.2 Monitoring soft tentacle movement .....	93
5.4 Discussion and Summary .....	94
<b>Chapter 6 Case Study: Soft Tactile Sensor and Soft 2D Strain Sensor .....</b>	<b>96</b>
6.1 Case Study 1: Soft Tactile Sensor .....	97
6.1.1 Materials and design .....	97
6.1.2 Test configuration .....	98
6.1.3 Results .....	100
6.1.4 Discussion .....	105
6.2 Case Study 2: Soft 2D Strain Sensor .....	106
6.2.1 Fabrication .....	106
6.2.2 Pull test .....	107
6.2.3 Results .....	110
6.2.4 Discussion .....	115

---

6.3 Summary .....	116
<b>Chapter 7 Discussion and Conclusion .....</b>	<b>118</b>
7.1 General Discussion.....	119
7.1.1 Materials and fabrication .....	119
7.1.2 Experiments .....	121
7.2 Contribution and assessment of research objectives .....	122
7.3 Outlook .....	124
7.4 Conclusion.....	125
<b>Reference .....</b>	<b>129</b>

# List of Tables

Table 2-1 Summary of soft material in soft sensor application .....	21
Table 3-1 Parameters of fully elastomeric sensors .....	41
Table 3-2 Requirements of different soft sensors .....	42
Table 4-1 Variation of fabrication methods .....	48
Table 4-2 Test results of different formulations of conductive hydrogels.....	60

---

# List of Figures

Figure 2-1 Hard and soft robots .....	7
Figure 2-2 Early stage of the development of soft robots.....	9
Figure 2-3 Design and fabrication of V-SPAs .....	9
Figure 2-4 Integrated fully soft autonomous robots .....	10
Figure 2-5 Dielectric soft actuators with fluidic strengthening .....	11
Figure 2-6 Soft actuators for cardiac assistance .....	11
Figure 2-7 Soft robotic ventricular assist device .....	12
Figure 2-8 Recent developments of soft robots .....	13
Figure 2-9 The categories of soft sensors .....	14
Figure 2-10 Array of magnetic soft tactile sensor .....	16
Figure 2-11 Illustration of a sample plane-parallel capacitive sensor .....	16
Figure 2-12 Dielectric elastomer tactile sensor with stretchable hydrogel electrodes.	17
Figure 2-13 Soft resistive tactile sensor using tomographic imaging .....	18
Figure 2-14 Carbon nanotube and silicone elastomer tactile sensor.....	18
Figure 2-15 Fabrication of a typical carbon-elastomer soft sensor.....	20
Figure 2-16 Fabrication and configuration of a soft sensor using liquid conductor ....	22
Figure 2-17 Fabrication methods of soft sensors .....	23
Figure 2-18 Hydrogel with high mechanical performance .....	27
Figure 2-19 Stretchable dielectric elastomer actuator (DEAs) made by hydrogel .....	27
Figure 2-20 Capacitive soft strain sensors with ionic hydrogel.....	28
Figure 2-21 Highly stretchable tactile sensors using pure elastomeric structures .....	29
Figure 2-22 Polymerisation of PDMS .....	31
Figure 2-23 Reaction of UV crosslink silicone rubber .....	32
Figure 2-24 Application of UV-crosslinked silicone rubber .....	33

---

Figure 2-25 3D printable silicone elastomers .....	34
Figure 2-26 Physical interactions between hydrogels and elastomers.....	35
Figure 2-27 Transparent, compressible pressure sensors made of PEDOT:PSS coated on PDMS.....	36
Figure 2-28 Highly stretchable Functional living device .....	36
Figure 3-1 Conceptual design and applications for fully elastomeric soft sensors.....	42
Figure 3-2 Fabrication methods and test methods for fully elastomeric soft sensors..	43
Figure 4-1 Fabrication process of UV-cured hydrogels .....	46
Figure 4-2 Experiment setting for hydrogels properties .....	50
Figure 4-3 The tensile test results for the conductive hydrogels in different concentrations of acrylamide .....	52
Figure 4-4 The tensile test results for the conductive hydrogels in different concentrations of MBAA.....	54
Figure 4-5 The tensile test results for the conductive hydrogels in different concentrations of Irgacure 2959.....	55
Figure 4-6 The tensile test results for the conductive hydrogels in different concentrations of NaCl .....	57
Figure 4-7 The tensile test results for the conductive hydrogels in different UV exposure time .....	59
Figure 4-8 Summary of different mechanical performances in tensile tests of different formulations of hydrogels. ....	61
Figure 4-9 Summary of different electrical resistance in tensile tests of different formulations of hydrogels .....	62
Figure 4-10 Fixture of compression test on hydrogels .....	64
Figure 4-11 Mechanical stress of hydrogels with different acrylamide concentrations .....	65
Figure 4-12 Electrical resistance of hydrogels with different acrylamide concentrations .....	66
Figure 4-13 Mechanical stress of hydrogels with different MBAA concentrations ....	67
Figure 4-14 Electrical resistance of hydrogels with different MBAA concentrations	68
Figure 4-15 Mechanical stress of hydrogels with different NaCl concentrations .....	69
Figure 4-16 Electrical resistance of hydrogels with different NaCl concentrations ....	70
Figure 4-17 Mechanical stress of hydrogels with different Irgacure concentrations...	71

---

Figure 4-18 Electrical resistance of hydrogels with different Irgacure concentrations .....	72
Figure 4-19 Mechanical stress of hydrogels with different UV exposure dose.....	73
Figure 4-20 Electrical resistance of hydrogels with different UV exposure dose .....	74
Figure 5-1 The design of the soft sensor.....	80
Figure 5-2 Chemical scheme of photo-grafting on the PDMS .....	82
Figure 5-3 Water retention test setup for hydrogel samples .....	82
Figure 5-4 Results of water loss test for hydrogel samples .....	83
Figure 5-5 Fabrication of a PDMS-coated soft strain sensor.....	84
Figure 5-6 Tensile strain test on baseline recipe of the hydrogel .....	87
Figure 5-7 Peel test setup on hydrogel-elastomer hybrid .....	88
Figure 5-8 Peeling test of hydrogel and PDMS bonding.....	88
Figure 5-9 Electrical property test .....	89
Figure 5-10 Case studies of the soft strain sensor.....	92
Figure 5-11 Soft strain sensor applied to sensing the bending of a pneumatic actuator .....	93
Figure 6-1 Schematic of the sequential scan.....	97
Figure 6-2 Configuration for multi-electrodes sensing.....	98
Figure 6-3 Photo for the indentation test .....	99
Figure 6-4 Test results for multi-electrode sensing .....	102
Figure 6-5 Fitted position of indentation .....	104
Figure 6-6 Fabrication of sensor array .....	107
Figure 6-7 schematic of electrodes distribution for the sensor array.....	108
Figure 6-8 Schematic of pull test on soft strain sensor array.....	109
Figure 6-9 Installation of sensor sample .....	109
Figure 6-10 Resistance changes during the 2 mm parallel pull test .....	110
Figure 6-11 Resistance changes during the 4 mm parallel pull test .....	111
Figure 6-12 Resistance changes during the 2 mm diagonal pull test.....	113
Figure 6-13 Resistance changes during the 4 mm diagonal pull test.....	114

# Chapter 1

## Introduction

Focus is rising on soft robotics, which has been developed by altering rigid materials and parts of robots to soft and compliant ones. This chapter presents the background of soft robotics and their related soft sensors. The motivation for research on soft sensors is clarified by understanding the shortcomings in the development of soft robotics and soft sensors. The research objectives are then proposed as the design, development and characterisation of a fully elastomeric soft sensor aiming at the unsatisfied need for soft sensors. The thesis structure is presented at last to organise the research content.

---

## 1.1 Soft Robotics and Soft Sensors

Soft robotics is a group of robot systems made of soft materials, soft parts and soft structures [1-3]. The transition from conventional ‘hard’ robots to soft robotics enabled safe and comfortable interaction between humans and soft robots [4]. Obstructions are cancelled along with rigid parts in the soft robotic system, resulting in an excellent performance in response to complex deformation. Those soft robots also advance more bio-mimic functions for robots that can sense, move and be constructed just like living beings [5].

Sensing is essential for soft robots to perform their functions, and it provides feedback of action, which are needed for soft robots to achieve accurate controls and safe interactions. Environment perception is also required for soft robots working in universal applications. These sensors used in soft robotics systems require flexibility, integrability, in addition to the robustness, accuracy and speed needed by conventional robots. On this occasion, soft sensors aim to address those needs of sensing for soft robotics systems.

Existing research on soft sensors has been developed for tactile, strain, thermal, and pH sensing. In addition, some research has advanced in applying soft sensors to soft robots. For example, the softness of soft sensors is coordinated with the compliant interaction for soft robots, and soft sensors are also stretchable, facilitating flexible movement for soft robots.

## 1.2 Research Motivation

Despite the advantages of soft sensors in safe interaction, biocompatibility and motion complexity, there are still obstructions to them to be widely applied for long-term usage and in a harsh environment,

- 
- 1) properties of soft materials such as stretchability and durability remain enhanced for practical use,
  - 2) adaptive design of soft sensors for soft robotics, considering installation, cooperation, and fabrication, has not been proposed.

By thoroughly investigating the literature and state-of-the-art research on soft sensors, the gaps in current research were found as,

- 1) The lack of highly applicable soft sensors limits the development of soft sensors. Novel designs and concepts of soft sensors are still worth studying.
- 2) High-performance materials have been applied in existing research on soft sensors, but the durability, stability and flexibility of the soft sensors remain to improve.

This research aims to locate under-researched areas in the literature reviews and address potential techniques. It is to propose a fully elastomeric soft sensor,

- 1) a soft sensor with softness, stretchability, elasticity, durability and transparency is necessary to be integrated,
- 2) fully elastomeric materials for soft sensors need to be researched,
- 3) in-depth research on the mechanical and electrical properties of soft sensing materials, such as strain, stiffness and electrical resistance, remains to be conducted,
- 4) optically transparency is required to extend applications to occasions requiring optical clarity.

In general, an integration of soft strain sensor with softness, stretchability, elasticity, durability and transparency has not been proposed yet. For sensing ability, compared to a soft sensor filled with non-elastomeric materials such as nanowire and conductive liquid, a soft sensor made of fully elastomeric soft materials will enable

---

linearity in strain measurement by its linear modulus. And thoroughly research on ratio change of soft material recipe can achieve tunability on mechanical and electrical properties for adaptive measurement range and various working environments. And for sensing applications, transparent encapsulation and soft sensing material can bring a fully transparent soft sensor to extend applications to occasions requiring optical clarity.

## **1.3 Objectives**

The thesis raised a research question that how to improve the performance of a soft sensor from aspects of soft materials, design and fabrication. The technique gaps identified in the literature reviews indicate the soft sensor could be improved by softness, stretchability, durability and visibility. Following the research question, the objectives of the thesis defined to achieve are:

- 1) To design a conceptual soft sensor and address the approaches to the concept in aspects of materials, fabrications and experiments.
- 2) To develop a characterisation method to understand the mechanical and electrical properties of selected soft materials.
- 3) To develop hybrid material techniques to improve the stability and durability of selected soft materials.
- 4) To fabricate, evaluate and demonstrate a fully elastomeric soft sensor through the developed design, material and experimental techniques.
- 5) To demonstrate the potential of the developed sensing techniques by conducting case studies in different applications.

## **1.4 Thesis Structure**

The thesis has the following structure and contents:

*Chapter 1 – Introduction*

---

The chapter will present the background of this thesis. The soft sensor will be introduced briefly, and the motivation, objectives of this thesis will be described.

### *Chapter 2 – Literature review*

The chapter will include detailed reviews on the development of soft robots and soft sensors. The focus will then be on the materials, fabrication and encapsulation of conductive hydrogels.

### *Chapter 3 – Concept and methodology*

This chapter will briefly describe the concepts and methods of fully elastic soft sensors to provide a clear overview of the materials, fabrication, and experimental aspects of this thesis.

### *Chapter 4 – Conductive hydrogels*

The chapter will investigate the fabrication methods and variant recipes of conductive hydrogels. Variations of hydrogel recipes will be characterised by mechanical and electrical properties.

### *Chapter 5 – Fully elastomeric soft sensor*

The chapter will present the fully elastomeric soft sensor, including the fabrication, characterisation and application.

### *Chapter 6 – Case studies*

The chapter will provide two case studies expanding the usage of ionic conductive hydrogels for soft sensor arrays.

### *Chapter 7 – Discussion*

This chapter will discuss the results and limitations of fully elastic soft sensors. Prospects for applications and future work will also be addressed.

# Chapter 2

## Literature Review

To fully understand the development of soft sensors and investigate the gap in the research field, an in-depth literature review should be conducted. Firstly, the general development of soft robotics, including soft actuators, are looked through to locate the aim and purpose of a soft sensor. Then, an overall investigation of the soft sensor is conducted to determine the remaining gap. Next, to design and fabricate a novel soft sensor, several soft materials and fabrication methods are reviewed. Lastly, a promising technology of conductive hydrogels is focused on improving the performance of soft sensors.

## 2.1 Soft Robotics

Conventional robotic systems are made of precisely manufactured and engaged rigid parts, while soft robots are developed with flexible and compliant parts. Figure 2-1 illustrated two extremes of hard and soft robots. Hard robots are rigid linked, with actuators for every joint. Soft robots, on the other hand, have actuators integrated and distributed throughout the robot. The rigid parts of robotic systems sometimes become a threat to human safety in the scenes of interactive working with robotic systems. Due to their precision of movement, perception, and cognition, robotic systems are now widely applied in industrial manufacturing and many other contexts. To achieve their desired abilities, complex mechanisms had been designed and implemented, which often limited their adaptability. Complexity, limited adaptability, unsafe interaction with humans and lack of compliance are gaps between machines and people. Soft robots can fix those problems in conventional robotics for their potential in adaption, sensitivity and agility [6]. The critical challenge in soft robots is that new components such as sensors, actuators and computation with ideal material and novel control algorithms remain to be developed.

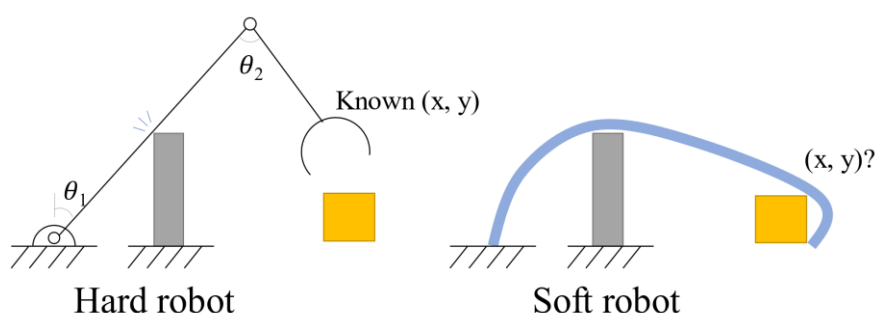


Figure 2-1 Hard and soft robots. The conventional robots have predictable but limited trace while soft robots have complex moving more complex and adaptive movement trajectory.

---

The use of soft and compliant materials in soft robotic systems sets them apart from conventional robotic systems. Young's modulus is a widely used measure to represent stiffness and rigidity of materials in robotic system [7]. Usually, a range of materials with Young's modulus between  $10^4$ - $10^9$  Pa are applied in soft system which is very close to natural organisms and tissues. By using soft materials, the soft systems obtain similar compliance to natural biological materials, reducing the potential harm of hard contact [8]. Compliant materials also have good adaptivity to other objects which largely help to improve the performance of tasks such like grasping [9] and moving over soft surface [10]. Soft systems simplified the mechanism, while in another way, pushed more computation on control such like morphological algorithm [11].

The first design of the soft robot date back to 1992. Suzumori [12] *et al.* demonstrated an effectively flexible micro-actuator with pneumatic actuation composed of elastomer, shown in Figure 2-2(a). Channels in the elastomer are inflated by air, and asymmetry structures are deformed to drive components to actuate. This approach achieved lifelike motions by the continuous, adaptive and compliant move. Then this micro-actuator was optimised by the finite-element method (FEA) in 1997 to reduce the complicity of the fabrication process [13]. The pneumatic actuating technologies were also further developed for planar mobile worm robot [14], pneumatic wobble motor [15], swimming robot [16], shown in Figure 2-2(b)-(d), respectively.

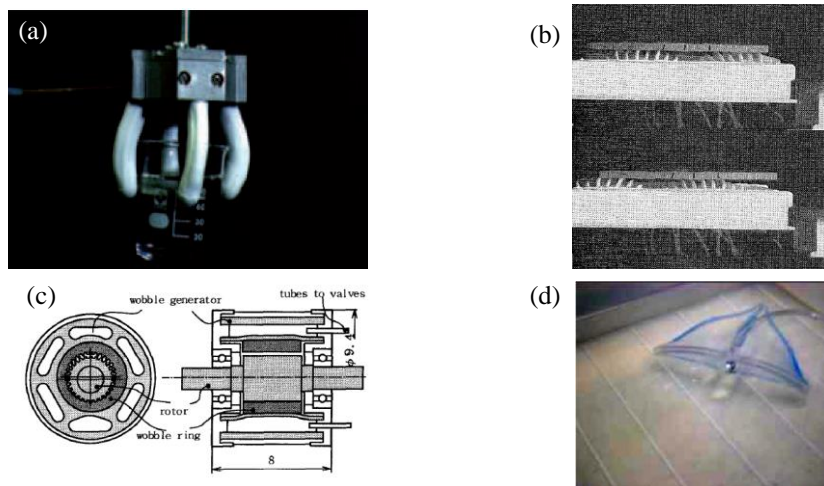


Figure 2-2 Early stage of the development of soft robots. a) flexible gripper composed of inflated elastomer [12]. b) planar mobile worm robot [14]. c) pneumatic wobble motor [15]. d) soft swimming robot [16].

Recently, through the path of early-stage soft robots, Robertson and Paik [17] introduced a vacuum-powered soft pneumatic actuator (V-SPAs) with multiple degrees of freedom. As shown in Figure 2-3, foams were applied as cores of actuators and enclosed with silicone layers which improved the productivity of industrial and massively fabrication. This device achieved multiple tasks such as multimodal locomotion, object manipulation, and stiffness tuning with simple structures and proposed modular peripheral mechanisms. While one of the drawbacks of V-SPAs was that system was working under vacuum conditions which weakened its strength when actuating.

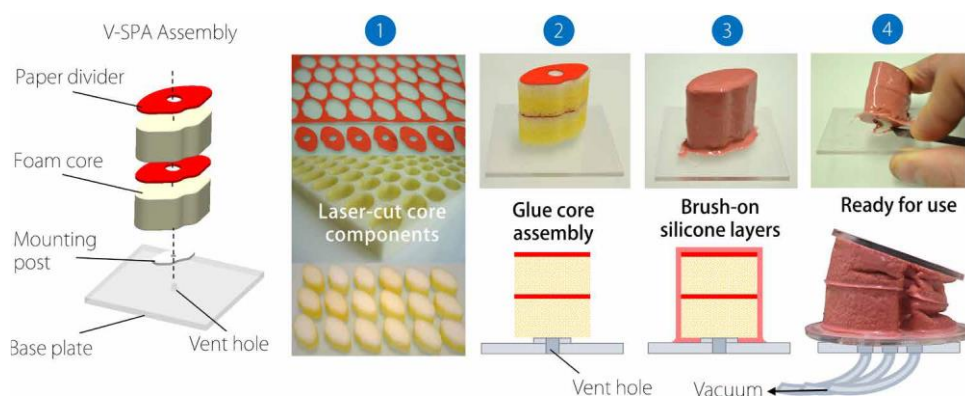


Figure 2-3 Design and fabrication of V-SPAs [17]. The V-SPAs consist of foam core, divider and base. Silicone layers are brushed on to form a vacuum chamber for actuation.

Wehner *et al.* [18] designed an autonomous soft robot under an integrated fabrication method, shown in Figure 2-4. Stretchable electronics, including a fluidic controller, were implanted and then the embedded 3D print was applied to shape the robots. The microfluidic circuit design provided a miniaturized solution for soft robots which relied on a fluidic or pneumatic drive. Developing a fully soft robotic system also enlightens this research field in a more practical method.

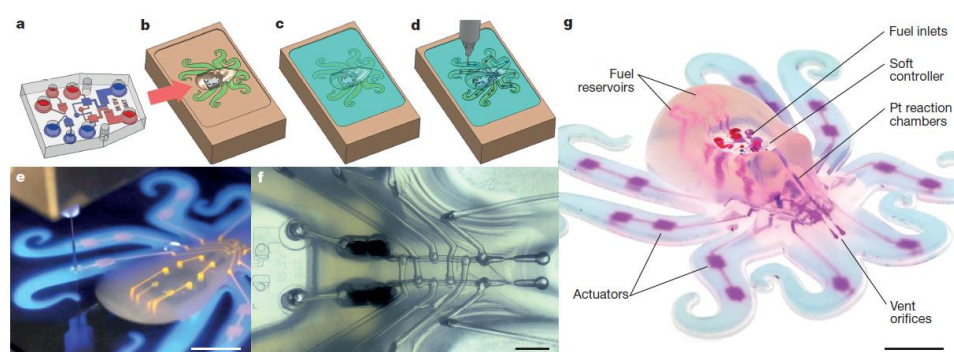


Figure 2-4 Integrated fully soft autonomous robots [18]. A microfluidic circuit was applied to a miniaturized soft robot made by 3D print. a)–d) a miniaturized soft robot made by embedded 3D print. e)–f) A microfluidic circuit was applied to the soft robot. g) overview of the structures and controls of the autonomous soft robot.

Apart from improving fabrication technologies, the adaptive and inspired design also made soft robots a step further. For example, Kellaris [19] *et al.* integrated the advantages of fluidic actuators and electrostatic actuators to build a flexible actuator shown in Figure 2-5. The actuators were strengthened by fluid using a facile heat-sealing method with commercially available materials. The prototype demonstrated a strain rate of 900% per second and actuation at 50 Hz by the implementation of electric field. The fluidic actuators also advanced in high optical transparency and self-sensing of their deformation. This research paved the way for hybrid design in soft robotics, which provides more outstanding performance.

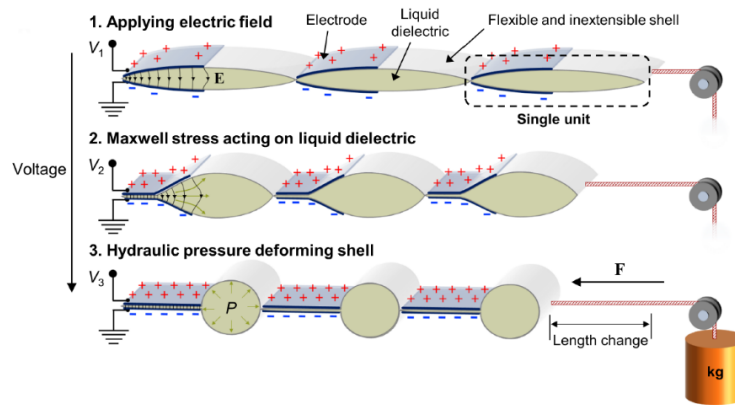


Figure 2-5 Dielectric soft actuators with fluidic strengthening [19]. The actuator changed length by applying an electric field to close the flexible and inextensible shells.

Adaptive design of soft robots led to a more effective path to the application. For example, very different designs can achieve the same goals for a similar cardiac problem. Roche *et al.* [20] develop a soft robotic sleeve to assist heart muscle shown in Figure 2-6. The sleeve consists of two layers of soft actuators implanted around the heart in a helical and circumferential fashion and actively controlled to compress the heart. Efficacy of the soft robotic sleeve in heart failure assistance is demonstrated in pigs with acute heart failure. The biomimetic function of a soft robotic sleeve is proved similar to real cardiac muscle.

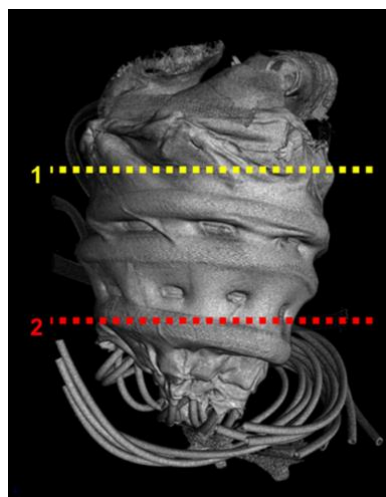


Figure 2-6 Soft actuators for cardiac assistance [20]. The sleeve-like soft actuator implanted around the heart to assist the heart to beat. The soft actuators consisted of two layers in a helical and circumferential fashion and actively controlled to compress the heart.

Payne *et al.* [21] proposed a soft robotic ventricular assist device aiming to assist heart failure, as shown in Figure 2-7. The device consists of a rigid semilunar frame with soft actuators attached around the inner surface. A brace bar crosses a ventricle wall with a septal anchor engaged with the interventricular septum (IVS). The actuators provide contractile motion when inflated to compress the ventricle. With engaging interventricular septum, this device may perform well in blood injection, which assists heart failure operatively.

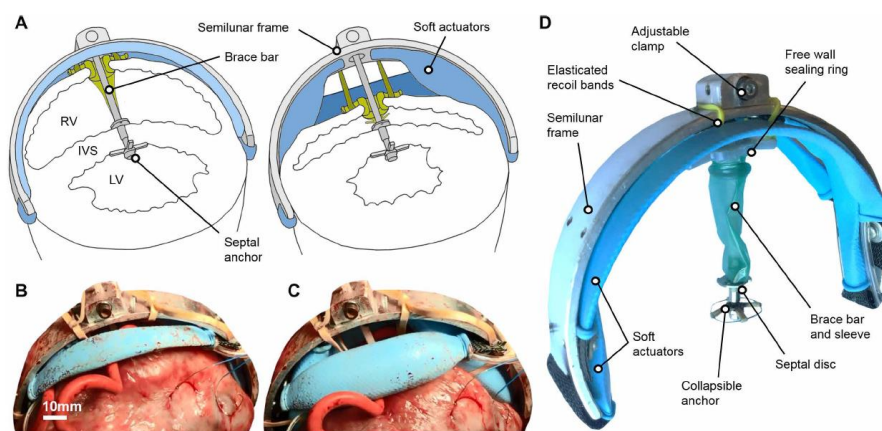


Figure 2-7 Soft robotic ventricular assist device [21]. The device consists of a rigid semilunar frame with soft actuators attached around the inner surface. The actuators provide contractile motion when inflated to compress the ventricle.

Figure 2-8 summarised the recent progress on different kinds of soft robots in the aspect of driving power, including pneumatic soft robots shown in Figure 2-8(a)(b)(c), magnetic soft robots shown in Figure 2-8(d)(e)(f), and electromotive soft robots shown in Figure 2-8(g)(h)(i).

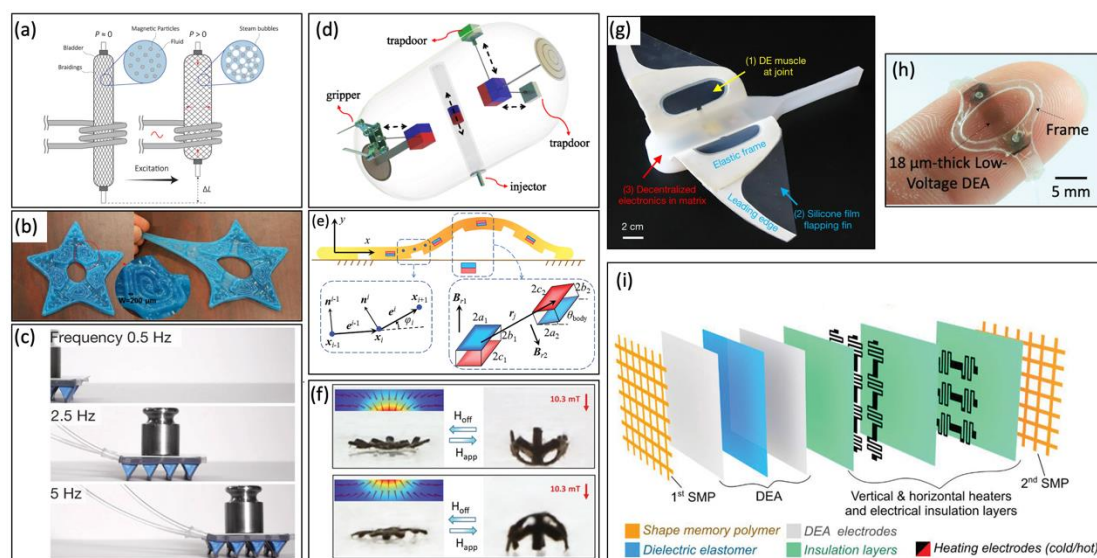


Figure 2-8 Recent developments of soft robots. a) A pneumatic artificial muscle is presented by filling metallic particles into a fibre-constraint balloon [22]. b) 3D-printed highly stretchable soft actuator is fabricated with the complex internal patterns and channels [23]. c) A soft robotic millipede walker is produced by the multi-material multi-nozzle 3D printing [24]. d) A multi-degree-of-freedom microrobot equipped with four onboard tools driven by a magnetic field is presented [25]. e) A biomimetic magnet embedded worm-like soft robot is designed [26]. f) A hydrogel milli-gripper with flexible and reversible shape deformations by magnetic field controlling is achieved [27]. g) A self-powered soft robot with a dielectric elastomer actuator reached the Mariana Trench [28]. h) A dielectric elastomer actuator is applied as a haptic feedback device [29]. i) A shape-programmable dielectric elastomer with different latched states is fabricated [30].

## 2.2 Soft Sensors

The rising studies on the soft actuators were the first steps of soft robotics. To further develop more flexible soft robots, there is a need to present other soft components. Soft sensors are the key components for soft robots to acquire environmental conditions and aware status of themselves in a flexible and compliant manner.

Soft tactile sensors were developed to obtain feedback and serve optimum contact force to aimed objects. For soft robotics, tactile sensors are adaptively addressed as low stiffness and high compliance objects [31, 32]. Existing approaches to this purpose measured force indirectly by converting other parameters into force itself including optical sensors [33], conductive liquid sensors [34], resistive sensors [35], capacitive sensors [36] and magnetic sensors [37], as shown as Figure 2-9.

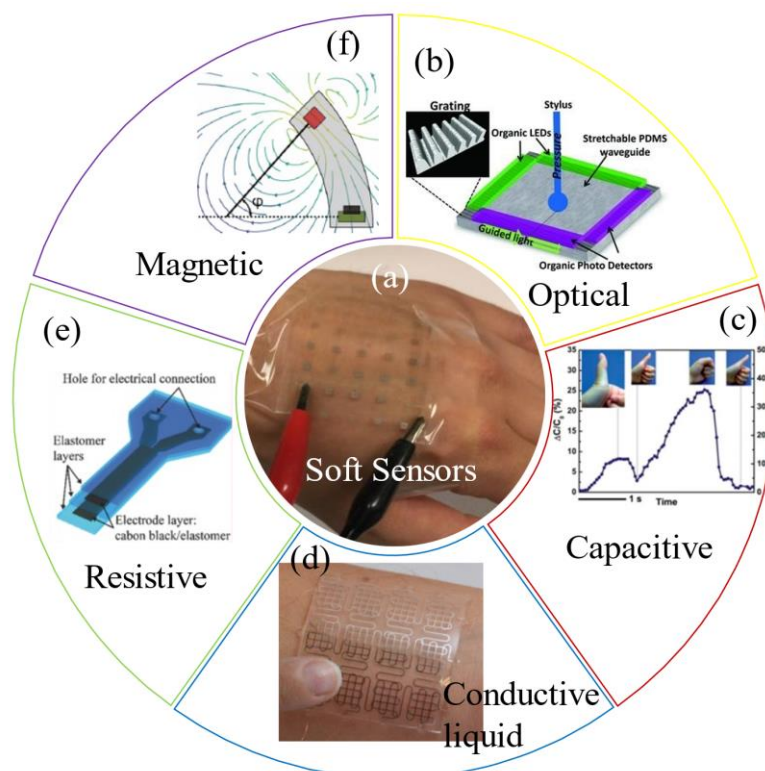


Figure 2-9 The categories of soft sensors. a) Soft sensors are stretchable and in low stiffness [38, 39]. b) Optical sensors monitor the shift of wavelength of light [40]. c) Capacitive sensors measure the capacitance change to indicate the deformation and force [41]. d) Conductive liquid sensors embed liquid conductors in its microchannels to measure the changes of electrical resistance [42]. e) Resistive sensors measure electrical resistance change [43]. f) Magnetic sensors monitor the magnetic field change when the sensor is triggered [44].

For example, Ohmura *et al.* realised a soft optical tactile sensor in 2006 [45]. The optical sensor detected the deformation of covered soft urethane foam and then transacted the measured light change. Hammond *et al.* presented a soft tactile sensor using conductive fluid filling in micro-channels embedded in soft elastomer layers [46]. In 2014, Sun *et al.* presented an ionic skin by creating a soft conductive hydrogel consisting of a dielectric elastomer [47]. The sensor was reported as a stretchable, large-area sheet of the distributed sensor. Kim *et al.* reported an all-carbon skin as a piezo-capacitive tactile sensor [48]. Elastic carbon nanotube microyarns fabricated the sensor. Different stimuli, including mechanical deformation, touch, temperature or humidity gradient, were measured on a single sensor.

---

Some research focused on magnetic field-based tactile sensors. Those sensors usually contained a magnetic field sensor and an attached magnet [49]. The magnetic field varied when the magnet was triggered by contact with a potentially sensing object. The magnet can be contained in a soft body that is fabricated at low cost as well as deformable and stretchable.

Magnetic field sensors provide a way to process a relatively soft and compliant component to safely interact with humans, which reveals more possibilities in design, fabrication for a soft tactile sensor. For example, with soft and compliant contact, magnetic-based tactile sensors can be also integrated into a robotic hand to help grasped fragile objects with a proper force [50, 51].

Aimed at a robust, low-cost soft tactile sensor, Goka *et al.* produced a magnetic type tactile sensor [52]. A magnet was injected inside a soft elastomer which was set on a substrate layer with four GMR (Giant Magneto Resistance) elements and four chip inductors. Distance change of magnet was detected by GMRs, and a force vector is calculated. In the case of magnetic tactile sensors, precise measurement of force relied on accurate evaluation of the magnetic field. A Hall-effect sensor was introduced to the field of the tactile sensor in 2013 [53]. In this study, a 3-D Hall-effect sensor was applied to locate the relative movement between the magnet and Hall-effect sensor. And force measurement was then further calculated considering the elasticity of the substrate. In 2014, Youssefian *et al.* highlighted a promising technology by applying a soft spherical shell to conventional soft tactile sensors which were based on hall-effect sensor and magnet as shown in Figure 2-10. Each set of soft tactile sensors contained a spherical shell made of silicone rubber, an attached magnet on top of the shell and an array of four Hall-effect sensors on the substrate PCB board. And several sets of soft sensors were arranged as a matrix for the large-area multiple sensing [54].

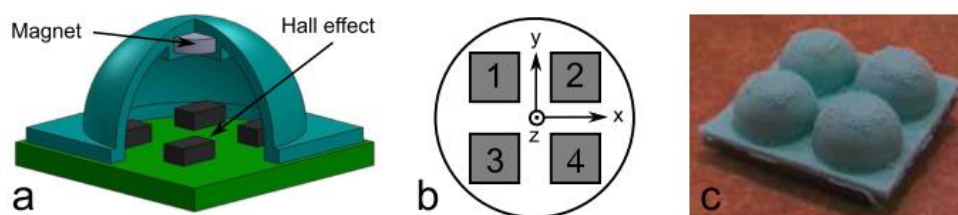


Figure 2-10 Array of magnetic soft tactile sensor [54]. The sensor detects the movement of a spherical shell made of silicone rubber by Hall-effect sensors on the substrate PCB board.

Despite the widespread application, the magnetic-filed sensors were still restricted with the rigid magnetic components and PCB board [52-54]. And the sensitivity of the magnetic-filed sensors was mainly determined by their contained Hall-effect sensor where was limited potential to enhance.

Soft capacitive sensors are another promising soft tactile sensor technology. In general, dielectric elastomers are fabricated to plane-parallel capacitive sensors, which are sandwiched by two flexible and compliant electrodes, as shown in Figure 2-11 [55]. The dielectric elastomer sensor was deformed by external pressure and the distance between two sandwiched electrodes changed correspondingly. Then capacitance change was captured to estimate the applied pressure.

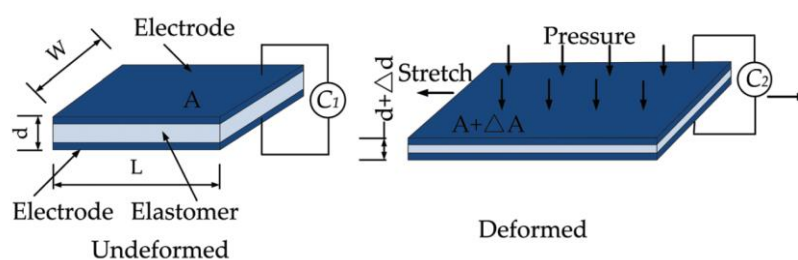


Figure 2-11 Illustration of a sample plane-parallel capacitive sensor [55]. The capacitive sensor detects the capacitance change caused by deformations under external pressure.

For example, Sun *et al.* presented a stretchable, large-area sheet of distributed sensors [47] which showed flexibility in the application of hydrogels as shown in Figure 2-12. Two hydrogel layers as electrodes and one dielectric layer were sandwiched. When the dielectric elastomer was pressed, capacitance changed by distance variation

between two electrodes. This measurement of capacitance enabled the sensor to detect the strain and pressure. As sensors arrays, the distributed sensors can also locate and measure contact.

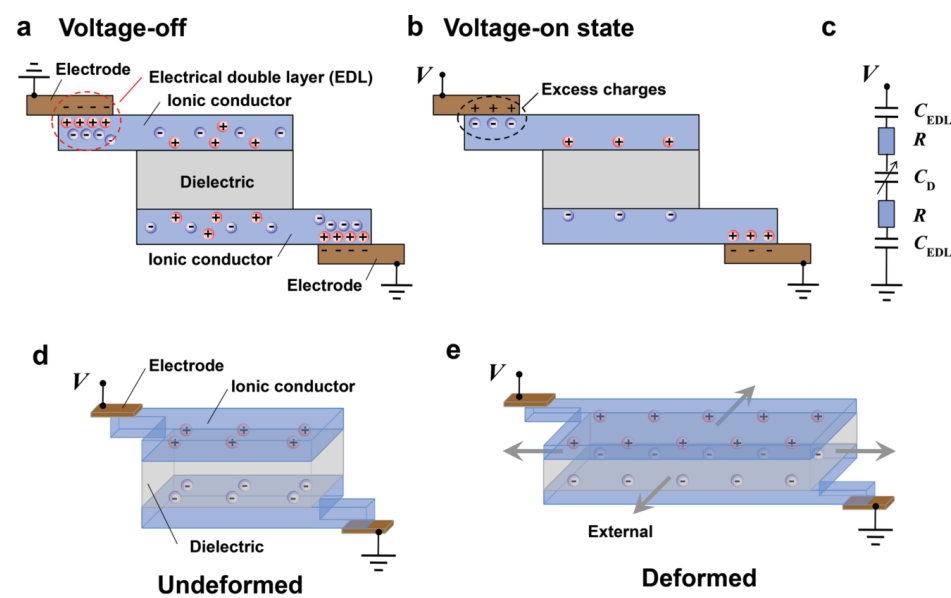


Figure 2-12 Dielectric elastomer tactile sensor with stretchable hydrogel electrodes [47]. This sensor is consisting of two conductive hydrogel layers and a sandwiched dielectric layer. The capacitance changes when the sensor is pressed.

Tomographic imaging is based on the inverse reconstruction of cross-sectional images from measurements made at boundaries, which is a common medical technique applied in human body imaging.

In 2015, Chossat *et al.* [56] presented a soft tactile sensor by tomographic imaging resistive change as shown in Figure 2-13. The sensor consisted of conductive soft electrodes fabricated by carbon nanofiber with coated nickel, silicone substrate with channels, room temperature ionic liquid. An electric impedance tomography method was applied to measure the electric current change among different electrodes through the conductive liquid. Then both location and magnitude of contact force were detected in the experimental section.

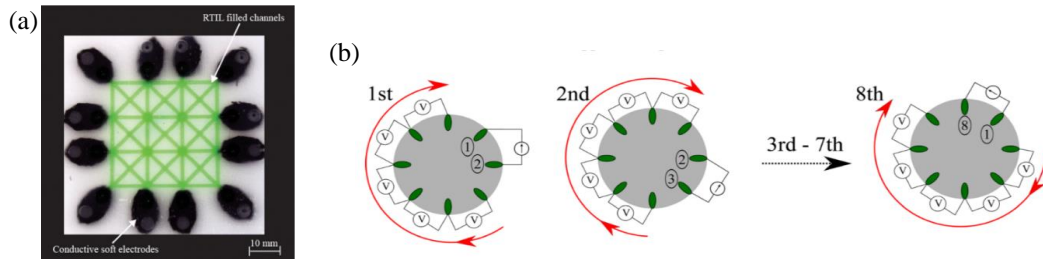


Figure 2-13 Soft resistive tactile sensor using tomographic imaging [56]. a) grids filled in with conductive liquid is built into the sensor, b) an electric impedance tomography method was applied to measure the electric current change.

Lee *et al.*[57] presented research on the soft tactile sensor by a mixture of carbon nanotube and silicone elastomer as shown in Figure 2-14. Powder of multiwall carbon nanotube was added into liquid silicone and injected the mixture into a casting mould. The thin fabric appeared an anisotropic piezo-resistivity corresponding to the morphological deformation. Anisotropic electrical impedance tomography was then applied as a stress mapping test with a successful estimation of stretch displacements, surface normal forces, and multi-point contact locations.

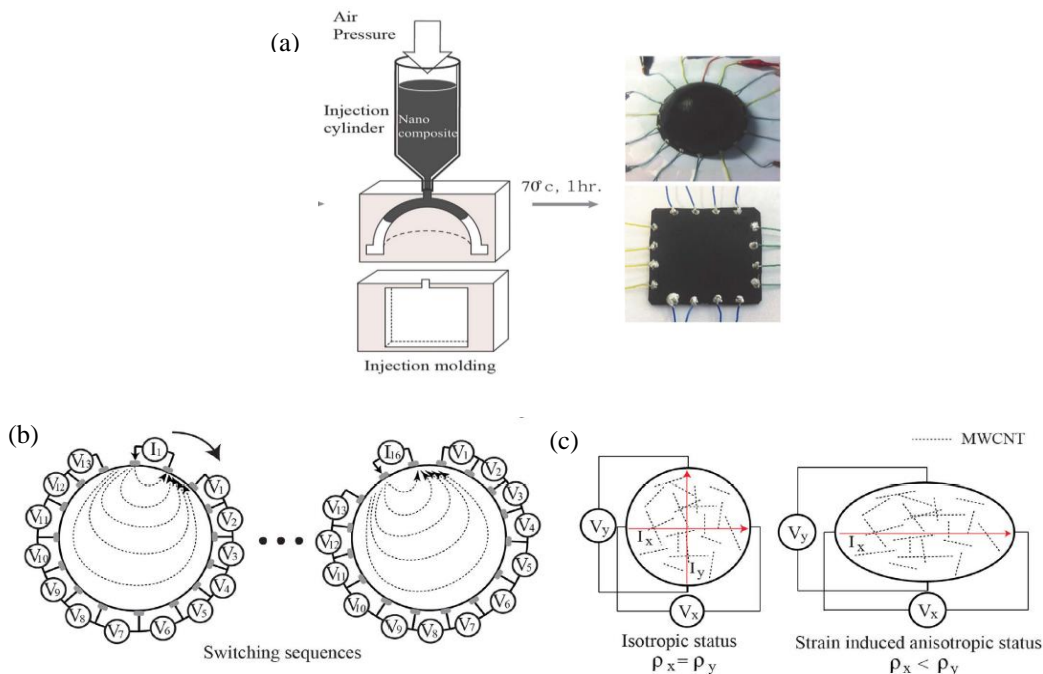


Figure 2-14 Carbon nanotube and silicone elastomer tactile sensor [57]. a) Anisotropic electrical impedance tomography is applied as stress mapping for the tactile sensor. b) - c) Detecting process of the anisotropic electrical impedance tomography

---

## 2.3 Soft Materials for Soft Sensors

### 2.3.1 Conductive soft materials

In order to proceed highly stretchable and sensitive soft tactile sensor, research focus had been transmitted on selecting and fabricating soft materials that showed potential in the mechanical property and electrical property. This research focuses on the conductive and resistive soft materials which change their electrical resistance when deformed. Those soft materials can be divided into three categories, conductive carbon-elastomer mix, liquid conductor and conductive hydrogel.

For carbon-based soft materials, studies mixed in conductive carbon and soft elastomers. Typically, conductive carbon particles with high electrical conductivities are injected or encapsulated into a highly stretchable and low stiffness elastomer. For example, Roh *et al.*[58] presented a strain sensor made of single-wall carbon nanotubes (SWCNTs) embedded on a PDMS elastomer with polyurethane-poly(3,4-ethylenedioxythiophene) polystyrene-sulfonate (PU-PEDOT:PSS) coating as shown as in **Error! Reference source not found.** This strain sensor achieved electrical conductivity by SWCNTs. Based on the mechanical properties of PDMS and PU-PEDOT:PSS, it had high stretchability, up to 100%. This sensor also brought optical transparency of 62%.

Table 2-1 summarizes a list of soft sensors that show differences between different soft materials.

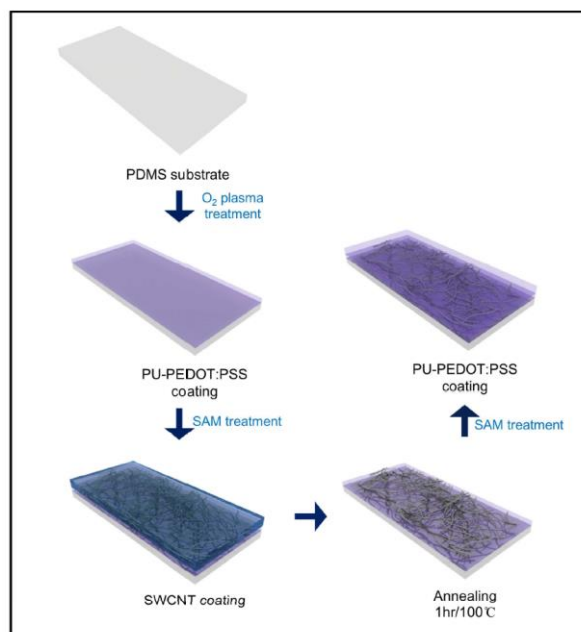


Figure 2-15 Fabrication of a typical carbon-elastomer soft sensor [58]. Conductive carbon nanotubes are implemented in soft materials for resistive sensing.

Carbon nanotubes, graphene and carbon black have been widely used in the field of carbon-elastomer soft sensors due to its high electrical conductivity and various morphology. [62-71] For example, Wang *et al.* [63] presented a wearable and highly sensitive strain sensor using graphene. Graphene that was grown on copper mesh by chemical vapor deposition (CVD) was transferred to a PDMS film. High gauge factor of  $10^6$  under higher strains ( $>7\%$ ) was achieved in this sensor configuration. Shin *et al.* [64] fabricated a highly stretchable conductors and piezo-capacitive strain gauges using carbon nanotubes (CNTs). Modified vertical CNTs were encapsulated inside a moulded PDMS responding to strain applied on PDMS. This sensor can be stretched up to 450% strain length fully functionable. Kong *et al.* [65] presented conductive and elastomeric carbon composites mixing carbon black particles and PDMS pre-solution. This composite was then moulded to a wire-like or mesh-like shape, embedded into a PDMS substrate as strain sensor. It also achieved a high stretchability of 80% strain length.

Table 2-1 Summary of soft material in soft sensor application

Authors	method	Categories	achievement or application	shortage	Ref.
<b>Hughes and Iida</b>	A resistive sensor fabricated by EcoFlex 0020. Carbon fibre and Carbon black were added as conductive element.	Carbon	Conductive particles and a non-conductive silicone matrix. Wearable Physiological Sensing both pressure and strain. Monitoring of foot load, calf muscle, breathing rate and heart rate. The simple procedure enables further formation.	Strain is reported over 200% and stiffness not reported. Conductive layer is not transparent.	[59]
<b>Sun et al.</b>	Conductive hydrogel electrodes and stretchable dielectric elastomer as a capacitive sensor	Hydrogel	A stretchable, large-area sheet of distributed sensor is fabricated which offered tissue-level softness and high optic transparency.	Fabrication method are not state-of-art. Lack of bonding between polymer as hydrogels.	[47]
<b>Lee et al.</b>	multiwall carbon nanotube silicone elastomer nanocomposites and anisotropic electrical impedance tomography (aEIT)	Carbon	A strain sensor and a pressure sensor were presented. Multi-dimensional strain measurements and multi-contact stress measurements were achieved.	Stretchability and softness and visibility	[57]
<b>Cai et al.</b>	single wall carbon nanotube (SWCNT), graphene, and silver nanowire in self-healing hydrogel	Carbon	By applying SWCNT, graphene and silver nanowire into hydrogel, this research achieve extremely stretchable conductive layer. A soft strain sensor was proposed using the conductive layer. This sensor is capable of self-healing due to the properties of self-healing hydrogels.	Visibility is still an unsolved problem.	[60]
<b>Park et al.</b>	Liquid conductor eutectic gallium indium is filled in microchannel moulded inside silicone rubber	Liquid conductor	A thin multi-layered resistive sensor was created with low stiffness and high stretchability.	Complicated structures and fabrication methods. Soft stiffness and visibility are limited.	[34]
<b>Muth et al.</b>	Conductive ink made of carbon conductive grease and silicone oil, injected to uncured silicone rubber	Liquid conductor	A printed strain sensor was presented with low stiffness and high stretchability.	Soft stiffness and visibility are limited.	[61]

For liquid conductors, studies focus on improving the conductivity of liquid conductors and encapsulation of liquid conductors in elastomers. Typical configuration of liquid conductor based soft sensor including a highly stretchable elastomer with multiple channels filling up with a highly conductive liquid conductor. Electrical properties changes, such as resistance, capacitance and impedance, of liquid conductor were detected to evaluate applied strain or stress.

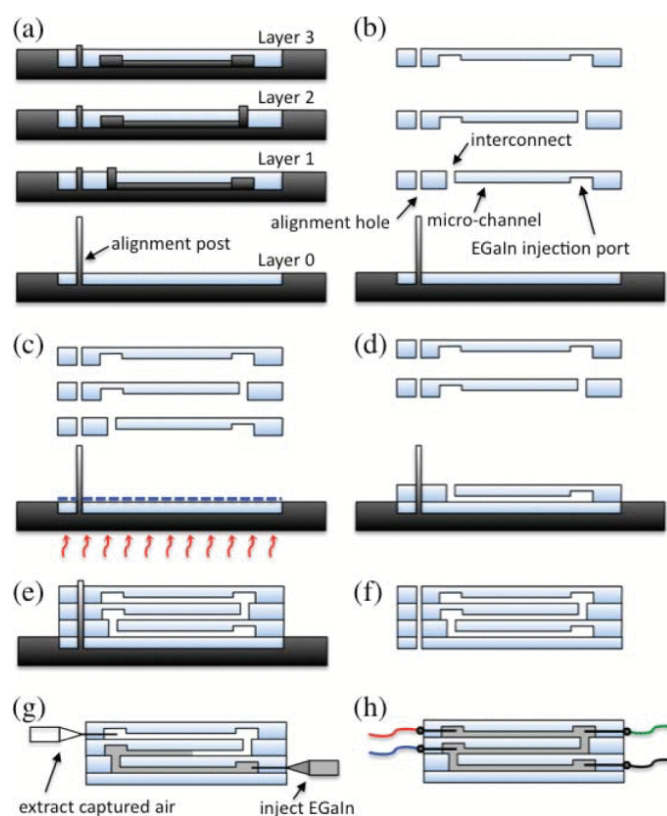


Figure 2-16 Fabrication and configuration of a soft sensor using liquid conductor [72]. Several layers of silicone rubber with groove are fabricated and stacked together to form vacuum channels filled with a liquid conductor.

For example, Park *et al.* presented a soft artificial skin by embedding a liquid conductor into a silicone rubber substrate, as shown in Figure 2-16 [72]. Eutectic gallium-indium (EGaIn) was selected as a liquid conductor due to its high surface tension and high electrical conductivity. With multiple layers of channels filled up with the liquid conductor, this sensor can reach a strain of 250%.

This type of soft sensor altered its electrical properties for wide and various sensing applications by adjusting the liquid conductor. For high conductivity, research applied Gallium-based alloy or its Oxide composites [73-77]. Liquid metal and alloy are outstood in high electrical ( $3.4 \times 10^4$  S/cm) conductivity and low viscosity. Soft sensors based on those materials maintain high electrical performance when stretched. Another group of liquid conductors is the ionic liquid solution. Soft sensors filled up with ionic liquid are also called microfluidic sensor [78-82]. Ionic liquid conductors covered a wide range of materials such as polymerised ionic liquids [83, 84], saline solution [85]. Liquid conductors can also be tuned to different conductivity, viscosity, and even chemical stability, which has significant potential in sensor application. Another aspect of the soft sensor is the attachment of conductive materials to a soft substrate. An excellent soft elastomeric substrate can improve the mechanical performance of soft sensors. Figure 2-17 summarizes widely used attaching methods during sensor fabrication.

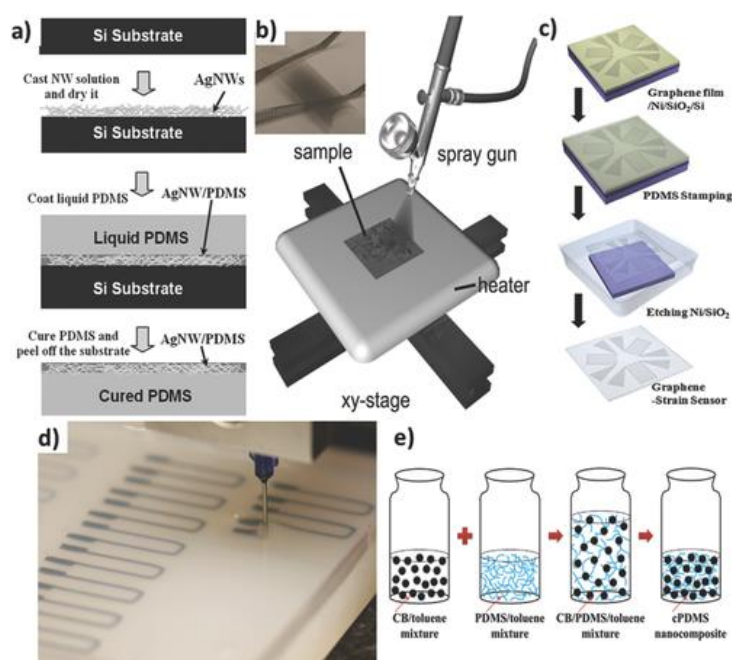


Figure 2-17 Fabrication methods of soft sensors. a) Filtration methods. Penetrating conductors into the elastomeric substrate. [86] b) Spray coating methods. Coating conductors onto the surface of soft elastomers. [87] c) Stamping or transferring methods. Transmitting a thin layer of conductive materials

---

on elastomers. [88] d) 3D printing methods. Injecting conductors (usually liquids or gels) into uncured elastomer pre-solution. [61] e) Pre-mixing solution. By mixing conductive particles and elastomer pre-solution to fabricate a conductive elastomer. [65]

### 2.3.2 Dielectric elastomer

In the last decades, the field of soft robots came into the view of materials scientists, enabling the development of new materials for actuation and sensing, including shape-memory materials [89-91], ionic liquids and polymers [92-96], polyelectrolyte gels [97], electroactive polymers [98-100], and carbon nanotubes [101].

Dielectric elastomers are a kind of electroactive polymers that are sensitive to mechanical deformation such as strain. Since dielectric elastomers were firstly developed in the 1990s [102-104], they were applied to transduce electric energy to mechanical energy or reversely from mechanical energy to electric power. Dielectric elastomer sensors have been another bunch of promising approach to soft sensors. Properties of large strain, compliance, low cost were highlighted among dielectric elastomer sensors [105].

In this configuration, the soft electrodes and dielectric elastomers were further developed to achieve better performance on dielectric elastomer sensors. For dielectric elastomers, silicone, Polydimethylsiloxane (PDMS) and acrylates were widely applied. For example, Fassler [106] *et al.* presented a soft pressure sensor made with a soft elastomer of silicone rubber (EcoFlex 0030). Both capacitance and inductance change were captured triggered by deformation. The same research group also presented a soft-matter capacitive sensor to measure shear and pressure by combining two different stiffness of silicone materials [107]. The applied pressure was measured both in magnitude and position with an array of electrodes. By computational analysis, the shear force was also obtained by this sensor. As for PDMS, for instance, back in 1997,

---

Lötters [108] *et al.* demonstrated the mechanical properties of PDMS and applied it to tactile sensors. Lee [108] *et al.* developed a PDMS dielectric elastomer sensor for pressure measurement. The PDMS elastomers provided good properties of low cost, high flexibility and high sensitivity in this research, which were essential for a soft pressure sensor. Mannsfeld [109] *et al.* achieved an extensive array of tactile sensors by PDMS with high sensitivity and flexibility to mimic human skin. This research showed the potential of PDMS in casting modelling and micro-structuring, which inspired low-cost practice and massive production. Research in acrylate such as VHB™ was also developed by various scientists for its high commerciality and good performance. For example, Kaltenbrunner [110] *et al.* designed a thin plastic tactile sensor film utilising VHB as a dielectric elastomer layer. High strain performance helped the ultra-thin film sensor form a non-plane sensor network. Pu [111] *et al.* presented a revised sandwiched design of a dielectric elastomer tactile sensor using two VHB elastomer layers clamping one electrode layer. The tactile sensors can also be applied as an energy generator by mechanical energy.

Despite the relatively mature application of dielectric elastomers, the focus had been placed on the compliant, stretchable, durable and conductive electrodes. There are three groups of soft electrodes being developed widely, namely the fluidic alloy [112-115], conductive carbon [73, 116-119] and conductive hydrogels [120-123].

### **2.3.3 Conductive hydrogels**

Hydrogels are a group of polymers syntheses with high molecular weight and water content. Most hydrogels are soft, stretchable, optically clear and biocompatible. A hydrogel is easily converted to an ionic conductor by adding ions to contained water. Its mechanical deformation usually initiates changes in electrical properties, which makes ionic conductive hydrogel a good material for soft tactile sensing. For example,

---

Sarwar *et al.* presented a sensor array using conductive hydrogels as electrodes [124]. Conductive hydrogels were structured and coupled as arrays of capacitors to measure the magnitude and location of the deformation of a sensor in the form of bending, stretching and touching. Kim *et al.* presented a touch panel using an ionic hydrogel as a conductor bridging two electrodes [125]. The current detected from two electrodes changed when the hydrogel was touched due to its resistance change.

Hydrogels have better safety performance when contacting humans than fluidic alloy, especially in medical applications. Another drawback for fluidic alloy electrodes is that an external package is required to prevent leakage. While one shortcoming of hydrogels comparing to the fluidic alloy is the durability due to the easy dehydration of hydrogel in open air. Hydrogel-based sensors are fully elastic with better mechanical properties such as high strain limit and high compliance in terms of conductive carbon electrodes. While conductive hydrogels still need to improve their electrical stability in comparison with the carbon electrodes. With the promising potentials and the intention to improve, research attention on hydrogel was raised largely.

Sun *et al.* [126] studied a highly stretchable hydrogel to overcome the limitations of conventional hydrogel and expand its application range in actuators and sensors, as shown in Figure 2-18. This study mixed two types of crosslinked polymer: ionically crosslinked alginate and covalently cross-linked polyacrylamide. Compared to conventional notch-sensitive hydrogels, this gel appeared to have high stretchability up to 17 times with notches, which widely expand the application of hydrogels. This research also revealed how the proportion of acrylamide affected its mechanical performance, which was inversely proportional to the elastic modulus of the hybrid gel.

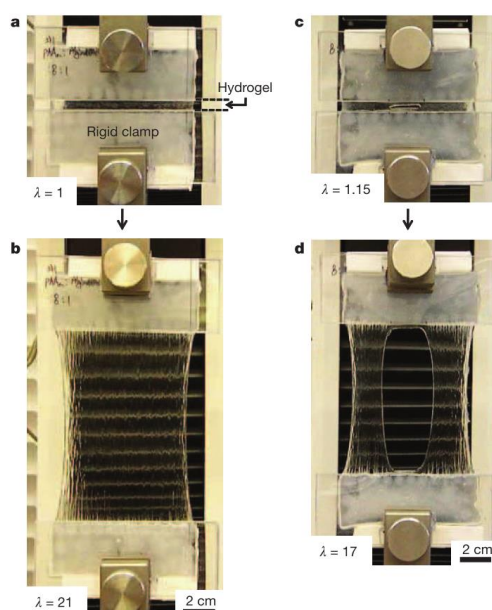


Figure 2-18 Hydrogel with high mechanical performance [126]. The highly stretchable hydrogel remains its robustness even with notch.

Keplinger [127] *et al.* demonstrated stretchable, transparent, ionic conductors using hydrogels, as shown in Figure 2-19. 1- $\mu\text{m}$ -thick VHB 4910 tape (3M) was used as the dielectric, and 100- $\mu\text{m}$ -thick polyacrylamide hydrogel containing NaCl was used as the electrolyte. This conductor was proven to have a quick response and large strain under high frequencies and voltages. Compared to existing electronic conductors, silver nanowires (AgNWs), single-wall carbon nanotubes (SWNTs), graphene, and indium tin oxide (ITO), this conductor had lower sheet resistance.

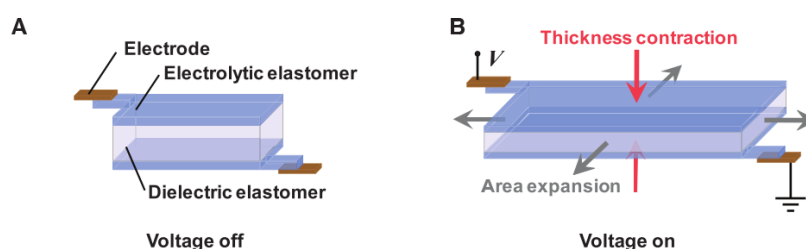


Figure 2-19 Stretchable dielectric elastomer actuator (DEAs) made by hydrogel [127]. When the electrical field was applied to the two conductive layers, the dielectric elastomer in the middle was compressed and expanded.

Frutiger [128] *et al.* proposed wearable and stretchable sensors for strain sensing, referred to as capacitive soft strain sensors (CS3), as shown in Figure 2-20. A composite fibre of four concentric layers is designed to contain two conductive hydrogel layers as conductors and two silicone elastomer layers as shell and dielectric. Multicore-shell fibre printing was applied for fabrication with flexibility and programmability. The CS3 fibre works appropriately with a large strain scale up to 250%, and dynamic response revealed desirable with wideband and quick response.

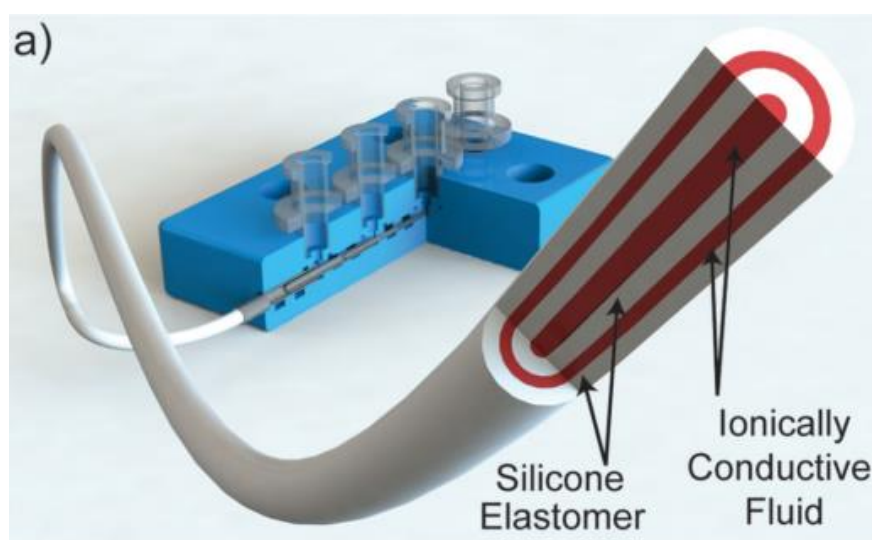


Figure 2-20 Capacitive soft strain sensors with ionic hydrogel [128]. The ionically conductive and silicone elastomer layers are fabricated simultaneously to form a strain sensor.

Larson *et al.* [129] presented a highly stretchable tactile sensor using pure elastomer structures, as shown in Figure 2-21. The conductive layer was fabricated by PAM-LiCl hydrogel as electrodes, while a silicone-based elastomer was used as a dielectric layer. Tactile sensing was achieved by capacitive variation when pressure was applied to the elastomers. In this research, the dielectric elastomer layer mixed with ZnS also provided a novel method for optical signalling. This research also showed the potential application of soft tactile sensors on soft actuators by testing capacitance change of sensor with pneumatic actuation of the soft actuator.

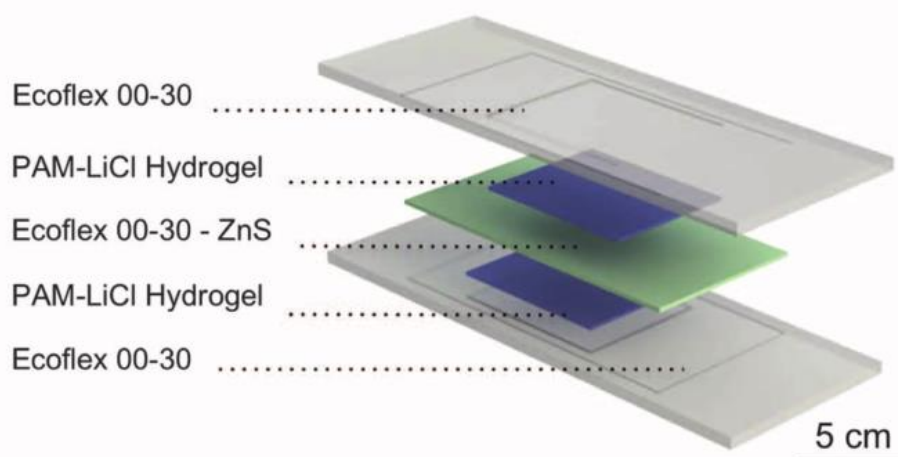


Figure 2-21 Highly stretchable tactile sensors using pure elastomeric structures [129]. The capacitive stress sensor consists of two encapsulation layers, two conductive layers and a laminating layer.

In 2014, Sun *et al.* presented an ionic skin by creating a soft conductive hydrogel consisting of a dielectric elastomer [47]. The sensor was reported as a stretchable, large-area sheet of the distributed sensor. Larson *et al.* [129] presented a highly stretchable tactile sensor using pure elastomer structures of hydrogel and silicone elastomer. PAM-LiCl hydrogels were used as two conductive layers, sandwiching a dielectric light-emitting layer in the middle to form a hyper-elastic light-emitting capacitor sensitive to applied pressure.

## 2.4 Process of Soft Materials

Functional soft materials are usually groups of polymer materials with high elasticity and strength. These functional soft materials are widely used as substrates of soft sensors or mixtures with conductive dopants to form soft sensors [125, 130, 131].

Among those functional soft materials, this research focuses on the process of polydimethylsiloxane (PDMS) and silicone rubber for their stretchability, softness, moulding ability and hydrophobic surface. They are widely applied as functional soft

---

materials in micro-electromechanical devices [132-134], soft sensors [135-137], microfluidic devices [138-140].

### **2.4.1 Polymerisation of soft materials**

Fabrication methods of soft materials largely depend on the polymerisation of those materials. Standard initiation methods for polymerisation are heat, ultraviolet and catalytic agent.

Heat is usually applied to silicone-based soft elastomer polymerisation such as EcoFlex and PDMS. The heat used in the elastomer cure has a significant effect on the curing speed, mechanical strength, and stiffness [141, 142].

The polymerisation of PDMS is initiated by Pt catalyst and accelerated by heat [143]. For example, one of the commercial PDMS, Sylgard<sup>®</sup>184 polydimethylsiloxane (PDMS) elastomer, is prepared in two parts. Part A, the base, contains dimethylsiloxane and Si-vinyl-siloxane (0.68 mol%) [144], and Pt catalyst [145]. Part B, the curing agent, contains a large amount of Si-H bonds [144]. The reaction of the two parts is shown in Figure 2-22.

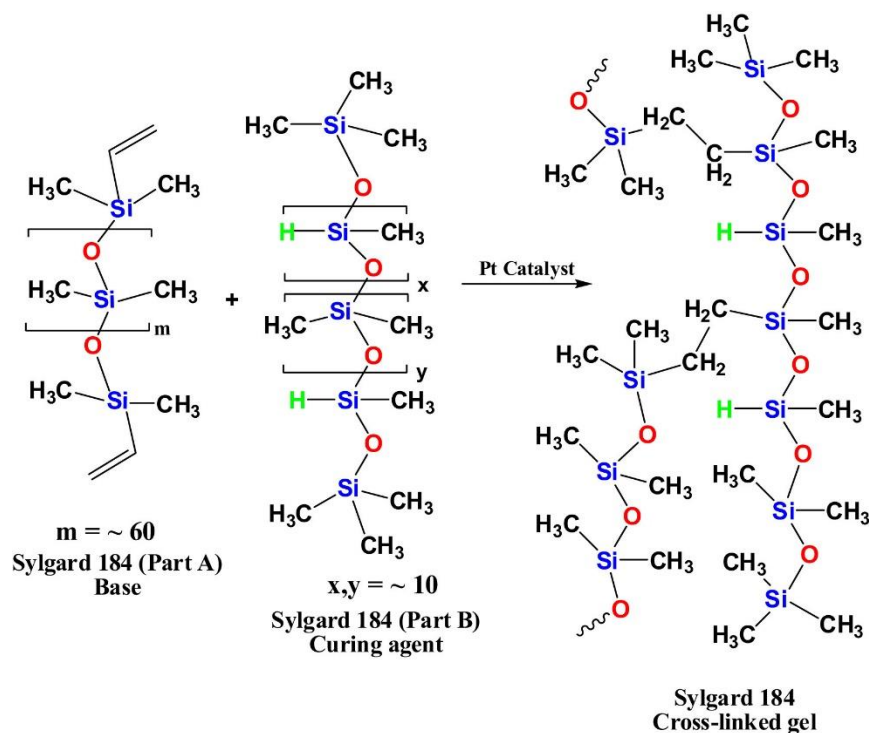


Figure 2-22 Polymerisation of PDMS [143]. The dimethyl-siloxane and Si-vinyl-siloxane react with Si-H bonds over Pt Catalysts to form PDMS.

The different temperature of heat affects the final product of PDMS. At low temperature ( $<300^{\circ}\text{C}$ ), the heat accelerates the cure of PDMS pre-mix gel while the air bubble is formed in PDMS due to a lack of time for the air to escape [146]. In this condition, a vacuum heat casting is required to reduce unnecessary air void in PDMS [147, 148]. At high temperatures ( $300^{\circ}\text{C}$ - $900^{\circ}\text{C}$ ), the PDMS pre-mix gel starts to lose weight mainly due to the loss of  $\text{H}_2\text{O}$  and  $\text{H}_2$ , resulting in a hard-ceramic PDMS product instead of a PDMS soft elastomer [149].

Ultraviolet radiation is emerging used in curing silicone rubber or pre-curing of heat curing silicone rubber [150]. In 2013, Xue *et al.* [151] presented a UV-curing silicone rubber prepared via thiol-ene reaction, as shown in Figure 2-23. High-molecular-weight polydimethylsiloxane containing vinyl groups as the gum, polymer-captopropylmethyl-siloxane as a crosslinker, TS-530  $\text{SiO}_2$  as reinforcing filler and 2,2-dimethoxy-2-phenylacetophenone as a photoinitiator. This UV-curing silicone rubber

presented good mechanical properties and excellent thermal stabilities and proved a silicone rubber curing system without heavy metal catalysts and high temperature.

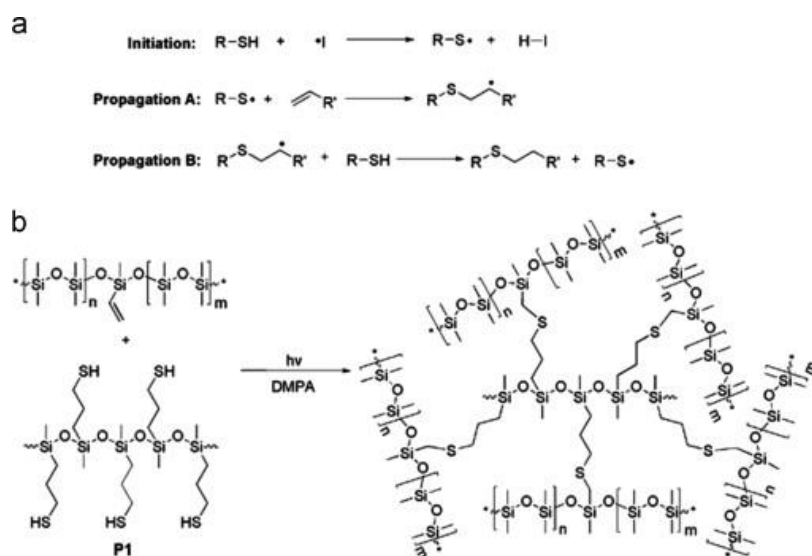
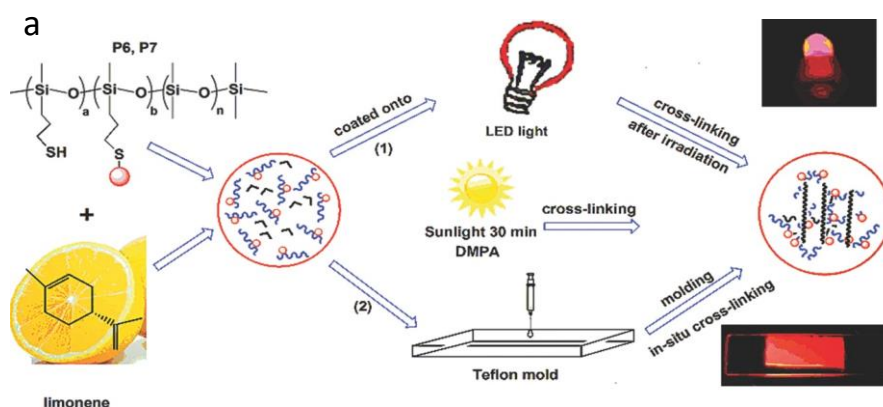


Figure 2-23 Reaction of UV crosslink silicone rubber [151]. High-molecular-weight polydimethylsiloxane containing vinyl groups as the gum, polymer-captopropylmethyl-siloxane as a crosslinker, TS-530 SiO<sub>2</sub> as reinforcing filler and 2,2-dimethoxy-2-phenylacetophenone as a photoinitiator.

The UV radiation curing methods enabled silicone rubber to be applied to luminescent films [152], superhydrophobic surface coating [153], and silicone-based gels [154, 155], as shown in Figure 2-24.



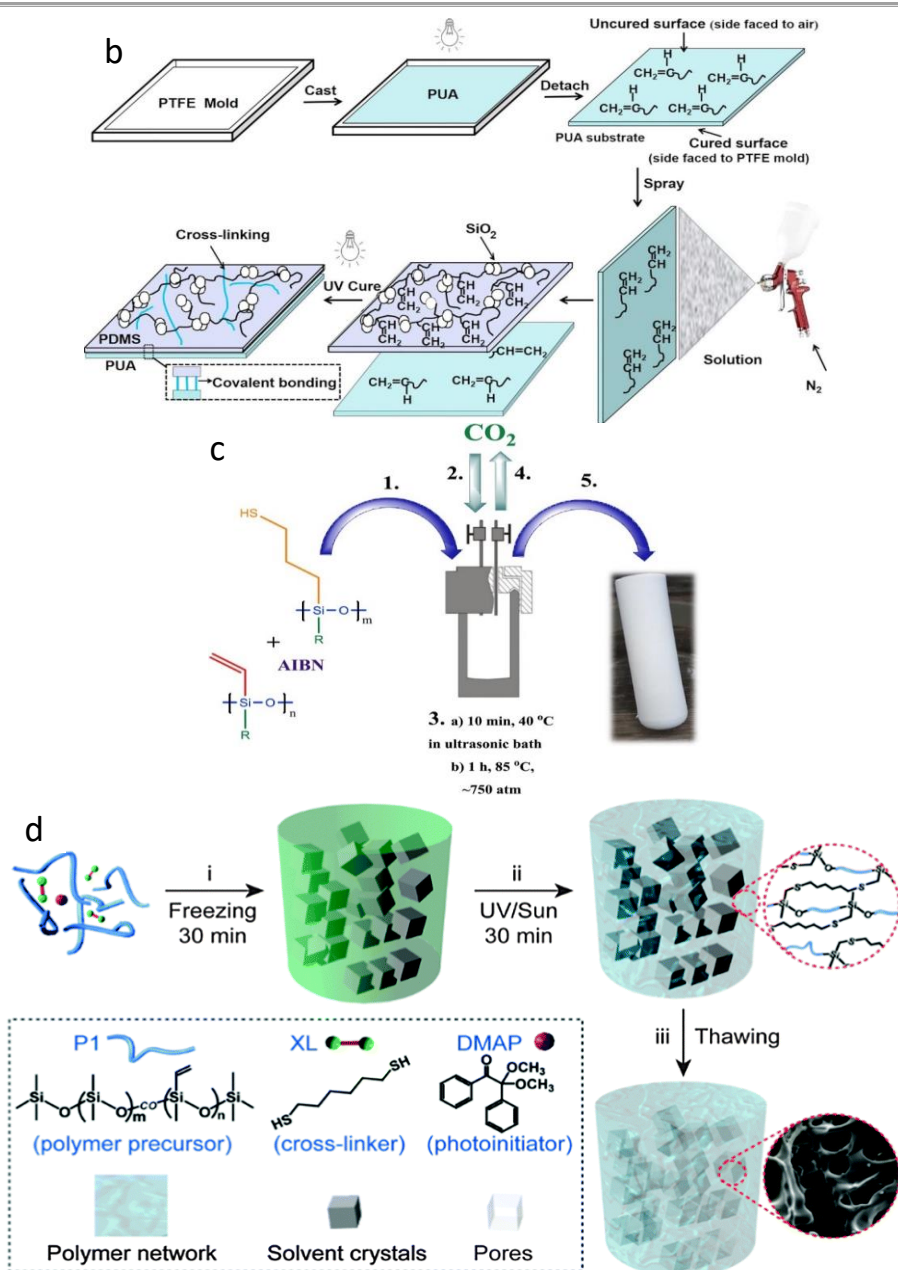


Figure 2-24 Application of UV-crosslinked silicone rubber. a) Sunlight-induced cross-linked luminescent films by UV crosslinked silicone rubber [152]. b) Superhydrophobic surface by UV cross-linking of coating onto oxygen-inhibited layer of substrate [153]. c) Flexible superhydrophobic aerogels [154]. d) Macroporous silicone-based cryogels [155].

The UV curing silicone rubber also benefits the additive manufacture or 3D print of silicone rubber [156-159]. The silicone rubber can be cured rapidly and form various structures with smooth surfaces and good accuracy. For example, Xiang [160] *et al.* presented a UV-curable, 3D printable and biocompatible silicone elastomer in

2019. The silicone elastomer was UV crosslinked via thiol-ene photo-polymerisation and formed a complex structure in 3D print, as shown in Figure 2-25.

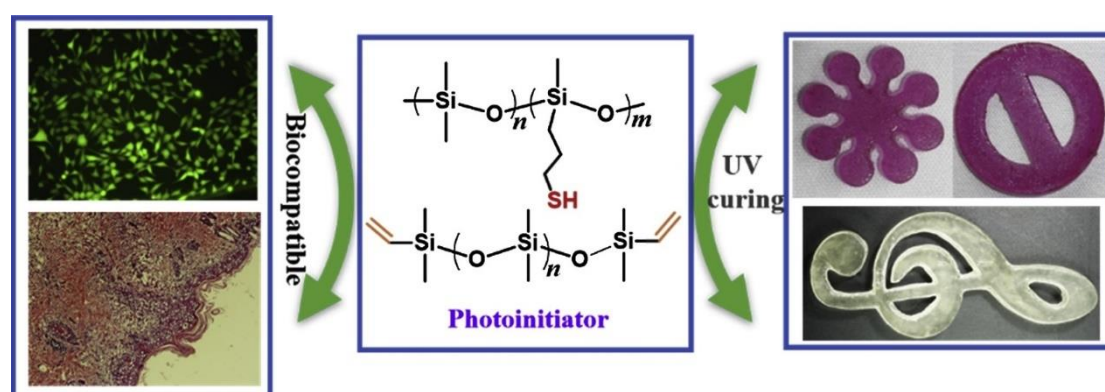


Figure 2-25 3D printable silicone elastomers [160]. The silicone elastomer was UV crosslinked via thiol-ene photo-polymerisation and formed a complex structure in 3D print.

## 2.4.2 Bond between different soft materials

In soft sensor applications, the materials are often required with various features in addition to softness and stretchability, such as durability, electrical conductivity, manufacturability and biocompatibility. Those features are not included in one single soft material, so integrations of soft materials are sometimes used in one soft sensor for its goal. For example, ionic hydrogels have good electrical conductivity but are easy to dehydrate to fail in function. At the same time, silicone rubbers own good hydrophobicity to prevent water evaporation within enclosed structures. Combining ionic hydrogels and silicone rubbers enable multiple features for soft sensors. Therefore, investigation of the bond between different soft materials is needed for soft sensor applications.

The bond between different soft materials is conducted by physical interactions and chemical bonds [161].

For physical interactions, closely attachment between two soft materials increases the van der Waals interactions, as shown in Figure 2-26. The interactions between PDMS and hydrogels are weak because of the hydrophobicity of PDMS. Oxygen plasma or ozone treatment converts the  $-CH_3$  groups in PDMS into  $-OH$  groups and forms a hydrophilic surface on the PDMS. The hydrogels are then promoted to attach to the PDMS for a strong bond [162, 163]. However, the bond is temperate, and its strength decreases as the hydrophilicity of the PDMS surface degrades [164].

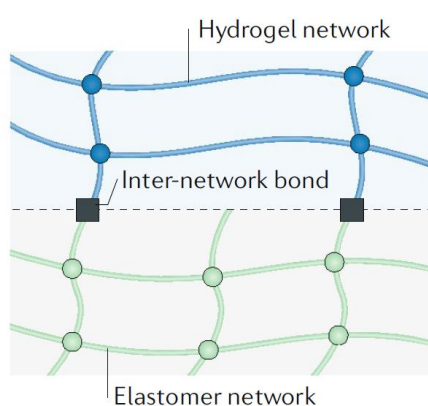


Figure 2-26 Physical interactions between hydrogels and elastomers [165]. The hydrogel network and elastomer network are tangled together as an inter-network bond.

Chemical bonds between soft materials are reported with a higher strength and durability [166]. For example, benzophenone is applied as a photo-initiator to anchor hydrogels onto various elastomeric soft materials [167, 168]. Performed elastomers such as PDMS are modified by benzophenone, and then hydrogel pre-solution is formed on the modified surface of elastomers to form tough chemical bonds. Silanes are also used as adhesion agents between soft materials [169]. Silanes can form covalent bonds to various materials. A silane crosslinked network adds strong adhesion to bond two different soft materials together.

The bond between hydrogel and PDMS stimulated the applications in flexible electronics, soft sensors and bioelectronics [170]. For example, Oh *et al.* presented a self-healing deformable electronic device using PEDOT:PSS coated on PDMS [171].

A demonstration case of foldable and stretchable LEDs showed high deformation based on the bond between two elastomeric materials. Lipomi *et al.* also presented research on the bond of PEDOT:PSS and PDMS [172]. A transparent conductive film was fabricated for the applications in organic solar cells and transparent pressure sensors, as shown in Figure 2-27.

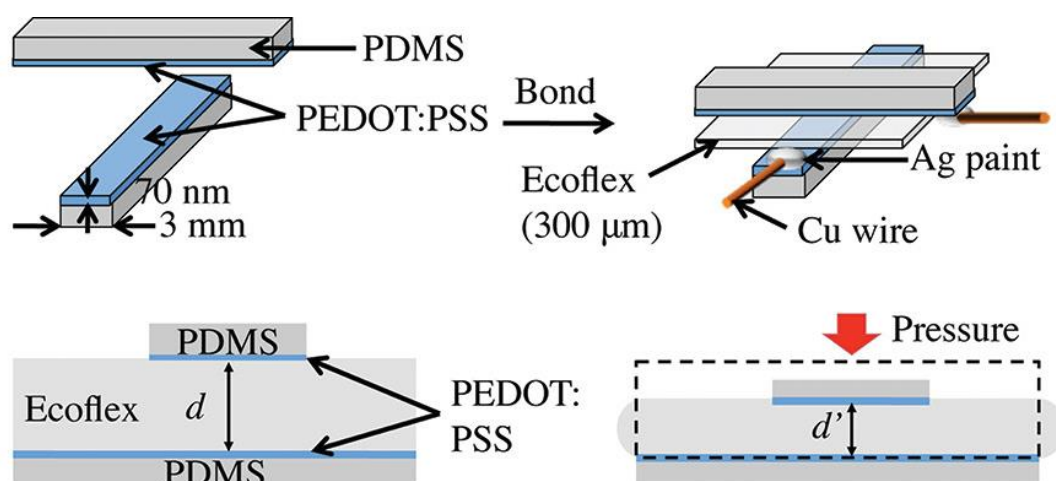


Figure 2-27 Transparent, compressible pressure sensors made of PEDOT:PSS coated on PDMS [172]. The PEDOT:PSS is bonded on the plasma-treated PDMS layer as a hybrid. Two hybrids sandwiched an Ecoflex layer to act as a capacitive pressure sensor.

In 2017, Liu *et al.* presented stretchable living materials and devices with hydrogel–elastomer hybrids [173]. The hydrogel was chemically bonded with PDMS elastomer, enabling the hybrid's large strength, as shown in Figure 2-28. The sensors were responsive to multiple chemicals and can be applied as chemical sensors in the form of skin patches and gloves-based sensors.

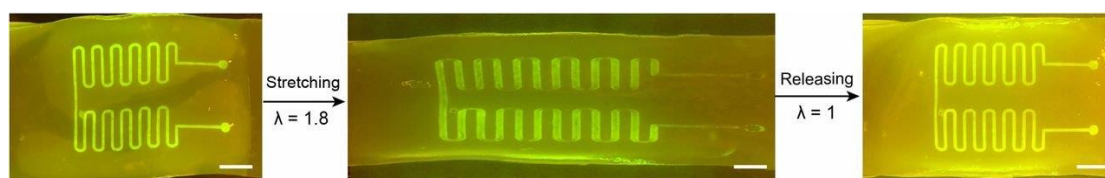


Figure 2-28 Highly stretchable Functional living device [173]. Hydrogels were encapsulated in the PDMS, and the encapsulated cell remained functional after large deformation.

---

## 2.5 Key findings and summary

In this literature review, the state-of-the-art research on soft robotics and soft sensors are reviewed. The reviews start with the importance of developing soft robotics over conventional robots, addressing that soft robotics advanced in safe and comfortable interaction with humans, flexible and complex actions in a wide range of different environments. Then the reviews focus on the necessary components of soft robotics, which is soft sensors. This part expands the design, material, fabrication, and application of soft sensors to an in-depth review of the recent development and future direction of soft sensors. The detailed review in this chapter enlightens current achievements and possible gaps in soft sensors.

The gap in the application of soft sensors in soft robots is that existing soft sensors lack high-performance materials and adaptive design. For soft sensors, this chapter firstly reviews the soft magnetic field sensors, which are limited in requiring magnetic components for sensing. Then the focus is on the soft capacitive sensors, which are constrained in adding extra dielectric layers.

In addition to the design of soft sensors, current soft materials are examined to compare their advantages and disadvantages for application to soft sensors. Conductive carbon-based materials, ionic conductive hydrogels and liquid conductors are reviewed to address their characteristics. Considering the advantages of hydrogels in terms of biocompatibility, mechanical and electrical properties, hydrogels were selected as promising representative materials for further review of materials, fabrication methods and aspects of soft sensors based on conductive hydrogels.

The focus is locked on the manufacturing and strengthening methods for soft materials in order to propose a capable soft sensor. The review has found there are two

---

primary goals in capable soft materials. On the one hand, researchers are trying to improve electrical performance, which contributes to the high sensitivity of sensor applications. On the other hand, mechanical properties such as stiffness, stretchability are essential for soft sensors. At the same time, conflicts between good electrical properties and mechanical properties are obstructing the development of soft sensors. Toning a good balance of those two perspectives has been the main topic in the research on soft materials.

Specifically, the research on polymerisation of soft materials is investigated, including silicone-based polymer and hydrogels in aspects of the mechanism of polymerisation and variation of polymerisation. Then, the bond mechanism between silicone-based polymer and hydrogels is surveyed to strengthen the hydrogels by encapsulating them and reducing their water loss.

And the finds of literature reviews determine that this thesis will focus on the following aspects,

- 1) To propose a soft sensor that is highly stretchable, elastomeric and sensitive,
- 2) To understand the mechanical and electrical properties of the conductive hydrogels,
- 3) To develop the techniques to modify the mechanical and electrical properties of conductive hydrogel for the aimed soft sensor,
- 4) To design, evaluate and demonstrate a fully elastomeric soft sensor,
- 5) To extend the application of the fully elastomeric soft sensor.

# **Chapter 3**

## **Requirements, Concept and Approach**

Fully elastomeric soft sensors are sensors made of fully elastomeric soft materials to measure force and position, such as tensile or compressive stress, and tactile stimuli in large deformation. In order to present a fully elastomeric soft sensor, this chapter defines the requirements of the target sensor in aspects of mechanical and electrical properties. The concept of a fully elastomeric soft sensor is also presented, including design, materials and applications. At last, the approach to the fully elastomeric soft sensor is described via fabrication and validation methods.

## 3.1 Requirements

Fully elastomeric soft sensors are to tackle the problems existing sensors cannot measure under complex interaction, especially for soft robots with flexible motions and human joint movement. Corresponding to those aims, the sensor is first required to be a mechanically and visually comfortable sensor as it is potentially installed on human skin. Then it is necessary to have low stiffness and high compliance to adapt to the compression or stress in the measurement. High elasticity and stretchability are also needed in case of large deformation of the sensors. As for sensing, the sensitivity of the sensor is also important to obtain a precise measurement. And durability is also considered for applications of sensors. The consideration of fully elastomeric soft sensors has been summarised within Requirement 1 to Requirement 4.

**Requirement 1** – Low modulus and optical clearance

*Design a small-size sensor suitable for being installed on skin with low modulus for mechanical comfort and high optical clearance for minimum visual obstruction.*

**Requirement 2** – High mechanical performance

*Fabricate a soft sensor with low stiffness, high compliance, high elasticity and stretchability.*

**Requirement 3** – High sensitivity

*To ensure sensitivity, the sensor should have a large electrical resistance change responding to deformation.*

**Requirement 4** – Durability

*Considering durability, the sensor must have strong bonding between different layers and a strong ability of water retention as an ionic conductor.*

According to the above requirements, related parameters are designed and listed in Table 3-1.

Table 3-1 Parameters of fully elastomeric sensors

<b>Items</b>	<b>Parameters</b>
Dimensions	20mm×8mm×1.8mm
Appearance	Optical clear
Modulus	<10kPa
Tensile strain	>300%
Electrical conductivity	>0.95S/m
Weight loss	<1%/day

## 3.2 Concept

A fully elastomeric soft sensor consists of two parts, the conductive layer and the substrate layer. Both the conductive layer and substrate layer are elastomeric and highly stretchable. The conductive layer used in this research is made of conductive transparent hydrogels filled in with the ionic liquid. At the same time, the substrate layer is made of casting PDMS rubber. The conductive layer is bonded with the substrate layer or encapsulated within the substrate layer. The general structures of fully elastomeric soft sensors are shown in Figure 3-1.

Fully elastomeric soft sensors will be prototyped as a single sensor device for soft robots or humans. For soft robots, proposed sensors can monitor their expansion and formation by strain sensing. The proposed soft sensor will also be served as a tactile sensor for the soft actuator to detect contacting force and normal stress. Besides, the proposed soft sensor can work as a wearable sensor for humans, such as joint movement monitoring, voice monitoring, breath and heartbeat monitoring. Soft sensors can also

detect stress on fingers, palms, and soles, enabling virtual haptics and particular medical usage. The potential applications of fully elastomeric soft sensors are shown in Figure 3-1 and their specific requirements are listed in Table 3-2.

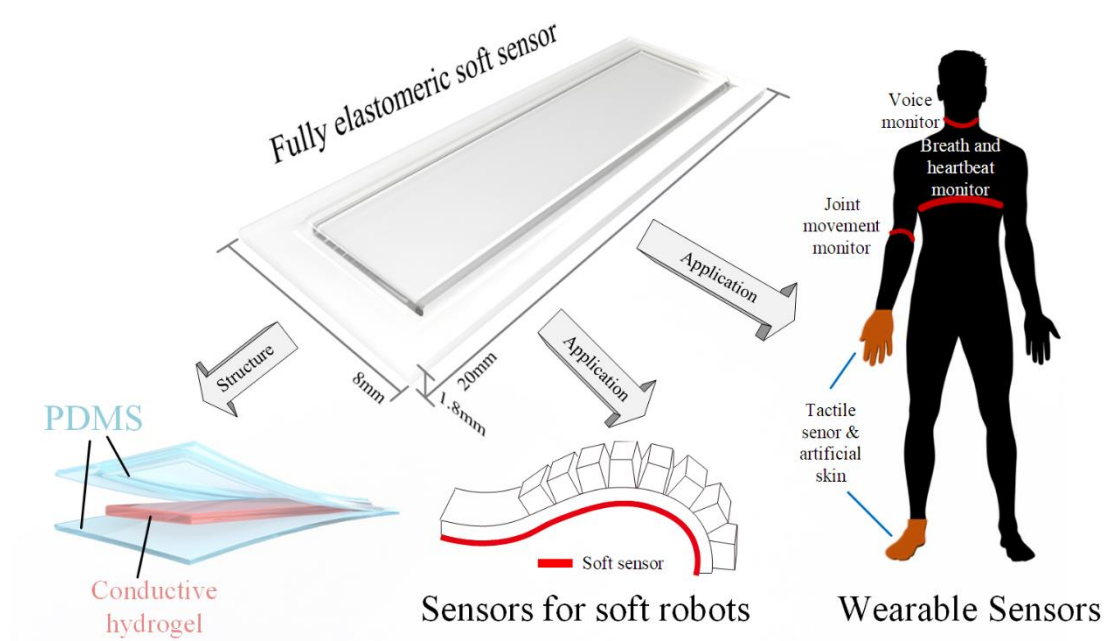


Figure 3-1 Conceptual design and applications for fully elastomeric soft sensors. The conductive hydrogel is encapsulated or engraved in PDMS as a soft sensor. The proposed soft sensor is applied on soft robots and human skin for motion sensing.

Table 3-2 Requirements of different soft sensors

Sensor type	Requirements
Soft strain sensors for soft robot	Flexible, less stiff than silicone rubber, light weighted
Human movement (joint movement, breath and heartbeat, vocal cords) monitor sensors	Non-destructive (soft and optical clear), biocompatible, durable, water-resistance, largely stretchable
Tactile sensor for artificial skin	Sensitive, non-destructive (soft and optical clear), compliant, biocompatible, tough, durable, water-resistance

### 3.3 Approach

To achieve the concept of the fully elastomeric sensor, the UV-initiating fabrication methods are applied for the hydrogel and the hydrogel-elastomer hybrid. Conductive hydrogel is used and optimised for specific sensor design by adjusting the components and concentration of hydrogel ingredients. The hydrogel and PDMS are bonded as a hybrid through surface modification and chemical reaction. The fabrication process of hydrogel-PDMS is researched, aiming to produce high-class and durable samples, improve the success rate and simplify the procedures. The fabrication methods are shown in Figure 3-2 (a).

The validation of proposed soft sensors is conducted by a test configuration for tensile and compressive tests. The test configuration records the mechanical and electrical properties of samples simultaneously to validate the sensors on both sides. A peeling test is also conducted to test the bond strength of the hydrogel-elastomer hybrid. Furthermore, the water loss test is implemented to verify the ability for water retention of the hydrogel-elastomer hybrid. All data is synchronised to a PC for further postprocessing. The testing methods are shown in Figure 3-2 (b).

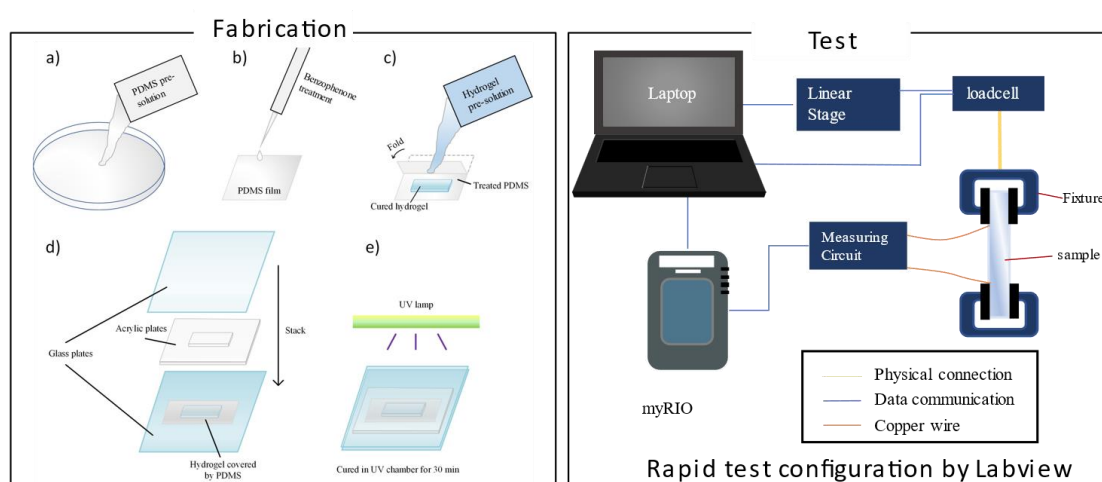


Figure 3-2 Fabrication methods and test methods for fully elastomeric soft sensors. a) The sensor is fabricated by UV-initiating hydrogel and hydrogel-PDMS bonding. b) The sensor is tested by a linear stage and real-time data acquiring device.

---

## 3.4 Summary

This chapter addressed the idea of fully elastomeric soft sensors. It began with the requirements of the proposed sensor relating to the aspects of appearance, mechanical and electrical properties. The concept was then proposed based on the Requirements. A qualified sensor design and its related applications were figured out. The sensor design had fulfilled Requirement 1 to have a mechanically and visually comfortable form. And the approaches to the proposed sensor was finally presented in material manufacturing, sensor fabrication and validation to meet Requirement 2 to Requirement 4.

The selected conductive hydrogel satisfied Requirement 2 and Requirement 3 in both mechanical and electrical performance. The development of UV-initiating conductive hydrogel techniques will be presented in Chapter 4.

The fabrication of the hydrogel-PDMS hybrid had guaranteed the durability of a strong bond and high water retention to meet Requirement 4. Chapter 5 will indicate the specific methods of fabricating hydrogel-PDMS hybrid and soft sensors based on the hybrid.

# **Chapter 4**

## **Ultraviolet Cross-link Hydrogels for Soft Sensors: Fabrication and Characterisation**

This chapter investigates a UV cross-link fabrication method for conductive polyacrylamide hydrogel. A polymerised hydrogel network by acrylamide and N, N-methylenebisacrylamide was created. NaCl solution is used as an ionic conductor to fill in hydrogels to enable their electrical conductivity. The hydrogel is firstly made by a basic formulation, and then the concentration of primary materials, including acrylamide, N, N-methylenebisacrylamide, Irgacure 2959, NaCl and UV exposure time are altered to test the influence of each component material. The hydrogels are characterised by mechanical property and electrical property.

## 4.1 Fabrication Method

### 4.1.1 Fabrication of hydrogels

This hydrogel fabrication method is processed based on a UV-polymerised acrylamide-bisacrylamide system. The hydrogel was synthesised using acrylamide (AAm; Sigma, A8887) as monomers. N, N-methylenebisacrylamide (MBAA; Sigma, M7279) as crosslinkers. 2-Hydroxy-4'-(2-hydroxyethoxy)-2-methylpropiophenone (Irgacure 2959; Sigma, 410896) was used to initialise the UV polymerisation under a wavelength of 365nm. Sodium chloride was added to the solution as an ionic conductor to obtain electrical conductivity. The fabrication process is presented in Figure 4-1.

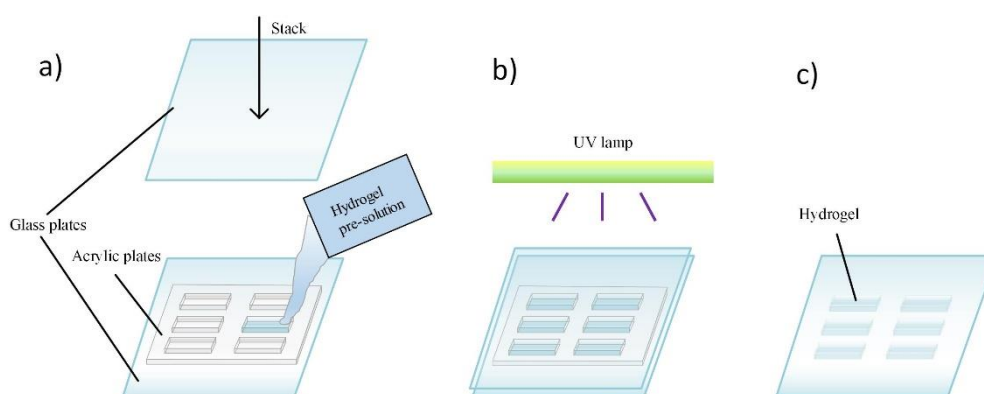


Figure 4-1 Fabrication process of UV-cured hydrogels. a) Hydrogel pre-solution is injected into the acrylic mould sandwiched between two glass plates. b) The mould is transferred into a UV chamber and exposed under 365nm UV. c) The glass and acrylic mould are removed to collect solid hydrogel after UV exposure.

The preparation of acrylamide-bisacrylamide solution is presented in the following order. AAm and NaCl were dissolved in deionised water, with AAm fixed at 2.2 M and NaCl fixed at 2.7 M. Add MBAA by 0.0006 weight of AAm. Add Irgacure 2959 by the ratio of 0.1%w/v into the solution. The solution was then stirred by a magnetic stirrer at room temperature (around 20 C°) for 5 min. Degas the solution in a

vacuum chamber for 10 min. The solution was poured into a mould, and the gels were cured using an ultraviolet light chamber of 365 nm wavelength at a constant power of 8 W for 90 minutes.

The mould for hydrogel consists of two optic clear glass plates sandwiching a clear acrylic frame. The transparent mould allows UV light to irradiate on hydrogel solution with maximum efficiency. The acrylic frame is cut by laser as a set of six triangle shapes with the same inner dimension of  $4 \times 10 \times 1$  mm each. The triangle shape was selected as it was a standard sample pattern for tensile test. The acrylic frame is laid on one of the glass plates and filled up with hydrogel solution. The surface tension of hydrogel solution drops remains inside the acrylic frame without leaking from the acrylic frame and glass plate. Then another glass plate is covered on the acrylic frame, squeezing surplus hydrogel out of the acrylic frame. The sandwiched mould then forms a closed mould fulfilling hydrogel solution. The cured hydrogel was then put into salted water with the same concentration at room temperature overnight to ensure the hydrogel fully absorbed the ionic conductor. The size of the sample will increase nearly two times to  $7.8 \times 18 \times 1.8$  mm.

### **4.1.2 Variation of formulations**

The ratio of monomers, crosslinkers and initiators and radiation time influences the final products of hydrogels in terms of stretchability and stiffness. As monomers and crosslinkers, the concentration of acrylamide and MBAA may affect the density of the polymer network and the strength of polymers, which further affects the stiffness and stretchability of polymers [47, 48, 125, 126]. As initiators, the concentration of Irgacure 2959 may affect the polymerization speed and may cause incomplete polymerization to lower the stiffness and stretchability [181]. The UV dose may also affect the strength and stiffness of final product of polyacrylamide hydrogels [181]. The saturation of NaCl

may affect the electrical conductivity of ionic hydrogels as NaCl is the ionic conductor in the conductive hydrogels. A set of hydrogels with different concentrations of substances mentioned above were prepared to explore their mechanical and electrical properties, as shown in Table 4-1. Variations of their concentration were based on existing research [47] (1.1M Acrylamide, 0.0006 MBAA/Acrylamide, 16% w/v NaCl, Ammonium Persulfate based heating polymerisation).

Table 4-1 Variation of fabrication methods

Formulations	Acrylamide	MBAA	NaCl	Irgacure 2959	UV exposure
<b>Baseline</b>	<b>1.1 M</b>	<b>0.0006</b>	<b>16% w/v</b>	<b>0.1% w/v</b>	<b>90 min</b>
Variable 1	0.6 M				
Variable 2	1.6 M				
Variable 3		0.0003			
Variable 4		0.0009			
Variable 5			8% w/v		
Variable 6			24% w/v		
Variable 7				0.04% w/v	
Variable 8				0.16% w/v	
Variable 9					120 min
Variable 10					150 min

## 4.2 Characterisation

To apply the presented conductive hydrogel as a strain sensor, the author tested the proposed conductive hydrogels and their variable formulations in mechanical and electrical properties simultaneously. The hydrogel samples were pulled to fracture for each test. Tensile stress and strain were recorded as the main characteristics of mechanical properties as it was required high stretchability and low stiffness in soft strain sensor application. Electrical resistance was recorded in the test for the electrical

---

property as its change over strain was crucial for strain sensing. All the variations of formulations were tested to characterise the influence of every substance on the mechanical and electrical properties of proposed hydrogels.

### **4.2.1 Tensile test and data acquisition configuration**

Test configurations are shown in Figure 4-2. Testing hydrogel samples are stored in 16% w/v NaCl solution for 24 hours before the test. All the samples are installed and tested within 2 mins to minimize the influence of hydrogel dehydration. An INSTRON 5943 (Instron, Norwood, MA, USA) universal testing system is used for a tensile test at a moving speed of 0.5mm/s until the hydrogel was broken down. Pulling force was obtained by a 50N loadcell and recorded at a sampling rate of 500 Hz. Two pairs of clamps installed on pneumatic grips (2712-05x, Instron, Norwood, MA, USA) are designed for holding hydrogel. On the one hand, hydrogels are easy to tear by the sharp edge; on the other hand, hydrogels are slippery and hard to clamp. In this case, double-sided foam tapes are stacked on a metal clamp to cover the hard edge of the metal clamp and increase friction to the hydrogel. The effective sample size of hydrogel, from the edge of the upper pair of clamps to the edge of the lower pair of clamps, is 8×20×1.8 mm.

In order to measure the electrical resistance of hydrogel during the tensile test, a copper foil is stacked on one side of the clamp. Copper foil is curved and rounded at the edge of the clamp to avoid sharp edges to protect hydrogels. Figure 4-2(a) shows the mechanical and electrical characterisation test configuration. As shown in Figure 4-2(b), the electrical resistance of hydrogel was measured between the edge of the upper pair of clamps and the edge of the lower pair of clamps. Wires were welded on the copper foil and connected to a measuring circuit shown in Figure 4-2(c). The analogy

measurement was recorded by a myRIO using its build-in ADC (0-5 V, 12-bit). Data was synchronised to the force data from INSTRON 5943 at 500 Hz.

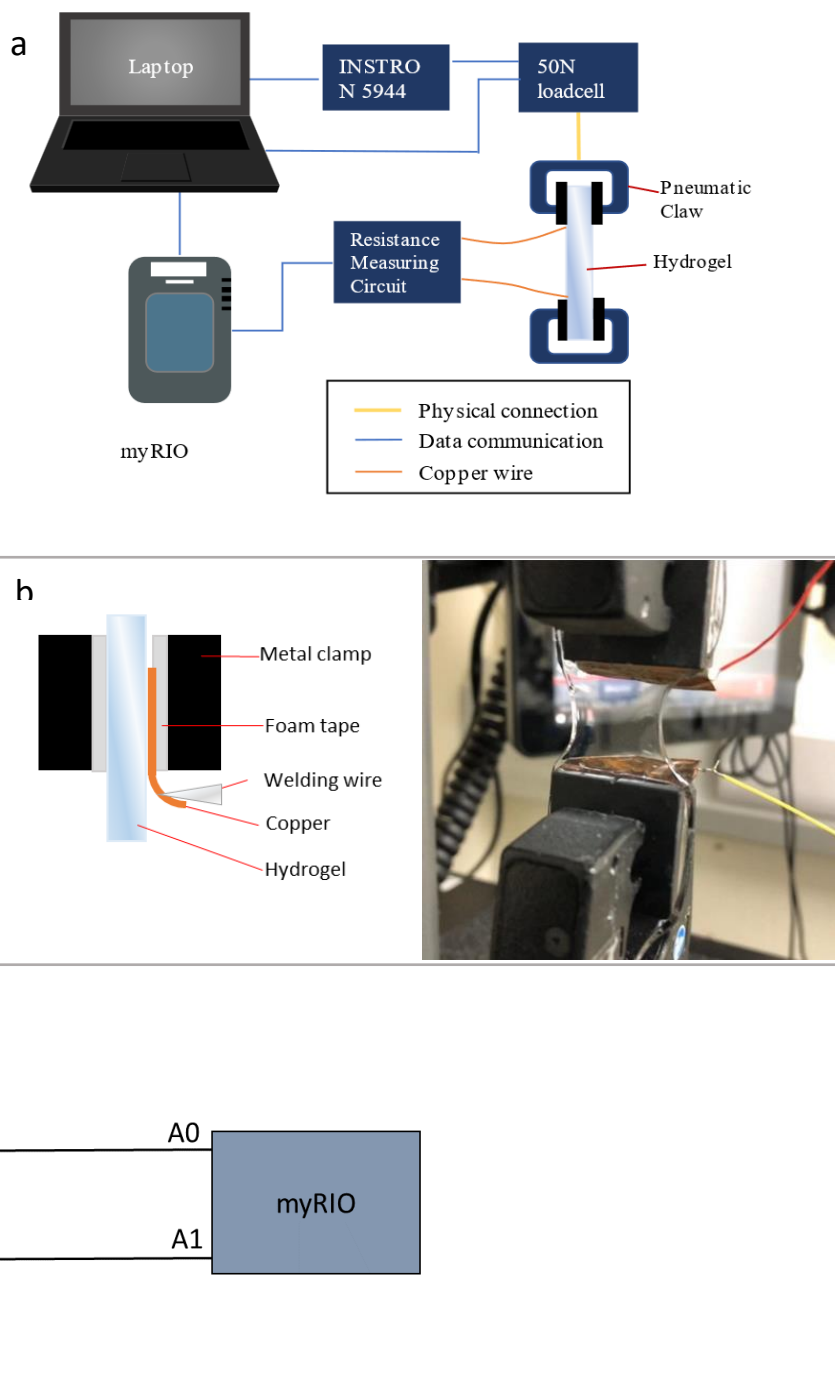


Figure 4-2 Experiment setting for hydrogels properties. (a) Overall test configuration for mechanical and electrical characterisation. (b) Clamps for hydrogel fixing. (c) Voltage divider circuit for resistance measurement

Figure 4-2(c) illustrates the circuit applied to the resistance measurement of the conductive hydrogel for tensile testing. A voltage divider is used in the circuit. The conductive hydrogel with changing resistance is connected to a known resistor in series by measuring the voltage of the power supply and the voltage on the hydrogel. The resistance of the tested hydrogel is solved as Equation (4-1).  $V_{cc}$  stands for the supply of voltage 5V provided by the myRIO 5V pin.  $R_x$  represents the conductive hydrogel with changing resistance. During the tensile test, the resistance of the conductive hydrogel is rising. On the two ends of the conductive hydrogel, the circuit is connected to the analogue input pins of the myRIO with 12 bits resolution ADC (0-5V, 1.221 mV step). A known resistor of 2 k $\Omega$  is connected to the conductive hydrogel in series and is grounded on the other side. A 2 k $\Omega$  resistor is selected as  $R_1$ , which is close to the mid-range of the changing resistance of the conductive hydrogel in the tensile test.

$$R_x = \frac{R_1(V_{cc} - V_1)}{V_{cc}} \quad (4 - 1)$$

where  $R_1$  is the resistance of divider resistor,  $V_{cc}$  is the supply voltage,  $V_1$  is the measured voltage of  $R_1$ ,  $R_x$  is the resistance of the conductive hydrogel sample.

## **4.2.2 Results of tensile test on electrical and mechanical properties of conductive hydrogels**

In the tensile test of the conductive hydrogels, the pulling force applied to the samples is recorded. The displacement and running time of the tensile test are also recorded. The electrical resistance changes of conductive hydrogel in the tensile test are also recorded. As five variants of the formulation of the conductive hydrogel are controlled, the results are presented in five groups.

## Concentration of acrylamide

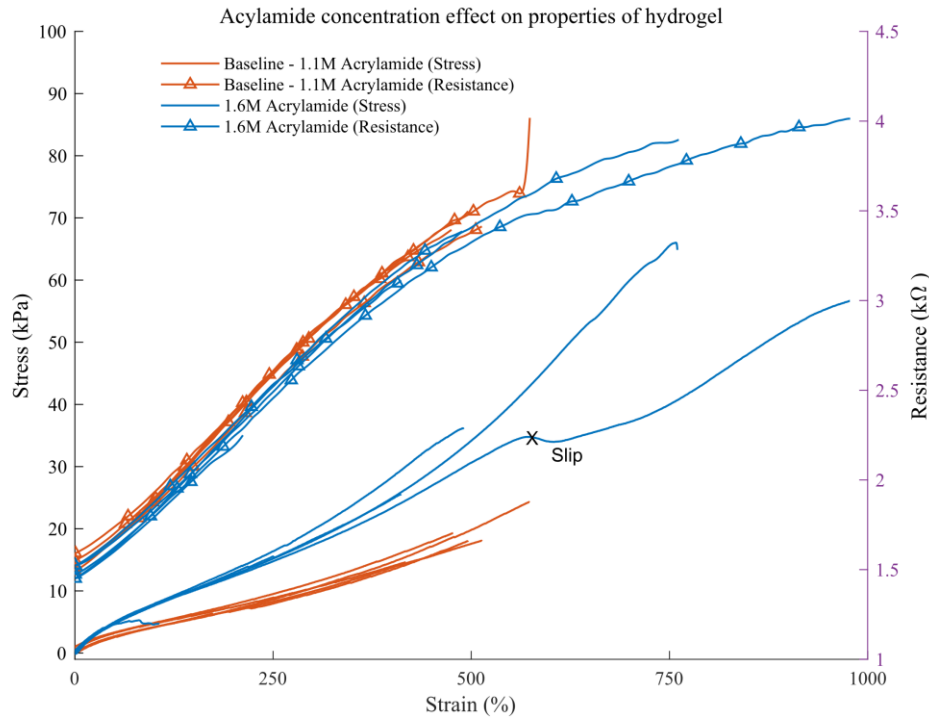


Figure 4-3 The tensile test results for the conductive hydrogels in different concentrations of acrylamide. The concentration of acrylamide varied from 1.1M to 1.6M. Both electrical resistance and mechanical stress increase as the strain of tested hydrogel samples increases in different concentrations of acrylamide.

Figure 4-3 shows the results of the tensile strain test in different concentrations of acrylamide. As the concentration of acrylamide increased, the stiffness of hydrogels increased. The stress  $\sigma$  was obtained by,

$$\sigma = \frac{F}{A} \quad (4 - 2)$$

where  $F$  is the force measured by the INSTRON test bench and  $A$  is the section area of the sample calculated by measured width and thickness.

The strain  $\varepsilon$  was obtained by,

$$\varepsilon = \frac{\Delta L}{L_0} \quad (4 - 3)$$

---

where  $\Delta L$  is the changing length of the sample recorded by the INSTRON bench during the tensile tests.  $L_0$  is the initial length of the sample.

As the stress gain was not strictly linear to strain gain, a fitted overall modulus  $K$  was defined by the slope of strain  $\sigma$  and stress  $\varepsilon$  to quantify the stiffness of different hydrogels.

$$K = \frac{\sigma}{\varepsilon} \quad (4 - 4)$$

As the acrylamide concentration went up from 1.1M to 1.6M, the average modulus  $K$  increased from 3.42 KPa to 5.99 KPa.

For electrical resistance, initial resistance and the changing rate of resistance were presented in the results.

At the beginning of the tensile test, the initial resistance was recorded by the myRIO through the attached measurement circuit. The upper and lower clamps that clipped hydrogels were kept at the same distance with measuring electrodes. In this condition, the average initial resistance decreased from 1.64 k $\Omega$  to 1.49 k $\Omega$ , where the initial length of hydrogels was constant at 20 mm.

In the 0.6M acrylamide concentration group, samples failed to cure in the same concentration of MBAA, NaCl, Irgacure and UV dose.

## Concentration of MBAA

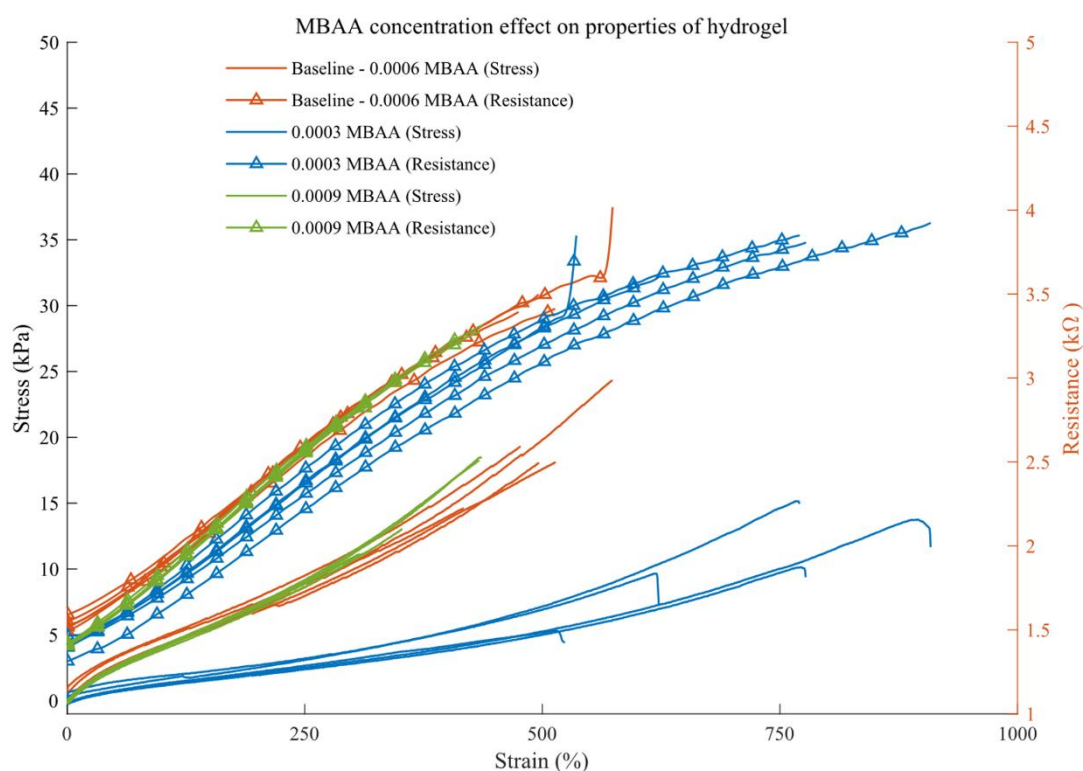


Figure 4-4 The tensile test results for the conductive hydrogels in different concentrations of MBAA. The concentration of MBAA varied from 0.0003 to 0.0009 weight of acrylamide and mainly affected the mechanical stress of tested hydrogel samples.

Figure 4-4 shows the results of mechanical stiffness and electrical resistance results of proposed hydrogels tensile tests in different concentrations of MBAA. Each formulation of different concentrations of MBAA was based on the ratio of MBAA and acrylamide. And results of five samples were carried out for each formulation.

As illustrated in Figure 4-4, the stiffness increased with the increasing concentration of MBAA. The fitted overall modulus  $K$  increased from 1.33 KPa at 0.0003 MBAA/ acrylamide to 3.42 KPa at 0.0006 MBAA/acrylamide and to 3.58 KPa at 0.0009 MBAA/acrylamide. The modulus changed more sharply in the stage between 0.0003 to 0.0006 MBAA/acrylamide, which indicated that variation in this interval might have more effort to modulate the stiffness of hydrogels.

The stretchability of hydrogels also varied when the concentration of MBAA changed. In the low ratio of 0.0003 MBAA/acrylamide, the hydrogels were tearing down at an average strain of 724% in the tensile test. The maximum tensile strain reached 909%. In the baseline formulation of 0.0006 MBAA/acrylamide, the hydrogels were broken at an average strain of 496%. And in the sample set of 0.0009 MBAA/acrylamide, the breaking point decreased to an average strain of 370%.

As for electrical resistance, initial electrical resistance varied with MBAA concentration. The measured initial electrical resistance increased from 1.4 k $\Omega$  at 0.0003 MBAA/ acrylamide to 1.64 k $\Omega$  at 0.0006 MBAA/acrylamide, then decreased to 1.41 k $\Omega$  at 0.0009 MBAA/acrylamide. While for the sample set of 0.0003 MBAA/ acrylamide, its electrical resistance had a larger deviation during the tensile test.

### Concentration of Irgacure 2959

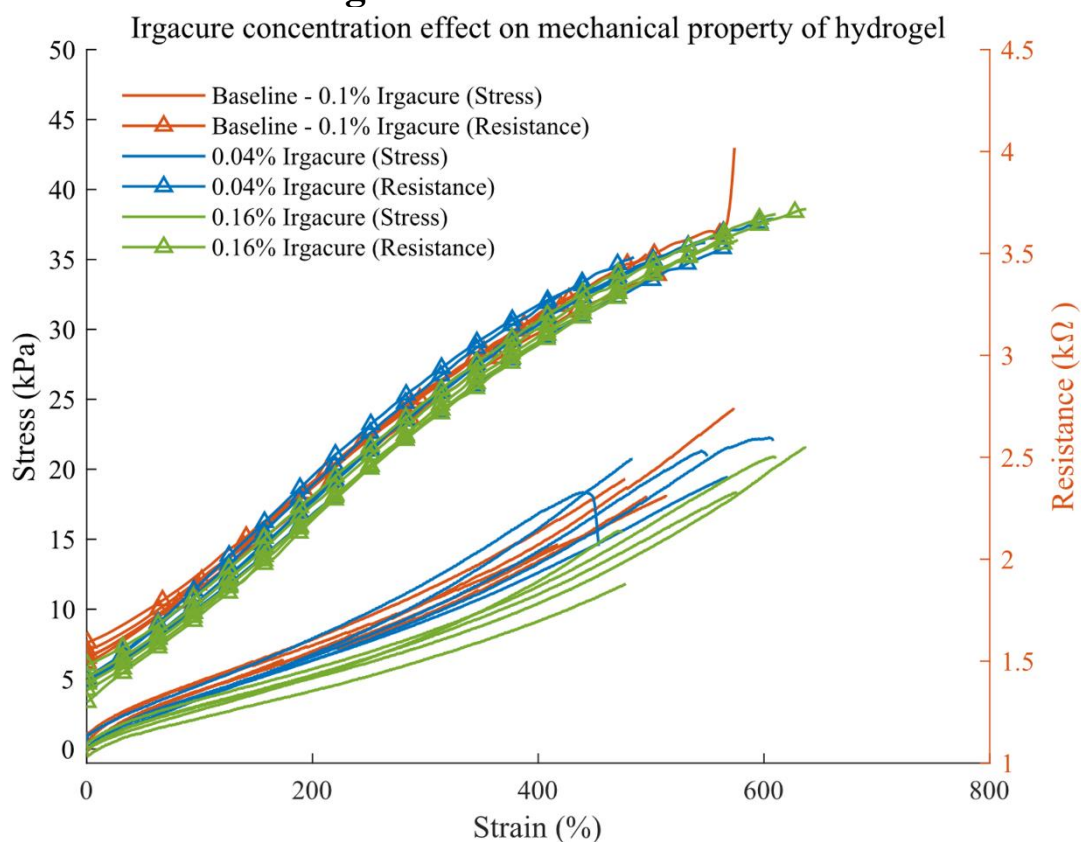


Figure 4-5 The tensile test results for the conductive hydrogels in different concentrations of Irgacure 2959. The hydrogels with a higher concentration of Irgacure revealed lower mechanical stress in the test.

---

Figure 4-5 showed the effect of different Irgacure 2959 concentrations on the mechanical and electrical properties of the hydrogel. The mechanical and electrical properties of the hydrogel were both altered from the tensile test results of three different concentration groups of five samples each.

The tensile tests of different groups of hydrogels showed that the stiffness increased when the concentration decreased. The overall stiffness  $K$  decreased from 3.71 kPa at 0.04% w/v of Irgacure 2959 to 3.42 kPa at 0.1% w/v of Irgacure 2959, and to 2.95 kPa at 0.16% w/v of Irgacure 2959.

The stretchability of hydrogels also varied when the concentration of Irgacure 2959 changed. Specifically, the average breaking strain is 533%, 496% and 555% at different concentration of 0.04% w/v, 0.1% w/v and 0.16% w/v respectively. However, deviations occurred in each set of results, resulting in overlap in breaking strain ranges. For 0.04% w/v concentration of Irgacure 2959, the ranges of breaking strain were between 418% to 573%. For the baseline, 0.1% w/v concentration of Irgacure 2959, the ranges of breaking strain were between 454% to 611%. For 0.16% w/v concentration of Irgacure 2959, the ranges of breaking strain were between 474% to 636%.

The initial electrical resistance also changed among different concentrations of Irgacure groups. The average electrical resistance is 1.41 k $\Omega$ , 1.64 k $\Omega$  and 1.39 k $\Omega$  at different concentration of 0.04% w/v, 0.1% w/v and 0.16% w/v respectively.

## Concentration of NaCl

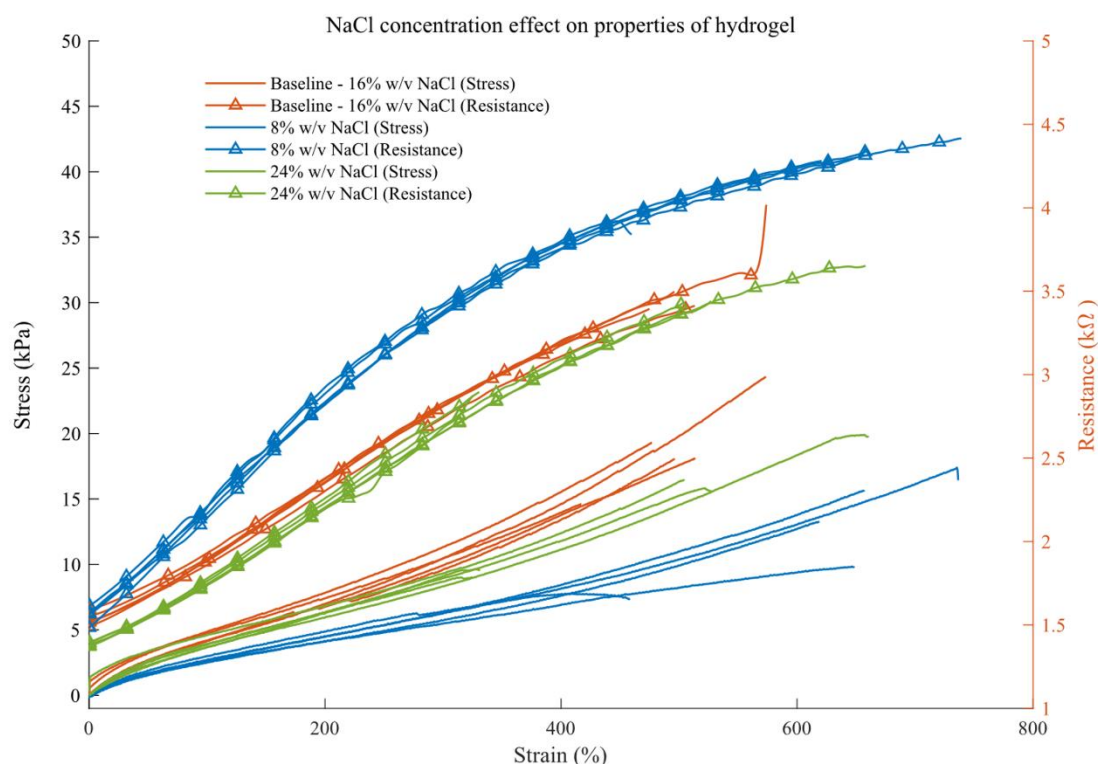


Figure 4-6 The tensile test results for the conductive hydrogels in different concentrations of NaCl. The concentration of NaCl varied from 8% w/v to 24% w/v and affected both electrical resistance and mechanical stress of the proposed hydrogel.

Figure 4-6 addressed that NaCl concentration affected both the mechanical and electrical properties of hydrogels in tensile tests.

For mechanical properties, the overall stiffness  $K$  changed non-linearly when the concentration of NaCl increased. At a lower concentration of 8% w/v NaCl, the average overall stiffness  $K$  was 1.86 kPa out of 5 samples. At the baseline concentration of 16% w/v NaCl, the average overall stiffness  $K$  increased to 3.42 kPa in 5 test samples. But at a higher concentration of 24% w/v NaCl, the average overall stiffness  $K$  decreased to 2.74 kPa in 5 test samples.

---

In another aspect, the stretchability was also varied when the concentration of NaCl changed. In the 8% w/v NaCl hydrogel samples group, the average breaking tensile strain was 625% in the range of 460% to 736%. 4 out of 5 samples were stretched over 600% strain before they were broken. For the baseline group of hydrogels with 16% w/v NaCl, the average tensile strain was 496% in a range of 454% to 611% before they were cracked. In the group of 24% w/v NaCl hydrogels, the average breaking tensile strain was 470% in the range of 325% to 660%. While 2 out of 5 became relatively weak and broke at tensile strain below 350%.

NaCl concentration had a remarkable effect on the electrical resistance as the ions came from it. The initial electrical resistance at a 20 mm distance between two electrodes was 1.57 k $\Omega$ , 1.64 k $\Omega$  and 1.38 k $\Omega$  at different concentrations of 8% w/v, 16% w/v and 24% w/v NaCl, respectively.

Despite differences in initial electrical resistance, the 8% w/v NaCl group showed a remarkable difference in how electrical resistance was changed as the hydrogel samples were strained. The hydrogel samples of 8% w/v NaCl gained electrical resistance more sharply than other sets of hydrogels. Compared to the baseline formulation of 16% w/v NaCl, the 8% w/v group has a 16% lower electrical resistance when the hydrogel sample is at its initial length of 20 mm. The electrical resistance difference of 24% w/v group to the baseline was 4% at the initial position. When the tensile strain reached 200%, the average electrical resistance of the 8% w/v group was not lower but 21% higher than the baseline 16% w/v group. But the 24% w/v group only has a difference of 5% compared to the baseline of 16% w/v.

## UV exposure time

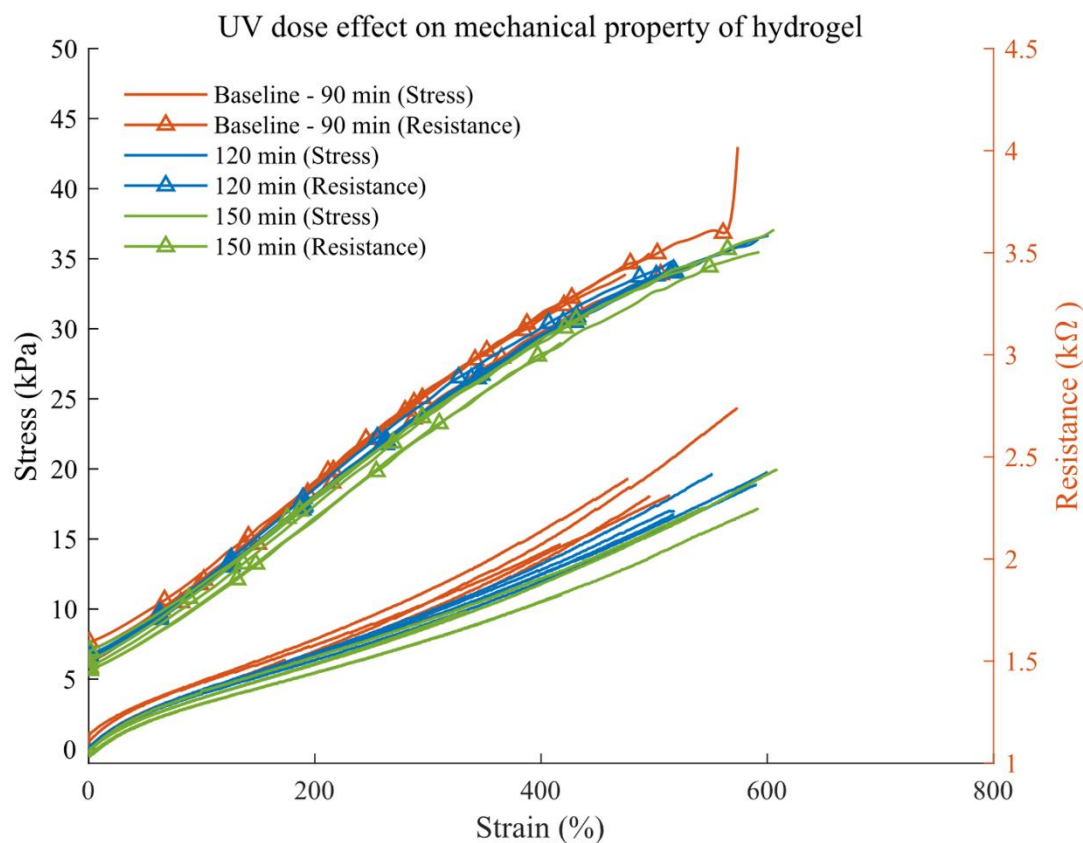


Figure 4-7 The tensile test results for the conductive hydrogels in different UV exposure time. The UV exposure time varied from 90min to 150min. Both electrical and mechanical properties of the hydrogel are affected by different UV exposure times.

Figure 4-7 shows the effort of different UV exposing times on the mechanical and electrical properties of hydrogels.

The overall stiffness  $K$  decreased when the UV exposing time increased. When the samples were exposed for 90 min, the average overall stiffness  $K$  of 5 samples was 3.42 kPa. When the exposure time increased to 120 min, the average overall stiffness  $K$  went down to 3.05 kPa. Furthermore, when the exposure time increased to 150 min, the average overall stiffness  $K$  decreased to 2.77 kPa.

The stretchability of hydrogels also changed along the UV exposure time. Tougher hydrogels were obtained with an average breaking tensile strain of 556% under 120 min UV exposure. While in other groups of 90min and 120min UV exposure, the average breaking tensile strain was 496% and 499%, respectively.

As for the electrical resistance, the hydrogels exposed for 90min appeared to have the highest initial electrical resistance of 1.64 k $\Omega$ . As the UV exposure time went up, the initial electrical resistance decreased to 1.48 k $\Omega$  and 1.49 k $\Omega$  for 120 min and 150 min UV exposure.

## Summary of different formulations of conductive hydrogels

Table 4-2 Test results of different formulations of conductive hydrogels

Variables	K (kPa)	$\epsilon_0$ (%)	R <sub>0</sub> (k $\Omega$ )
Baseline	3.42	496	1.64
1.6 M acrylamide	5.99	554	1.49
0.0003 MBAA/acrylamide	1.33	724	1.40
0.0009 MBAA/acrylamide	3.58	370	1.41
8% w/v NaCl	1.86	625	1.57
24% w/v NaCl	2.74	470	1.38
0.04% w/v Irgacure 2959	3.71	533	1.41
0.16% w/v Irgacure 2959	2.95	555	1.39
120 min UV exposure	3.05	499	1.48
150 min UV exposure	2.77	556	1.49

Table 4-2 summarises the modulus, maximum strain and initial resistance of each variation of conductive hydrogels. The details of how each ingredient affected the properties are described as follows.

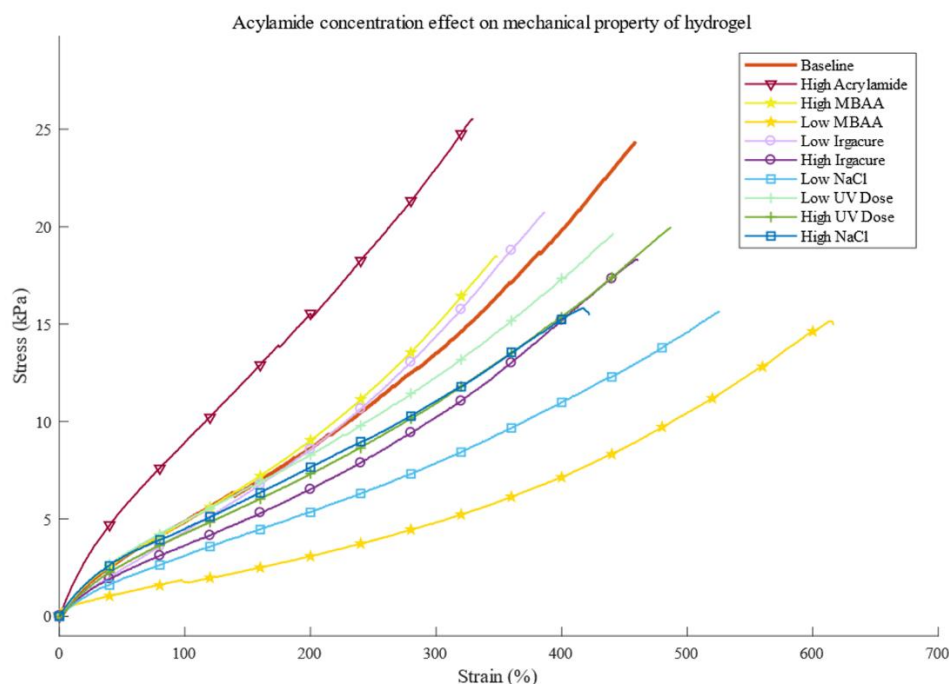


Figure 4-8 Summary of different mechanical performances in tensile tests of different formulations of hydrogels.

Figure 4-8 shows the effort of different formulations of hydrogels on the mechanical properties in tensile tests. The concentration of acrylamide and the ratio of MBAA/acrylamide had the most significant effect on the stiffness of hydrogels. By increasing the concentration of acrylamide to 1.6 M, the overall tensile modulus of hydrogel was able to reach as high as 5.99 kPa, which was 75% higher than the baseline formulations of 1.1 M acrylamide. By decreasing the ratio of MBAA/acrylamide to 0.0003, a 1.33 kPa overall tensile modulus of hydrogels was achieved, which was 61% lower than the baseline formulations of 0.0006 MBAA/acrylamide. Therefore, a range of 1.33 kPa to 5.99 kPa (450% scale) tensile modulus was obtained for the conductive hydrogels.

Figure 4-8 also indicates the stretchability of the proposed hydrogels. The lowest breaking tensile strain appeared when the ratio of MBAA/acrylamide went up to 0.0009, while the highest breaking tensile strain was achieved when the ratio of

MBAA/acrylamide went down to 0.0003. The range of breaking tensile strain was between 370% to 724%.

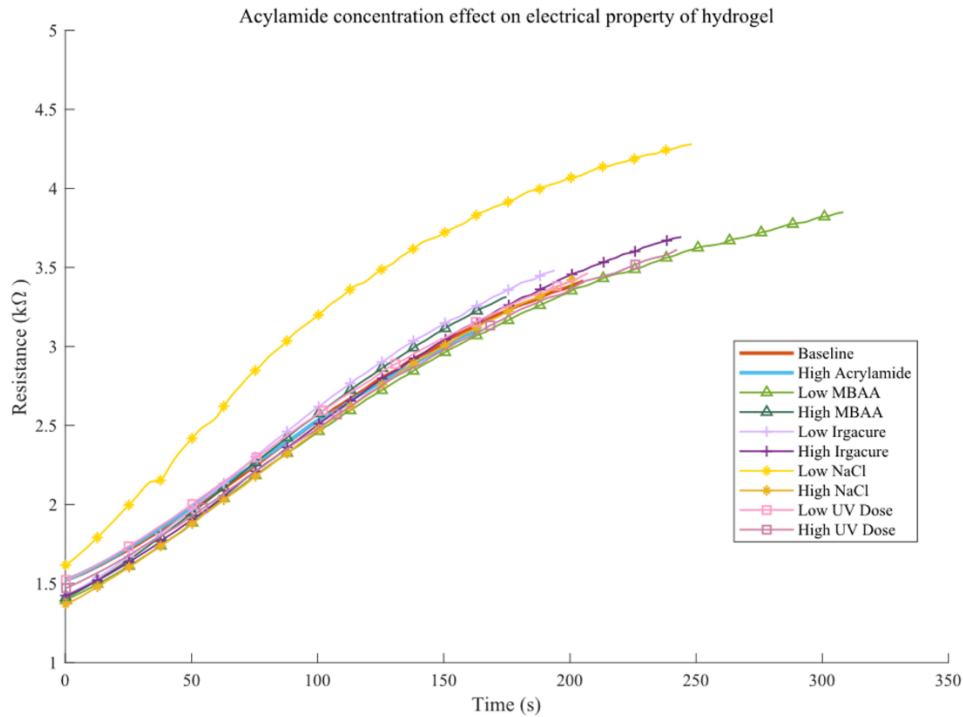


Figure 4-9 Summary of different electrical resistance in tensile tests of different formulations of hydrogels

NaCl is the dominating factor that affects the changing rate of electrical resistance while other factors also have an effect on the static or initial electrical resistance in the tensile test as shown in Figure 4-9. The initial electrical resistance was varied from 1.38 k $\Omega$  to 1.64 k $\Omega$  at the initial length of hydrogels of 20 mm. The electrical conductivity can be obtained by,

$$\rho = \frac{1}{\Omega} = \frac{l}{R \cdot A} \quad (4 - 5)$$

where  $R$  stands for the measured electrical resistance,  $l$  is the length of hydrogels clipped between two measuring electrodes and  $A$  is the section area of hydrogels samples. The electrical conductivity of the proposed hydrogels was between 0.847 S/m and 1.006 S/m.

---

### **4.2.3 Compression test on the electrical and mechanical properties of conductive hydrogels**

To further explore the performance of the proposed conductive hydrogel, compression tests were conducted to investigate the changes in electrical and mechanical properties of the conductive hydrogels under compression. Cylindrical samples of conductive hydrogel in 25×25×10 mm were made for the compression tests. The samples were fabricated in the same method as described in Chapter 4.2, but the mould was altered to obtain the required sample size. The mould consisted of two glass plates sandwiching laser cutting acrylic plates in the middle. Pre-solution of hydrogels was filled in the groove of acrylic plates. And the liquid was sealed by the glass plates over the surface tension of the liquid. In order to create a 10mm-height mould, two 5mm acrylic plates were overlapped as the frame of the fabricating mould.

The test configuration of the compression test was also carried out on the INSTRON 5943 universal testing system. The conductive hydrogels were compressing at a fixed speed of 0.5 mm/s until a 40% compression limit was reached. The tests were conducted in 5 cycles for each sample. Compression force was obtained by a 50N loadcell and recorded at a sampling rate of 500 Hz.

Two compression fixtures were used in the compression tests, the surface of the fixtures being flat metal, as shown in Figure 4-10. To avoid potential effects on the electrical conductivity of conductive hydrogels, the metal surfaces of the fixtures were taped with non-conductive tapes. In the compression test, copper films were attached to the fixture to act as electrodes for measuring the conductivity of the conductive hydrogels. The copper films are large enough to cover all the hydrogel sample area when compressed and flattened.

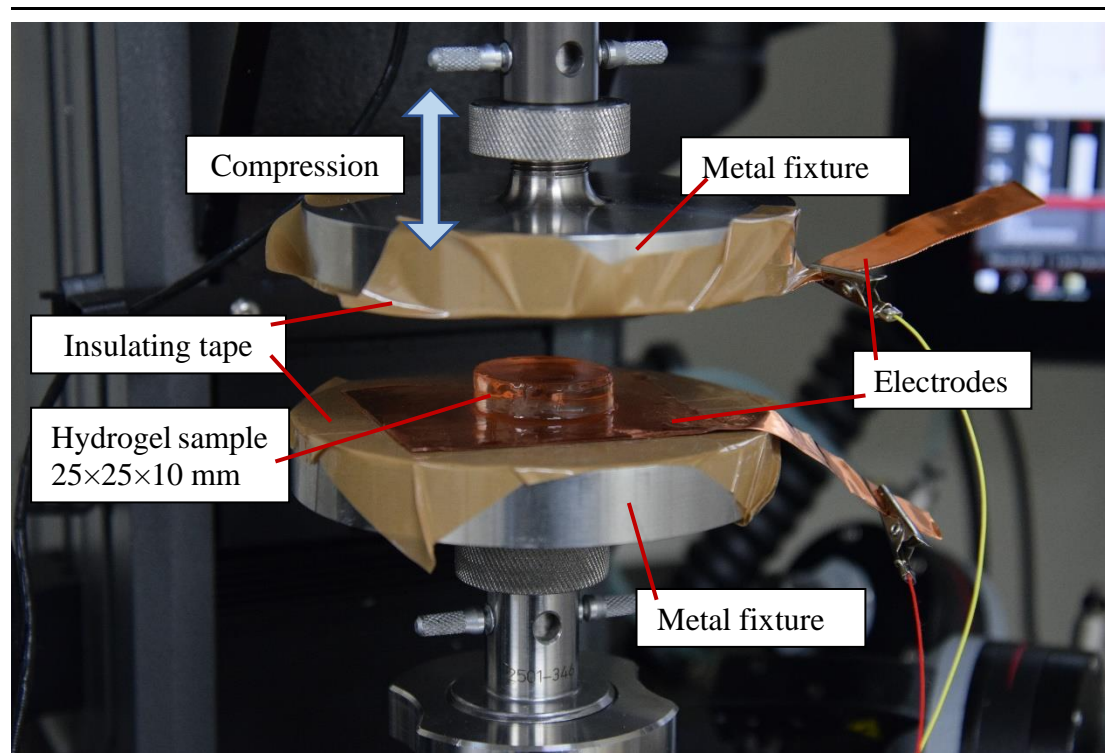


Figure 4-10 Fixture of compression test on hydrogels. Flat metal fixtures are used to compress the sample to set strain. Copper films are trimmed as electrodes to measure the electrical property of the conductive hydrogels. Tapes are applied to isolate the copper electrodes and the metal fixtures.

Figure 4-11 to Figure 4-20 showed the results of compression tests on the mechanical and electrical properties of the conductive hydrogels. Each graph has different curves for three different concentrations of one of the factors affecting the hydrogel. There are two samples of each concentration and five runs of the compression tests.

The raw data of the mechanical stress change over time is shown in the figures. There is stress data of 2 to 3 different formulations of the conductive hydrogels in each figure. And for each formulation, two samples are running five continuous tests in 80 seconds.

The compressive modulus  $K_c$  is defined by the compressive stress at the peak compressive strain to evaluate the stiffness of the hydrogel samples as Equation (4-6).

$$K_c = \frac{\sigma}{\varepsilon} \quad (4-6)$$

## Concentration of acrylamide

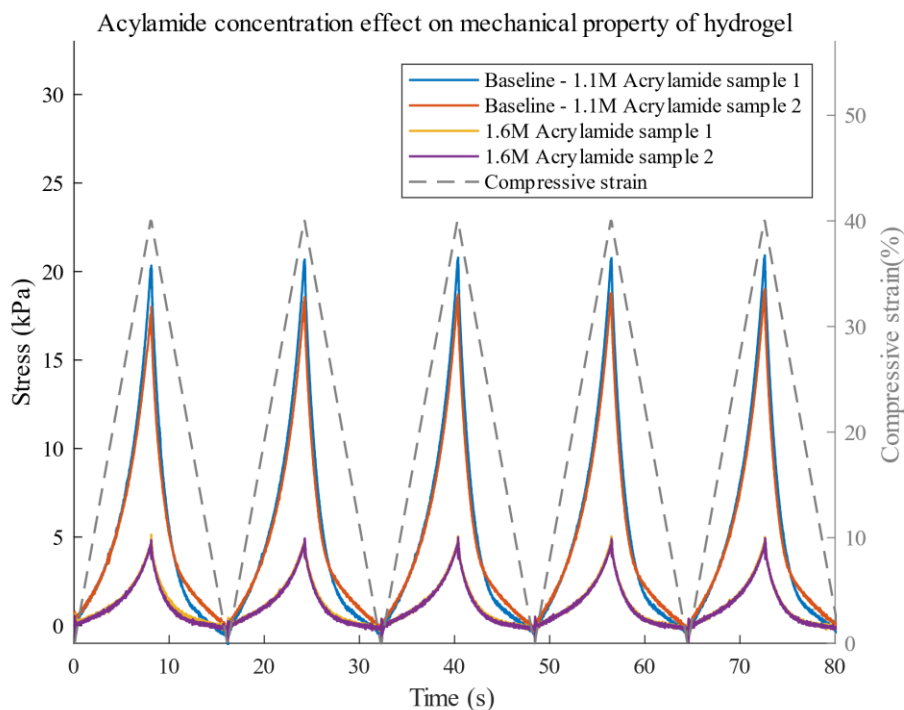


Figure 4-11 Mechanical stress of hydrogels with different acrylamide concentrations. The compression strain is from 0% to 40%, as shown in the grey dash line, and the compressive stress is shown in the coloured line. The concentration of acrylamide varied from 1.1M to 1.6M. A higher concentration of acrylamide showed lower compression stress.

Figure 4-11 shows the mechanical stress results in compression tests on conductive hydrogels with different acrylamide concentrations. However, the hydrogel pre-solution of a lower concentration (0.6 M) of acrylamide failed in forming a solid hydrogel. As the compressive strain increases, the stress of conductive hydrogels also increases. The peak of stress corresponds to the peak of compressive strain. As the concentration of acrylamide increase from 1.1 M to 1.6 M, a decrease in stress responding to compression occurs. By Equation (4-6), the compressive modulus of the hydrogels with 1.1 M acrylamide is up to 52.29 kPa, while the compressive modulus of the hydrogels with 1.6 M acrylamide is up to 12.86 kPa.

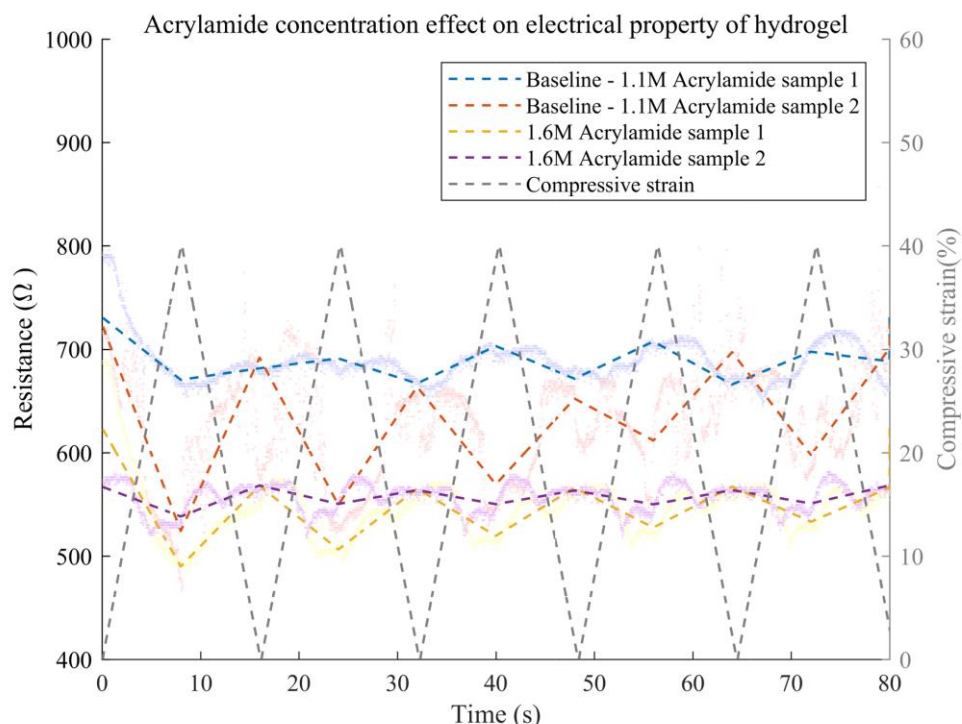


Figure 4-12 Electrical resistance of hydrogels with different acrylamide concentrations. Light-coloured scatters the raw data of electrical resistance. Coloured dash lines represent the segmented linear fitted curves of resistance. The concentration of acrylamide varied from 1.1M to 1.6M. A higher concentration of acrylamide showed lower electrical resistance.

Figure 4-12 shows the results of the change in resistance with time when hydrogels with different concentrations of acrylamide are tested in compression. As shown by the segmented fitted lines (coloured dashed lines), the change in resistance is related to the compressive strain. The resistance of most of the conductive hydrogel samples (1.1 M acrylamide sample 2 and 1.6 acrylamide samples) is inversely proportional to the compressive strain. One of the samples (1.1M acrylamide sample 1) does not correspond to the compressive strain. 1.1M acrylamide samples have a resistance range of 466  $\Omega$  to 918  $\Omega$ . 1.6M acrylamide samples have a resistance range of 483  $\Omega$  to 690  $\Omega$ . At the same compressive strain, 1.6M acrylamide samples have a lower resistance than 1.1M acrylamide samples. And the range of variation of the 1.6M acrylamide sample is smaller than that of the 1.1M acrylamide sample.

## Concentration of MBAA

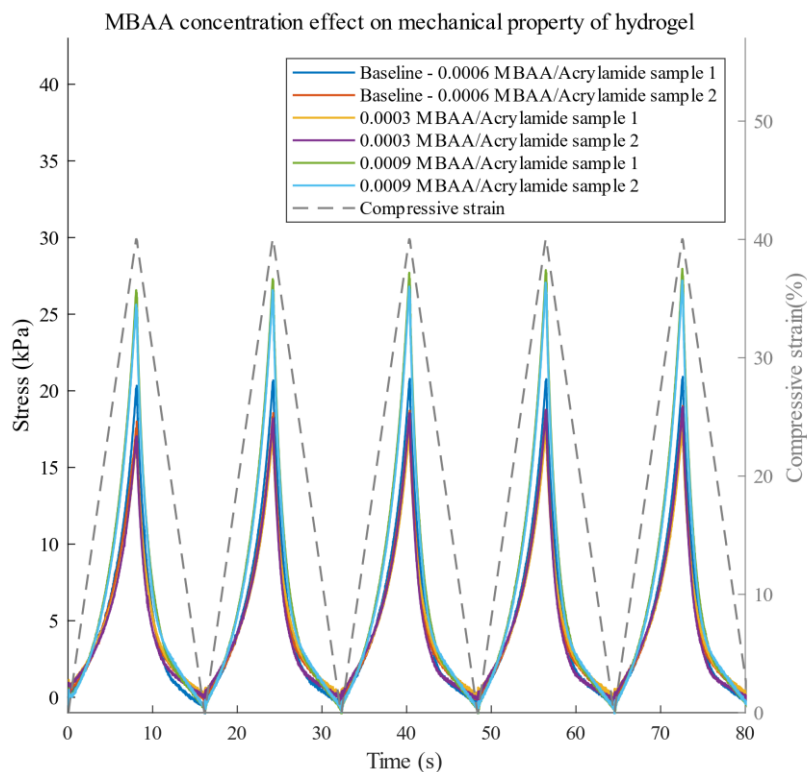


Figure 4-13 Mechanical stress of hydrogels with different MBAA concentrations. The compression strain is from 0% to 40%, as shown in the grey dash line, and the compressive stress is shown in the coloured line. The concentration of MBAA varied from 0.0003 to 0.0009 weight of acrylamide. A higher concentration of acrylamide showed higher compression stress.

Figure 4-13 shows the effect of different concentrations of MBAA on the mechanical properties of hydrogels in the compression test. The concentrations of MBAA affect the stiffness of the presented hydrogels. The peak stress occurs simultaneously at the peak compressive strain in the compression test. At the same time, hydrogels with higher MBAA concentrations have higher stress at the peak. For 40% of compressive strain, the compressive modulus for MBAA at 0.0003 weight of acrylamide is up to 44.73 kPa. As MBAA concentration rises to 0.0006 weight of acrylamide, the compressive modulus at 40% strain is as high as 52.29 kPa. The highest compressive

modulus is achieved for the hydrogels of MBAA at 0.0009 weight of acrylamide at 69.90 kPa.

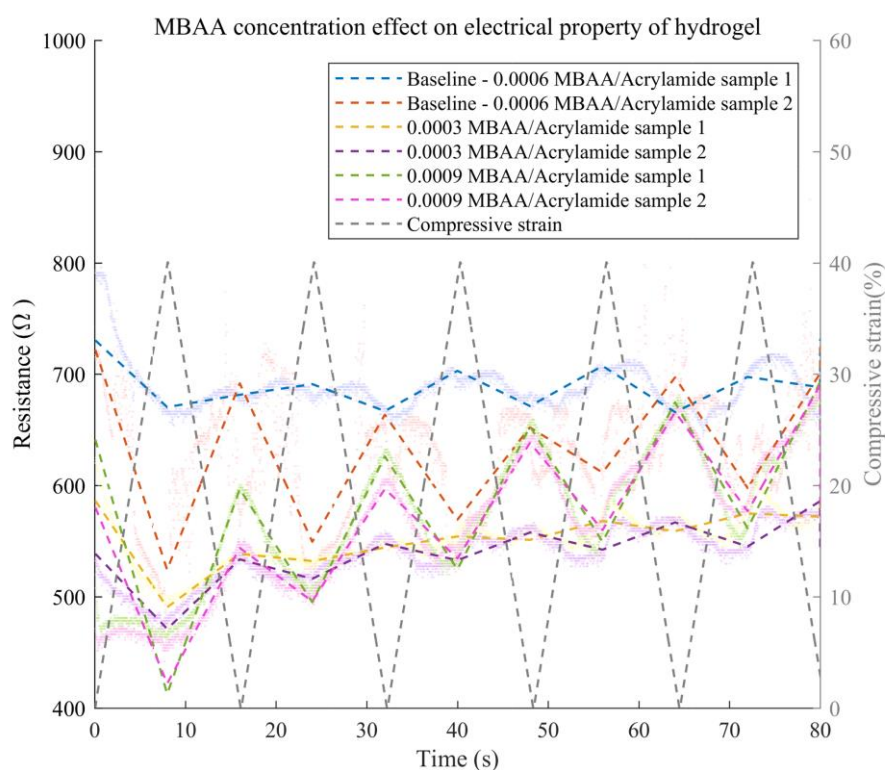


Figure 4-14 Electrical resistance of hydrogels with different MBAA concentrations. Light-coloured scatters the raw data of electrical resistance. Coloured dash lines represent the segmented linear fitted curves of resistance. The concentration of MBAA varied from 0.0003 to 0.0009 weight of acrylamide. A higher concentration of acrylamide showed lower electrical resistance.

Figure 4-14 shows the electrical resistance changes of conductive hydrogels with different MBAA concentrations in the compression tests. As shown as segmented linear fitted lines in Figure 4-14, most hydrogel samples of different MBAA concentrations are inversely proportional to the compressive strain, but some are switching from inversely proportional to the compressive strain to proportional to the compressive strain (0.0006 MBAA/acrylamide sample 1 and 0.0003 MBAA/acrylamide sample 1). For the samples of MBAA at 0.0003 weight of acrylamide, they have the smallest changes in resistance corresponding to the 40% compressive strain, which is from 488  $\Omega$  to 625  $\Omega$ . At the same time, the resistance of

samples of MBAA at 0.0009 weight of acrylamide changes the most from 457  $\Omega$  to 715  $\Omega$ . Other than the compression, there is a consistent increase in resistance for hydrogels samples. The hydrogel sample with MBAA at 0.0009 weight of acrylamide has the lowest initial resistance of 457  $\Omega$  but the highest rate of consisting resistance increasing.

## Concentration of NaCl

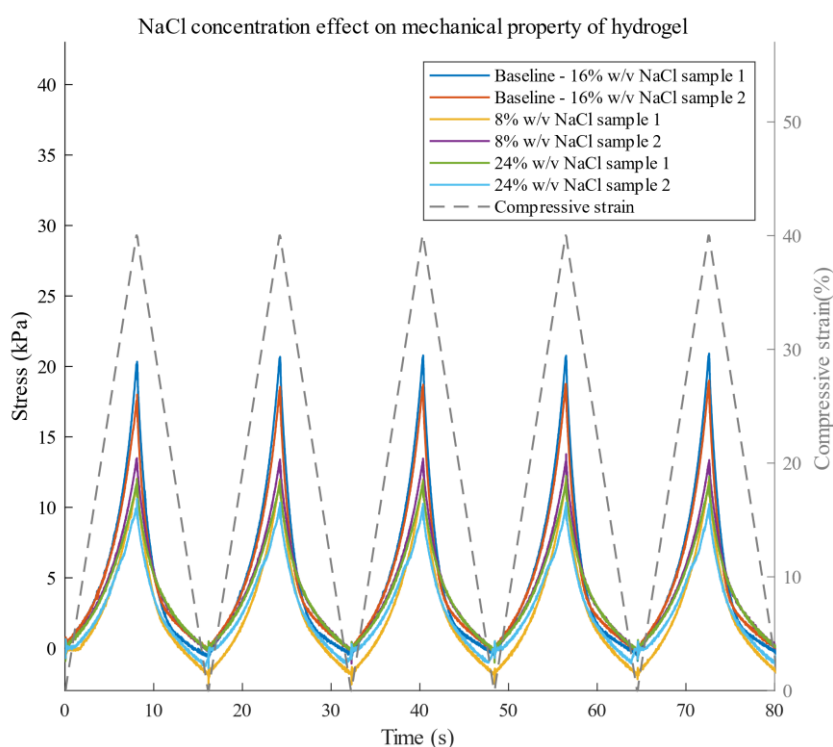


Figure 4-15 Mechanical stress of hydrogels with different NaCl concentrations. The compression strain is from 0% to 40%, as shown in the grey dash line, and the compressive stress is shown in the coloured line. The concentration of NaCl varied from 8% w/v to 24% w/v.

Figure 4-15 shows the mechanical stress results in compression tests on conductive hydrogels with different concentrations of NaCl. Both increasing and decreasing concentrations of NaCl decrease the compressive stress of hydrogels samples at the same compressive strain compared to the 16% w/v NaCl hydrogel samples. For 16% w/v NaCl hydrogel samples, the compressive modulus is up to 52.29 kPa which is higher than 34.44 kPa for the 8% w/v NaCl hydrogel samples and 30.59 kPa for the 16%

w/v NaCl hydrogel samples. In addition to the stiffness difference, as the concentrations of NaCl are varied, some samples show adhesion when compressive pressure have been unloaded. The adhesion results in the negative compressive stresses shown in Figure 4-15, as shown for 8% w/v NaCl hydrogel sample 1 and 24% w/v NaCl hydrogel sample 2.

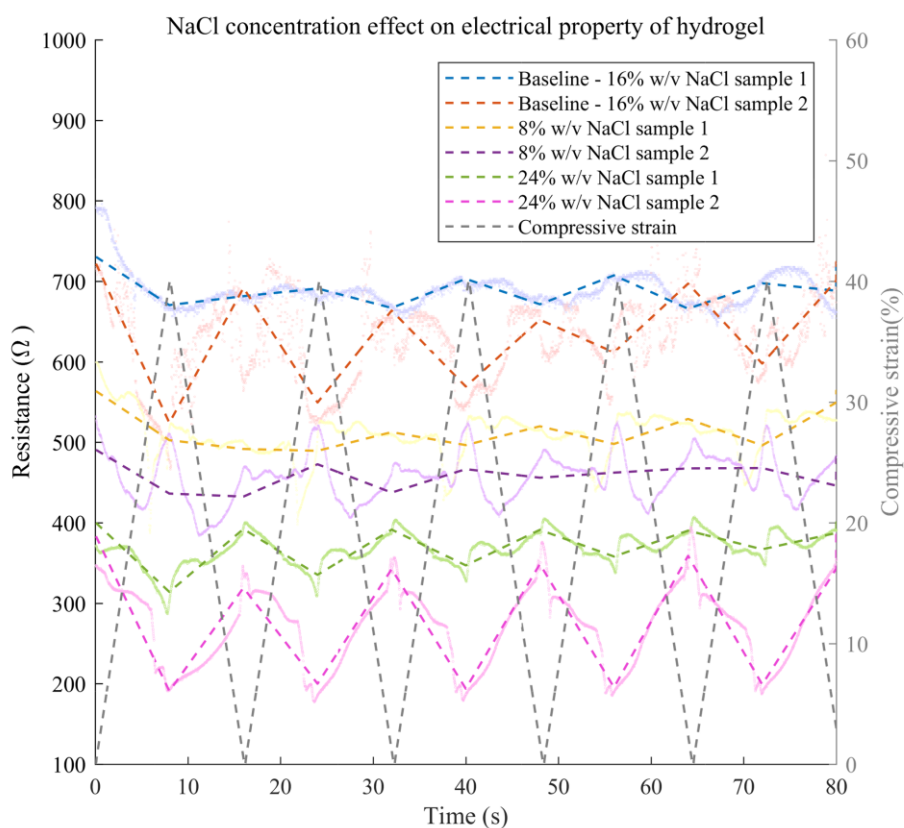


Figure 4-16 Electrical resistance of hydrogels with different NaCl concentrations. Light-coloured scatters the raw data of electrical resistance. Coloured dash lines represent the segmented linear fitted curves of resistance. The concentration of NaCl varied from 8% w/v to 24% w/v.

Figure 4-16 shows the results of electrical resistance changes of conductive hydrogels with different NaCl concentrations in the compression tests. For conductive hydrogel samples with different concentrations of NaCl, the initial electrical resistance without compression is different. The increase of concentrations of NaCl does not result in a decrease in the electrical resistance of conductive hydrogels. Despite the resistance difference between samples with the same resistance, the 16% w/v NaCl samples have

the highest initial resistance for 718  $\Omega$  and 793  $\Omega$ . In the contrast, the initial resistance of the 8% w/v NaCl samples are for 531  $\Omega$  and 599  $\Omega$ , and the initial resistance of the 24% w/v NaCl samples are for 347  $\Omega$  and 372  $\Omega$ . Furthermore, the 8% w/v NaCl samples show a different pattern of resistance change than other samples with different concentrations. As the compressive strain increase to around 20%, the electrical resistance of the 8% w/v NaCl samples stops falling and turn up, increasing to a peak at 40% of the compressive strain.

## Concentration of Irgacure 2959

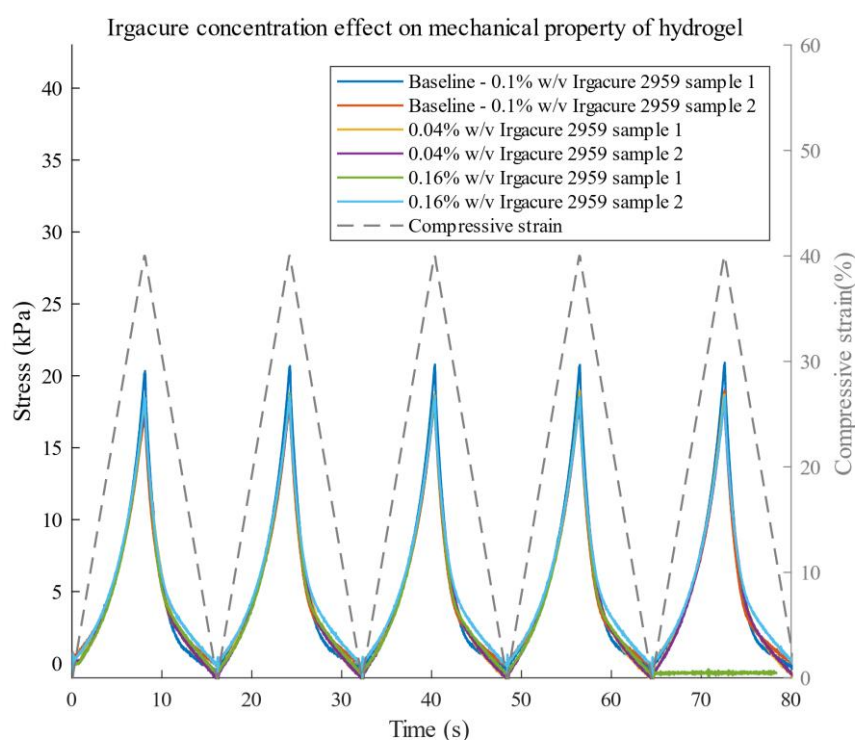


Figure 4-17 Mechanical stress of hydrogels with different Irgacure concentrations. The compression strain is from 0% to 40%, as shown in the grey dash line, and the compressive stress is shown in the coloured line. The concentration of Irgacure 2959 varied from 0.04% w/v to 0.16% w/v.

Note: The fifth test runs for 0.16% w/v Irgacure 2959 sample 1 was not correctly recorded as the green line shows.

Figure 4-17 shows the results of the mechanical properties of hydrogels tested in compression with different concentrations of Irgacure 2959. The compressive modulus

for 0.04% w/v Irgacure 2959 is up to 47.4 kPa in five test runs of two samples, and for 0.16% w/v Irgacure 2959 is up to 46.96 kPa, compared to 52.29 kPa for the baseline formulation of 0.1% w/v Irgacure 2959. Different concentrations of Irgacure 2959 have the least effect on the compressive modulus than the other factors.

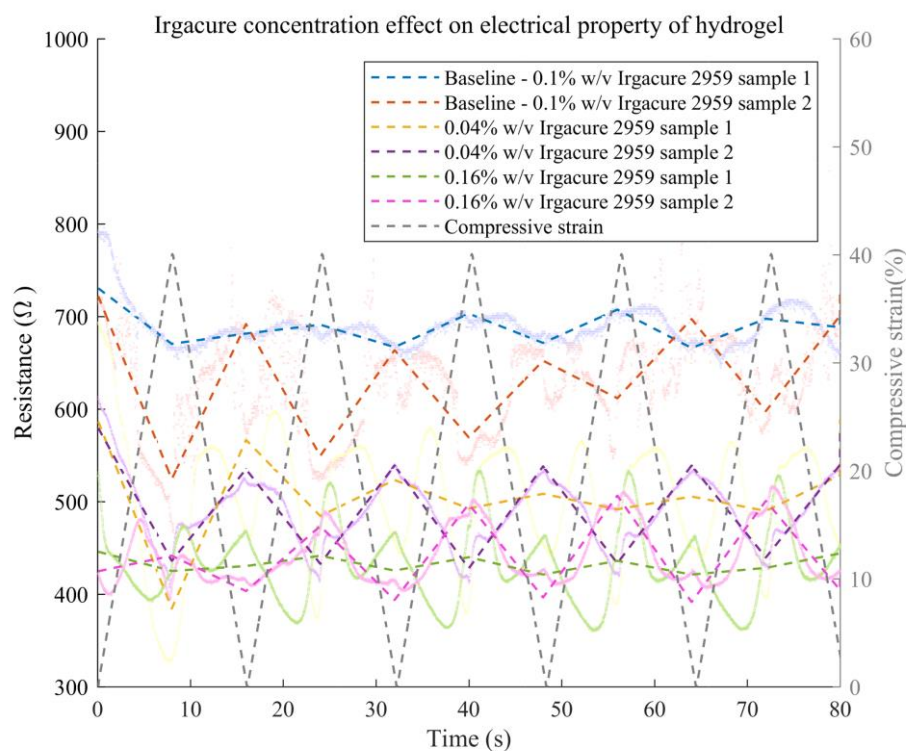


Figure 4-18 Electrical resistance of hydrogels with different Irgacure concentrations. Light-coloured scatters the raw data of electrical resistance. Coloured dash lines represent the segmented linear fitted curves of resistance. The concentration of Irgacure 2959 varied from 0.04% w/v to 0.16% w/v.

Figure 4-18 shows the electrical resistance changes of conductive hydrogels with different Irgacure 2959 concentrations in the compression tests. Overall, the 0.04% w/v Irgacure 2959 and 0.16% w/v Irgacure 2959 have lower electrical resistance, from 326  $\Omega$  to 693  $\Omega$  and from 360  $\Omega$  to 536  $\Omega$  respectively, than from 457  $\Omega$  to 715  $\Omega$  for the 0.1% w/v Irgacure 2959. Similar to the 8% w/v NaCl sample, the resistance changing pattern of hydrogels with 0.04% w/v Irgacure 2959 and 0.16% w/v Irgacure 2959 is not linear. The resistance decreases until the compressive strain goes up to 20% and then the resistance peaks at 40% compressive strain.

## UV exposure time

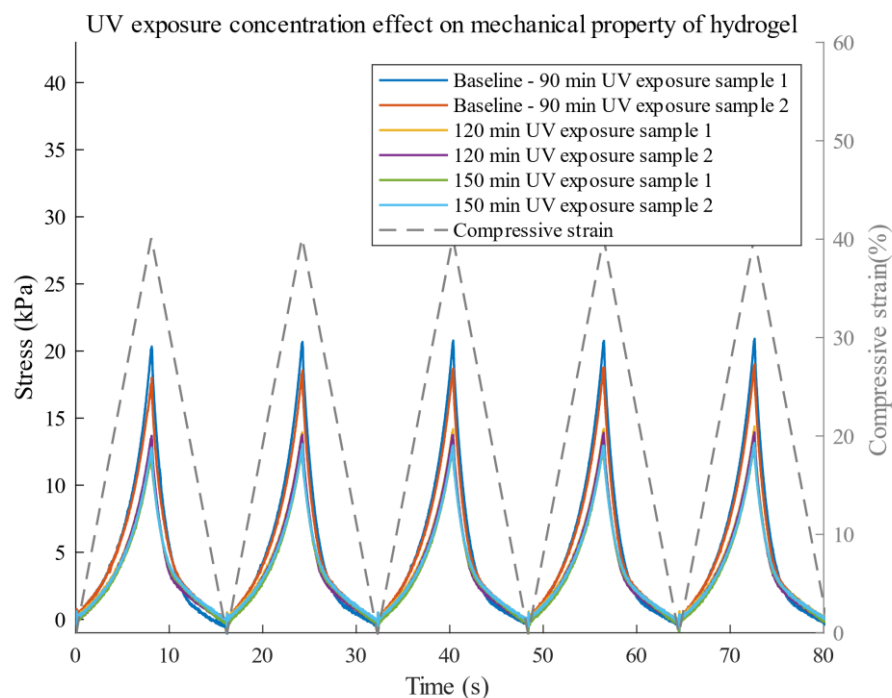


Figure 4-19 Mechanical stress of hydrogels with different UV exposure dose. The compression strain is from 0% to 40%, as shown in the grey dash line, and the compressive stress is shown in the coloured line. The UV exposure time varied from 90min to 150min. The longer UV exposure time of hydrogels showed lower compressive stress.

Figure 4-19 the results of mechanical stress in compression tests on conductive hydrogels with different UV exposure times during fabrication. Extending UV exposure time decreases the compressive stress of hydrogels samples at the same compressive strain compared to the baseline hydrogel samples. For 90 min UV exposure hydrogel samples, the compressive modulus is up to 52.29 kPa, higher than 35.95 kPa for the 120 min UV exposure hydrogel samples and 32.90 kPa for the 150 min UV exposure hydrogel samples.

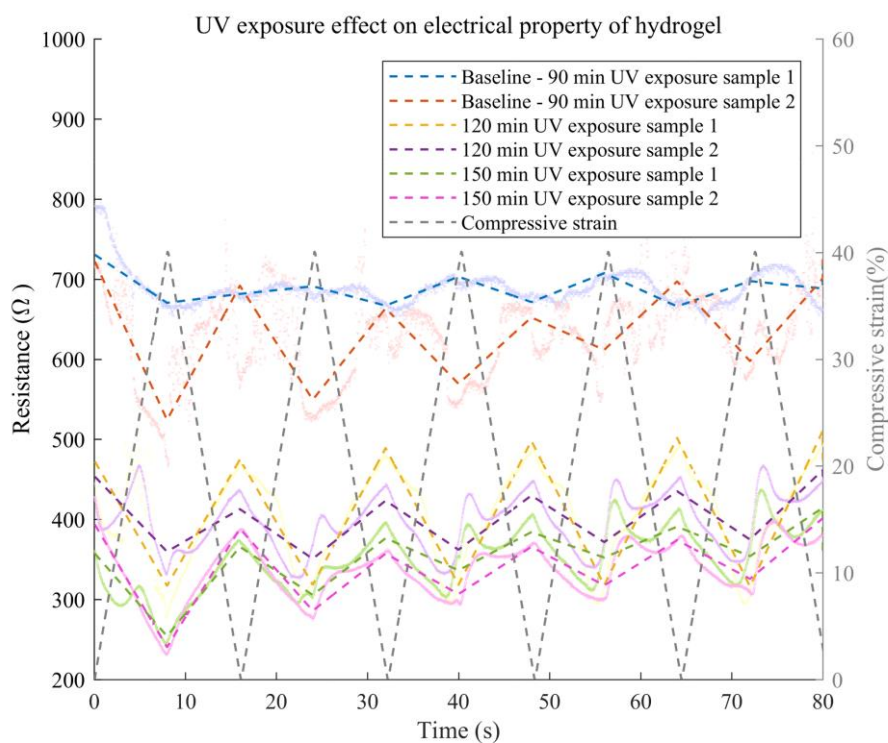


Figure 4-20 Electrical resistance of hydrogels with different UV exposure dose. Light-colour scatters are the raw data of electrical resistance. Coloured dash lines represent the segmented linear fitted curves of resistance. The UV exposure time varied from 90min to 150min. The longer UV exposure time of hydrogels showed lower electrical resistance.

Figure 4-20 shows the results of electrical resistance changes of conductive hydrogels with different UV exposure times in the compression tests. Overall, as the UV exposure time increases, both the initial electrical resistance and the change range of electrical resistance under compression decrease for the conductive hydrogels. The resistance change pattern of hydrogels for 120 min UV exposure and 150 min UV exposure is not linear. In the loading progress, as the compressive strain increase, the electrical resistance of those samples increases until 20% strain and turn down to the bottom at the peak of compressive strain. But in the unloading progress, the resistance is inversely proportional to the compressive stress.

---

## 4.3 Discussion and Summary

Additional information and failing cases of the fabrication and characterisation are discussed to improve the repeatability of this research. And main finds of the conductive hydrogel are summarised on fabrication and test results.

### 4.3.1 Fabrication

The mould consisted of two glass plates sandwiching laser cutting acrylic plates in the middle. Pre-solution of hydrogels was filled in the groove of acrylic plates, and the glass plates sealed the liquid over the surface tension of the liquid. In the UV curing procedure, UV was emitted from the top of the UV chamber. The top cover mould was firstly made of acrylic plates, but the hydrogel pre-solution failed to cure in the standard UV curing time (90 min). Then the glass plate was applied as the cover and bottom of the fabrication mould and the hydrogel succeeded to cure solid hydrogel samples. The reasonable speculations are that the glass and acrylic plate have different transparency for the UV, and the glass and acrylic plate have different hydrophobicity and surface energy, which affect the initial implant of hydrogel particles on the plate of the mould.

An ultraviolet light chamber is used to excite the initiator Irgacure 2959. Four ultraviolet lamps are installed parallelly on the top surface inside the chamber, emitting ultraviolet light of 365 nm wavelength. However, ultraviolet light is radical from the single ultraviolet light lamp, which causes overlaps or gaps between lamps. On the other hand, the ultraviolet light chamber is not in a vacuum. Air in the chamber will absorb part of the energy of ultraviolet light. Based on these two aspects, if two samples were placed in different positions, they should have absorbed different doses of ultraviolet light. Fixed planar position and vertical distance between ultraviolet light lamps and to-

---

be-cured solution largely ensure a constant procedure of fabrication. In addition, a constant starting temperature also helps to keep a constant air density that absorbs the same proportion of ultraviolet light lamps.

In the fabrication of hydrogel samples for compression tests, the height of the fabricating samples for compression tests should be controlled to avoid leakage of pre-solution of hydrogels. As the acrylic plates were laser cut with the groove, there were errors in verticality on the edge of the groove. And the errors would sum up to creating a tilting vertical surface. The tilting samples of hydrogel would affect the mechanical properties test. A higher resolution of the acrylic frame for the fabrication mould should help improve the accuracy of the compression test.

### **4.3.2 Tensile and compression test for the conductive hydrogels**

There are two common failures of the tensile tests for the conductive hydrogels—the slipperiness of the hydrogel strip samples and the early break of the hydrogel samples. In the failing cases of the slippery hydrogel tensile test, there was a dropping in stress when the slipperiness started, as shown as a slippery curve in Figure 4-3. And in the failing cases of early break of the hydrogels, the samples were obviously broken when the strain was less than the average strain of break. Both failures would largely affect the accuracy of the mechanical properties.

The solutions for both cases emphasised the clamp of the hydrogel samples. The samples were clamped by a pair of pneumatic claws with designed non-slippery conductive clamps in the presented test configurations. The pressure of pneumatic claws was crucial. High pressure would conduct mechanical damage to the hydrogel samples and cause an early break. Low pressure would cause the slipperiness of hydrogel

---

samples during the tensile test. A 10 psi pressure for the pneumatic claws was selected after the optimisation test. Besides, the non-slippery conductive clamps were designed. There was a copper film cover on the clamp as electrodes to contact the conductive hydrogels. The copper film should be thin and flexible to prevent damage to the much softer hydrogel sample. Also, there should be a soft edge when the edge of the copper film tends to curve to avoid any sharpness. In addition, the copper film was top stamped with dense cross patterns to increase non-slippery ability.

In the compression test, unlike the tensile test of the hydrogel, the compression tests will not break down the sample in the test range. Fewer samples are used in the test while each sample is cyclically tested. Two samples of each variant of conductive hydrogels are tested, which are fabricated in the same method but different batches.

The simultaneous compressive strains are also shown in the figures to understand the changes in mechanical and electrical properties about the course of the compression test. As for the figures of the results of the electrical property of hydrogels, the resistance data are linearly fitted in each segment of the tests. Each segment is divided by the running time of the compression test. In this case, the segment is 8 seconds from the initial position to the final position of compressing or returning in the test. Raw data of electrical resistance is shown in light-colour scatter in the figures, and fitted data are shown in coloured dash lines.

### **4.3.3 Summary of ultraviolet cross-link hydrogels**

This chapter presented a conductive polyacrylamide hydrogel with low stiffness, high stretchability and high conductivity. Varying formulations of polyacrylamide hydrogels were proposed to figure out the effect of each ingredient. The different hydrogel samples were then fabricated by UV-initiated crosslink. Tensile tests and

---

compression tests were conducted to characterise the proposed hydrogels' mechanical and electrical properties.

The test found that the concentration of acrylamide and ratio of MBAA/acrylamide had the most significant effect on the stiffness of hydrogels. And NaCl is the dominating factor that affects the changing rate of electrical resistance. The characterisation results showed that the proposed hydrogels meet the requirements in Chapter 3. The conductive polyacrylamide hydrogel will be used to fabricate the fully elastomeric sensors in the next chapters.

# **Chapter 5**

## **Fully Elastomeric Soft Strain Sensor**

In this chapter, a fully elastic and transparent soft strain sensor made of conductive hydrogel is presented. The soft strain sensor is coated by anti-dehydration polydimethylsiloxane (PDMS) elastomer layer. The fabrication process of the fully elastic sensor is described, including the fabrication of the hydrogel, the encapsulation of the PDMS layer and the insertion of the electrodes. Peeling tests were carried out to demonstrate the strength of the PDMS-hydrogel bond. The sensor was then characterised as a strain sensor. The results of the characterisation are presented in this chapter.

## 5.1 Design and Fabrication

### 5.1.1 Sensor design

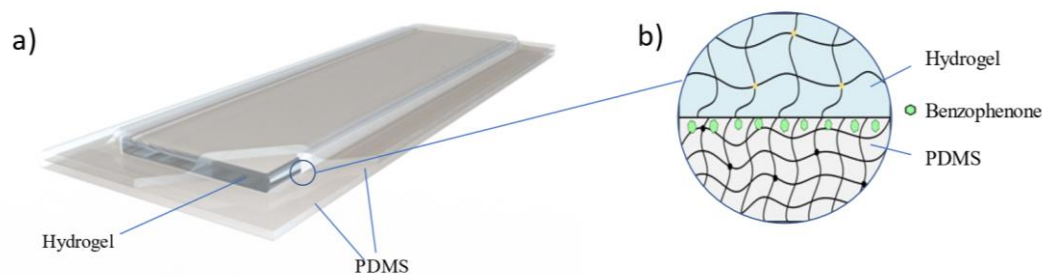


Figure 5-1 The design of the soft sensor. a) schematic of soft strain sensor. b) schematic of hydrogel and PDMS bonding with benzophenone treatment.

A fully elastomeric soft sensor has been designed by encapsulating a conductive hydrogel in PDMS. A simple configuration of the soft sensor consisted of an encapsulated conductive hydrogel with PDMS and two electrodes inserted inside the encapsulation, as shown in Figure 5-1. PDMS is applied to wrap the hydrogel to create a hydrophobic surface and decrease the dehydration of the hydrogel. Both the hydrogel and PDMS have high optical transparency and a clear appearance. The overall dimensions of the sensor are 50 mm x 20 mm, and the encapsulated hydrogel is 34 mm x 9 mm. This soft sensor can be strained in both the long-axis and short-axis directions. In this design, the soft sensor acts as a strain sensor in the long axis direction. Copper electrodes are inserted into the soft sensor to sense the electrical signals. The electrode has a wide head to expand the contact area with the hydrogel. And it has a slim body through the PDMS layer.

### 5.1.2 PDMS encapsulation and anti-dehydration

One drawback of presented conductive hydrogels is that it is easily dehydrated. After dehydration, the hydrogel is less stretchable and soft. At the same time, ionic

---

conductors dissolved in water such as NaCl start to crystallise, and the saturation of the ionic conductor becomes unstable, affecting its electrical conductivity. This shift of electrical resistance will critically fail the soft strain sensor.

To reduce dehydration of hydrogels, when used in strain sensors, they are encapsulated within a hydrophobic elastomer such as polydimethylsiloxane (PDMS). As elastomers are hydrophobic, bonding the elastomer to the water-filled hydrogel is difficult. The microdroplet of hydrogel pre-solution cannot be filled in the gap of PDMS chains, and the hydrogel will be cured without implanting into the PDMS. The bond between the hydrogel and the PDMS is weak, so when the PDMS-hydrogel hybrid is strained, once there is a difference in stress on PDMS and hydrogel, the hybrid will be decoupled. The water will continue to evaporate to the gap between the PDMS and hydrogel, which also cause dehydration of the hydrogel.

The solution is to form a hydrophilic surface on the elastomer and bond the hydrophilic surface to the hydrogel. And on the other hand, a strong chemical bond between elastomer and hydrogel is also essential to prevent slippery between layers. To create a robust bond between PDMS and hydrogels, benzophenone( $(C_6H_5)_2CO$ ) is used as a dopant for PDMS networks [166, 168, 170]. Benzophenone is photosensitive and is soluble in organic solvents. When benzophenone is exposed to UV light, it is excited to abstract a hydrogen atom from methyl groups of the PDMS. Graft polymerisation of vinyl monomers is excited, and acrylamide is grafted on PMDS, forming a polyacrylamide network. Benzopinacol is generated as a side product. In this way, a PDMS-hydrogel hybrid is bonded. The chemical reaction scheme is shown in Figure 5-2.

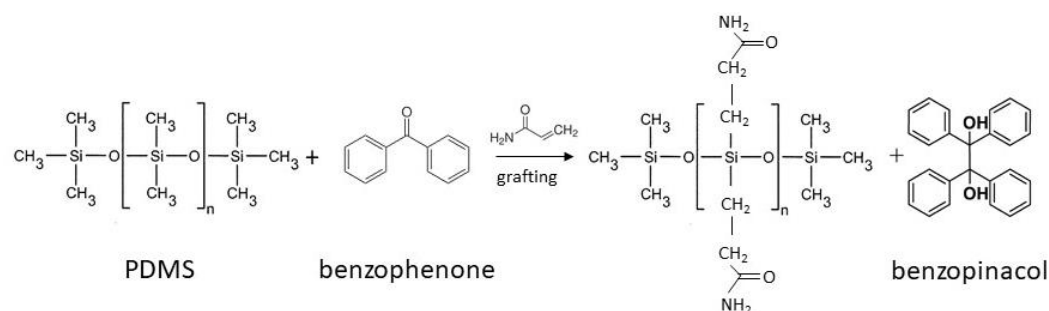


Figure 5-2 Chemical scheme of photo-grafting on the PDMS. Vinyl monomers are grafted on PMDS with the help of benzophenone.

The hydrogel solution is then filled between the modified PDMS and a cured hydrogel. After UV irradiation, a new hydrogel layer is formed connecting the modified PDMS and the cured hydrogel. In this case, the PDMS can be bonded to the hydrogel.

As shown in Figure 5-3 and Figure 5-4, a conductive polyacrylamide hydrogel and a PDMS encapsulated soft strain sensor was placed on a Petri dish in a ventilated room at room temperature for 24 hours. The humidity and temperature were recorded by a digital humidity and temperature monitor (Xiaomi, Beijing, China). The scale reading was taken every hour. The conductive hydrogel turned dried out, and the contained NaCl crystallised and lost 66.48% of weight after 24h. At the same time, the encapsulated hydrogel remained in its primary status and lost 0.43% of weight after 24h.



Figure 5-3 Water retention test setup for hydrogel samples. The hydrogel sample encapsulated by PDMS was exposed to the air for 24h at room temperature.

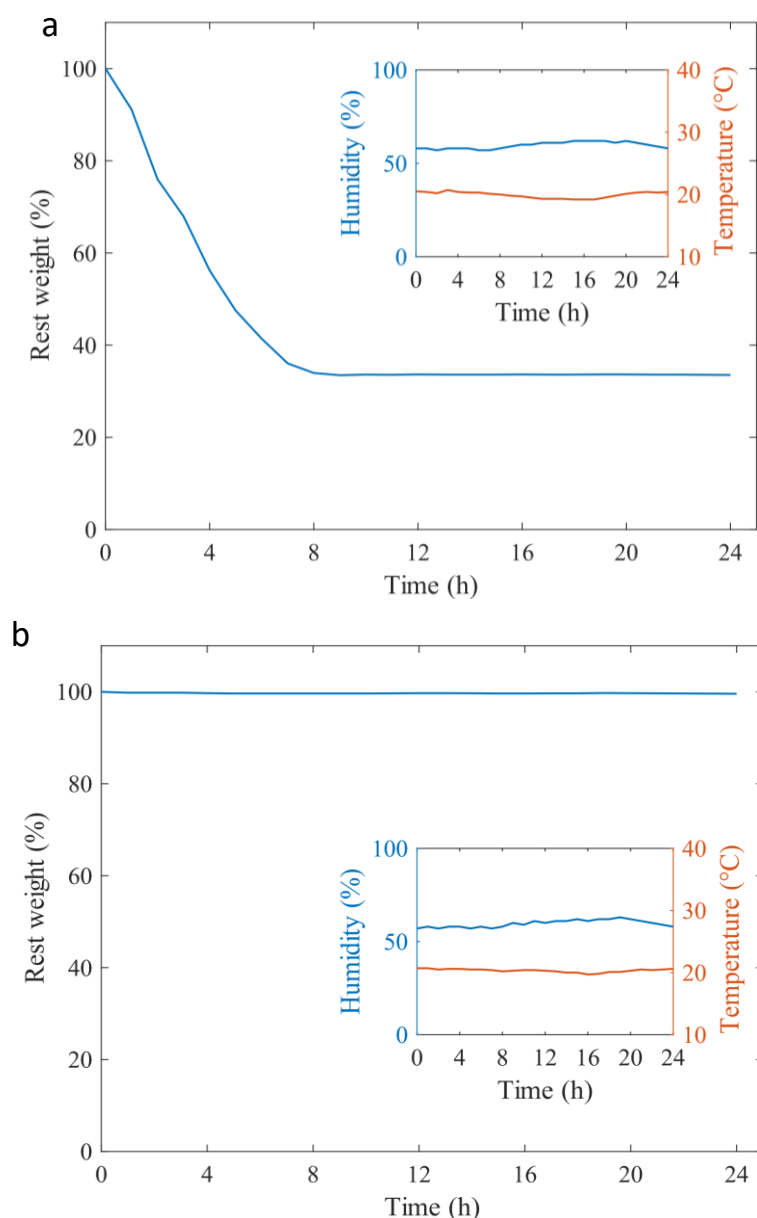


Figure 5-4 Results of water loss test for hydrogel samples. a) Water loss record for hydrogel sample without encapsulation. b) Water loss record for hydrogel sample with PDMS encapsulation.

### 5.1.3 Sensor fabrication

Figure 5-5 illustrates the encapsulation process of the hydrogel. A thin PDMS film was fabricated by pouring PDMS pre-solution into a Petri dish and curing it at room temperature (around 20 C°). The Petri dish was placed on a levelled plate to ensure that the PDMS pre-solution flowed horizontally and formed a uniform film. By calculating the weight of the PDMS pre-solution poured and the known area of the Petri dish, the

final thickness of the PDMS film was approximately 100  $\mu\text{m}$ . The fully cured PDMS film was then washed with methanol and deionised water for use in a later process. After PDMS was fully dried, a benzophenone solution (10 w/v% in ethanol) was applied to one surface of PDMS film for 2 mins to form a medium between the PDMS and the encapsulated hydrogel. The PDMS film was washed three times with methanol to remove excess benzophenone solution.

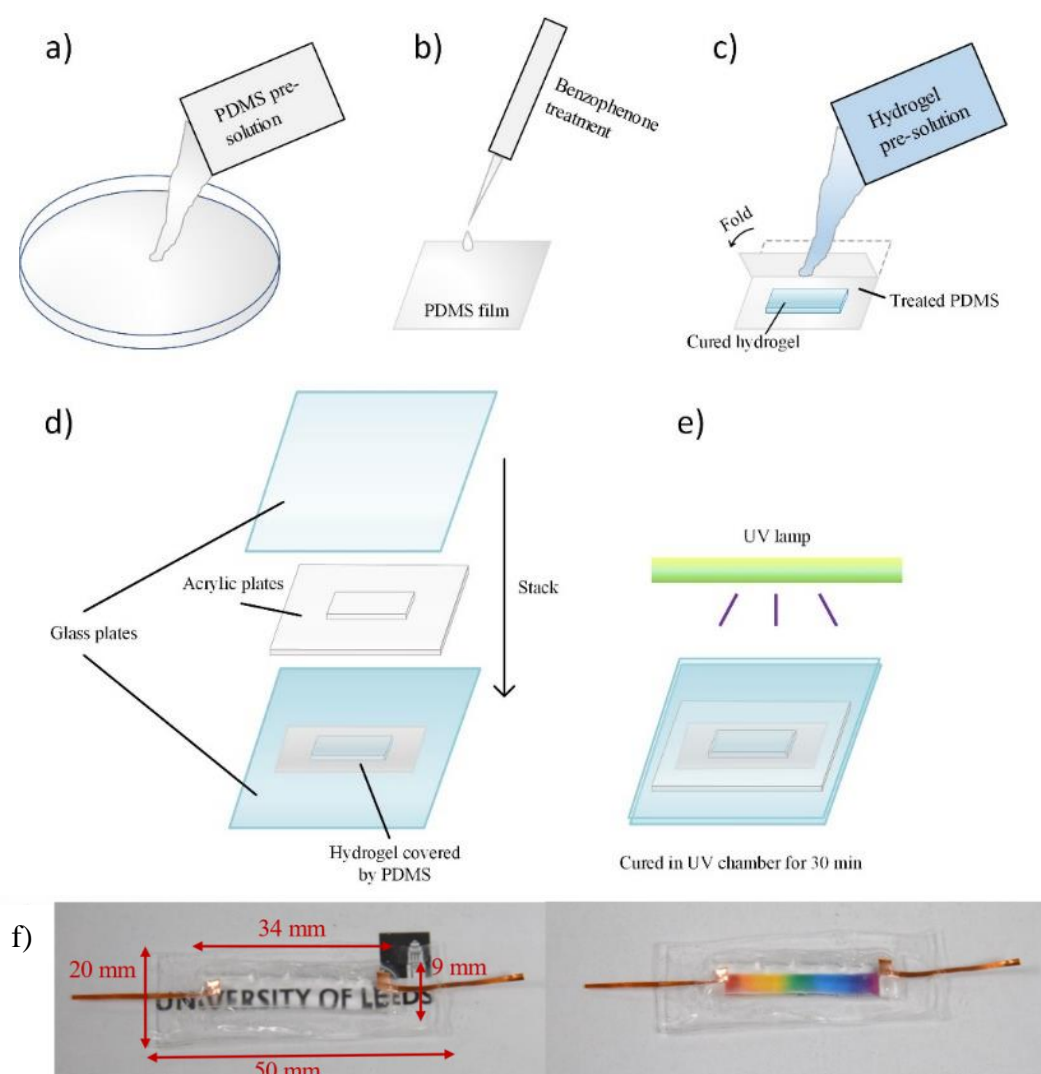


Figure 5-5 Fabrication of a PDMS-coated soft strain sensor. a) formation of a 100  $\mu\text{m}$  thick PDMS film. b) surface modification of PDMS by benzophenone. c) hydrogel covered by PDMS film. d) a mould was applied to constrain the hydrogel and PDMS film. e) the sensor was cured by UV oven of 365 nm wavelength. f) production of hydrogel-PDMS hybrid.

---

The PDMS film was cut into a rectangular shape (40×50 mm) and peeled from the Petri dish. A hydrogel (9×34×2 mm) was placed on the modified side of the PDMS. Two copper sheets (30×3×0.1 mm) were inserted into the edges of the hydrogel to act as electrodes. 2 ml of hydrogel solution was added to bond hydrogel and PDMS film. The PDMS film was then folded to encapsulate hydrogel and hydrogel solution inside.

An acrylic mould was covered on the PDMS and hydrogel to constrain its shape. The acrylic mould was made by laser cutting a rectangular slot (10\*36 mm) in a 3mm thick acrylic sheet. The volume of the slot in the acrylic sheet was larger than the hydrogel to ensure that additional hydrogel solution was filled inside the PDMS film to form the PDMS-hydrogel hybrid layer.

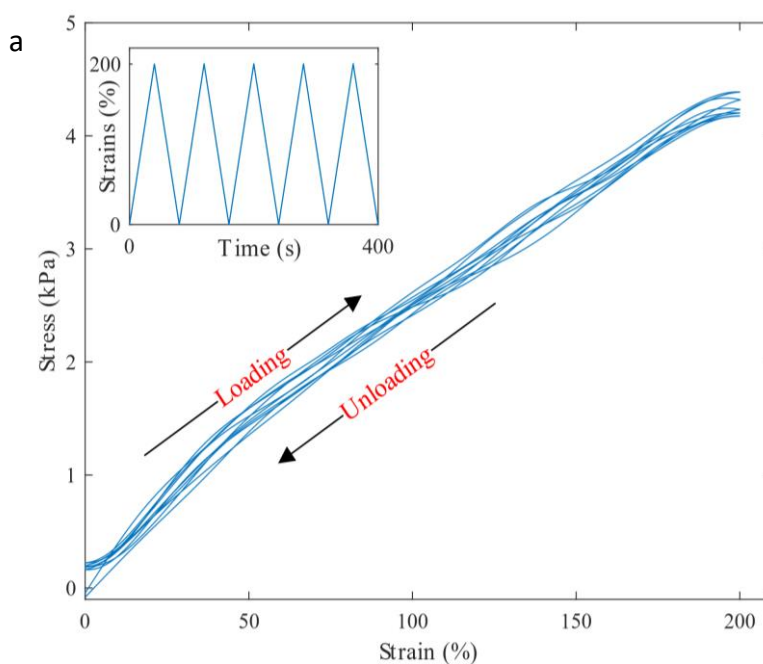
The sample was then placed in a UV chamber (365nm ultraviolet, UVP CL-1000) for 20 mins. Two glass plates were used to sandwich an acrylic plate to constrain the cross-linking process. Clippers were used to tighten the two glass plates and to drain extra hydrogel solution out of the mould.

## **5.2 Modelling and Characterisation**

This section presented the mechanical and electrical tests on the proposed fully elastomeric soft sensor. First, a cyclic test was conducted on the hydrogels made of selected formulation to testify the soft strain sensing materials were robust for repeat deformation. Then a peel test was conducted to validate the bond between hydrogel and PDMS, which ensured the stability and robustness of the soft sensors. At last, the strain sensor was tested for a cyclic load-unload case and a step tensile case to characterise its strain sensing ability.

## 5.2.1 Cyclic test on hydrogels

The results of the cyclic loading-unloading test for the baseline recipe of hydrogel (1.1 M acrylamide, 0.0006 MBAA of acrylamide, 16% w/v NaCl, 0.1% w/v Irgacure and 90 min UV exposure) are shown in Figure 5-6. Considering the potential applications of soft sensors on soft robots or human motion monitor, the hydrogel sample was set to stretch to 200% tensile strain at a speed of 0.5mm/s and released to its original length for five cycles using the same set-up as the previous tensile breakdown test. The tensile stress reached 4.29 kPa at the maximum strain of 200%. The electrical resistance of the conductive hydrogel was 41.2% higher at 200% tensile strain than its resistance at its original length.



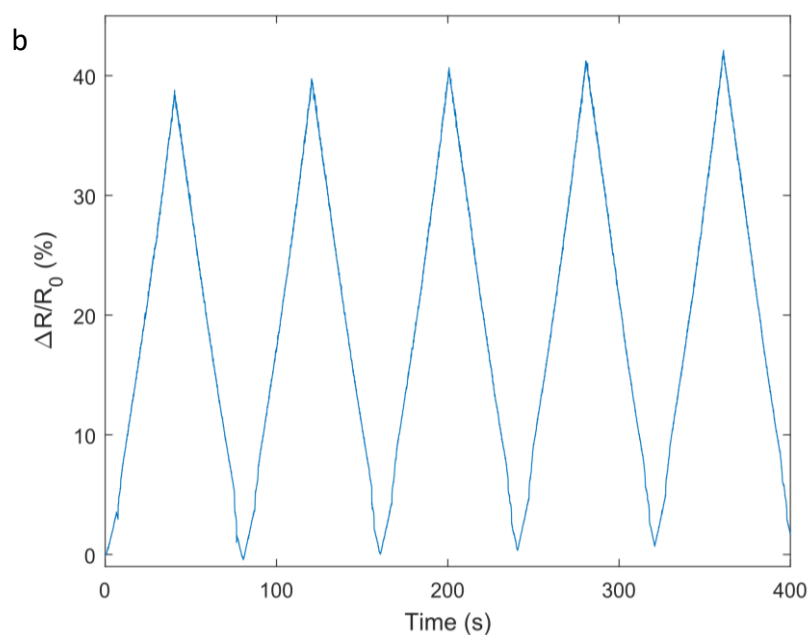


Figure 5-6 Tensile strain test on baseline recipe of the hydrogel. a) mechanical properties on tensile stress vs strain. b) electrical resistance changes during the tensile test.

## 5.2.2 Peel test of the soft sensor

Peel tests were conducted to test the bond strength of the PDMS-hydrogel hybrid [166]. A PDMS-hydrogel hybrid was fabricated in dimensions of 80mm by 10mm. One surface of the PDMS was treated with benzophenone to be bonded with the hydrogel. The PDMS side on the bottom was stuck by a double-sided tape (Scotch Permanent Double-Sided Tape, 3M) on a sliding rail to move horizontally. The adhesion between PDMS and double tape should be stronger than the PDMS-hydrogel bond in order to peel the hydrogel off the PDMS. Superglue was applied to stick hydrogel and a thin and bendable acrylic film. While the acrylic film and hydrogel were pulled up, the PDMS-hydrogel was moving horizontally to ensure the force measurement was all vertically. The test setup is shown in Figure 5-7.

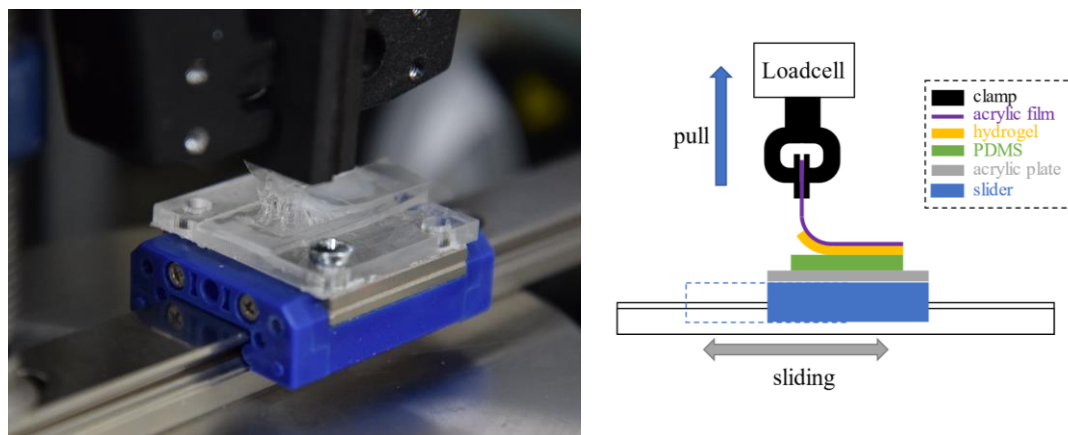


Figure 5-7 Peel test setup on hydrogel-elastomer hybrid. The PDMS-hydrogel hybrid was installed on a sliding rail to move horizontally. The hydrogel was stuck to an acrylic film, and it was peeling off the PDMS by pulling up the acrylic film.

The tests were carried out by pulling the acrylic film vertically, as shown in Figure 5-8. A tension test machine (INSTRON 5943) was used with a 50N loadcell (INSTRON). The pulling speed was set at 1mm/s for all samples. All the tests were carried out at room temperature.

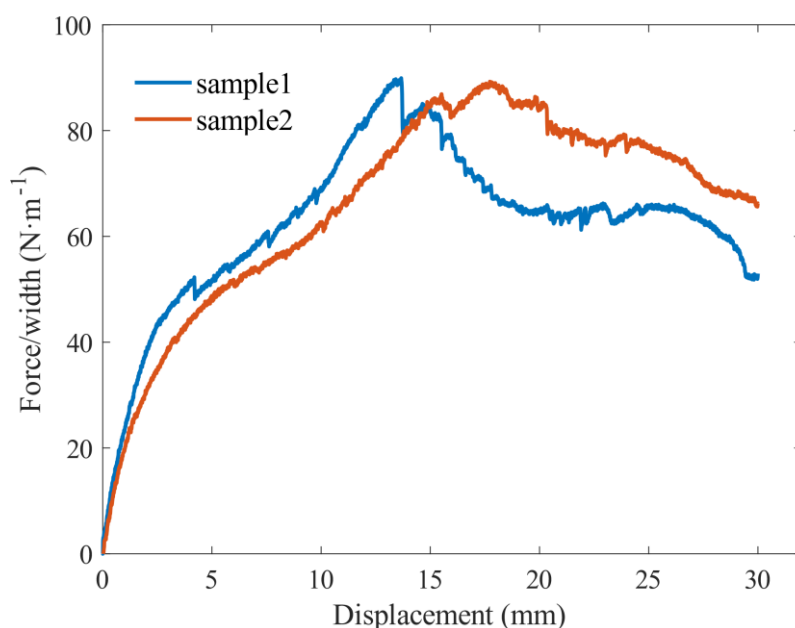


Figure 5-8 Peeling test of hydrogel and PDMS bonding. The force/width over the peeling displacement was recorded to show the bond strength of the hydrogel-elastomer hybrid.

### 5.2.3 Electrical properties test on the soft sensor

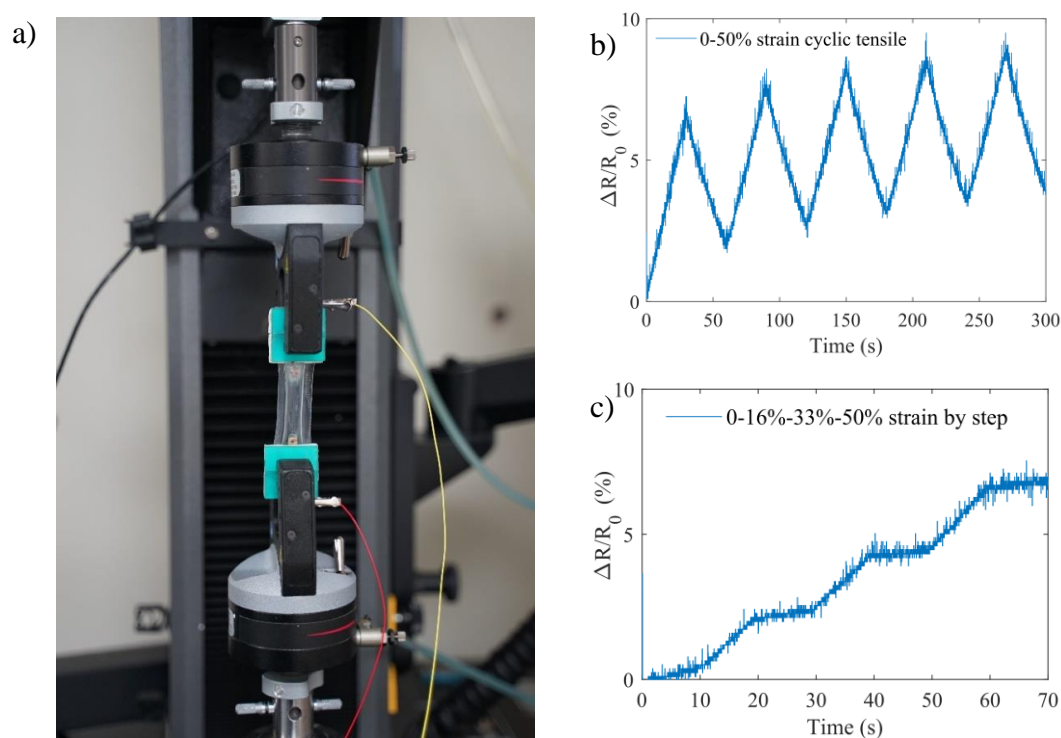


Figure 5-9 Electrical property test. a) Configuration of test and results of tensile test. b) 0-50% strain cyclic tensile test of  $\Delta R/R_0$  resistance change. c) 0-16%-33%-50% step strain tensile test of  $\Delta R/R_0$  resistance

Figure 5-9 (a) shows the configuration of the test and the results of resistance changes during the tensile test. The tested sample was fabricated by a hydrogel strip using the baseline above recipe (1.1M acrylamide, MBAA 0.0006 weight of acrylamide, 16% w/v NaCl, 0.1% w/v Irgacure, 90 min UV dose). This strain sensor sample used two copper films as electrodes to connect conductive hydrogels and outside measuring circuits. A myRIO was applied to record the analogy voltage signal with 12 bits ADC (0-5V, 1.221 mV step) from measuring circuits. A pair of pneumatic clippers clamped the strain sensor under a pressure of 7 kPa. The tensile test was conducted on an INSTRON 5943 test bench in a strain range of 0 to 50%.

---

## **Cycling load-unload test of soft sensor**

A cyclic 0-50% tensile test was conducted to confirm the stability of electrical resistance of the soft strain sensor as most stretched in the potential application was in 0-50%. The test bench repeatedly pulled the sample from an initial length of 20 mm to 30 mm (50% strain) at a speed of 0.5 mm/s and then released the sample to the initial length at the same speed. The resistance change of the soft strain sensor was recorded as shown in Figure 5-9 (b).

The loading and unloading test results of the soft sensor showed that a 7.25% higher resistance was recorded when the soft strain sensor was firstly pulled to 50% strain, compared to the unpulled soft strain sensor. The resistance of the soft strain sensor was also 1.6% higher when the sensor was relaxed to its initial place. When the loading and unloading test continued, the initial resistance of the soft strain sensor turned out to increase over test time. The peak resistance of the soft strain sensor also increased over test time. At the same time, the difference between peak resistance at 50% strain and its previous initial resistance at 0% remained the same.

## **Step tensile test of soft sensor**

A 0-16%-33%-50% step tensile test was also conducted to confirm the stability of electrical resistance of the soft strain sensor. The test was divided into 4 stages by strain of 0, 16%, 33% and 50%. The test bench was paused and held for 10 seconds at each stage and then pulled to another stage at a speed of 0.5 mm/s. The electrodes of the soft strain sensor were connected to the measurement circuit. The connected myRIO recorded the analogue signal of the measurement circuit.

The results of the 0-16%-33%-50% step tensile test were shown in Figure 5-9 (b). They suggested that the resistance of the soft strain sensor increased when the soft

---

strain sensor was stretched. When the soft strain sensor was pulled to 16%, an average 2.3% higher resistance was measured than the sensor at 0% strain. At 33% strain, the soft strain sensor had a 4.5% higher resistance than at 0% strain. The soft sensor had an average 6.8% higher resistance at 50% strain than the initial resistance. An increase in resistance was observed when the sensor was held at one stage. The increase was notable at 0% strain. At the end of holding the soft strain sensor at 0% strain for 10 seconds, the sensor's resistance increased by 0.6%.

## **5.3 Application of soft strain sensor**

The soft strain sensor addresses the problem of monitoring the movement of human joints or soft robots. Finger joints have a large bending angle up to  $120^\circ$ . It is usually hard to attach a sensor to the finger joint without disturbing its bend. A soft strain sensor, which is stretchable and soft, can adjust closely to the finger joint and not obstruct the movement of fingers. The movement monitoring of a soft actuator is similar to human joint monitoring. Soft actuators are easier affected due to their softness when attached with other objects like movement sensors. The soft strain sensor would be able to monitor the movement of soft actuators without affecting them.

### **5.3.1 Monitoring finger joint movement**

The proposed soft strain sensor was applied as a movement monitor at the finger joint. The soft sensor was taped on a finger covering the joint when the finger was relaxing. The tape (Scotch Permanent Double-Sided Tape, 3M) wined the finger to bond two soft strain sensor ends on the finger. Then the finger was relaxed and bent for 5 seconds repeatedly. When the finger was relaxing, the two sides of the joint were at  $0^\circ$ . While the fingertip was bent to touch the other side of the finger, the two sides of the joint were approximately  $120^\circ$ . The electrodes of the soft strain sensor were wired to the

resistance measuring circuit to measure the resistance of conductive hydrogel. The ratio of resistance changes was recorded by a myRIO during the movement, as shown in Figure 5-10.

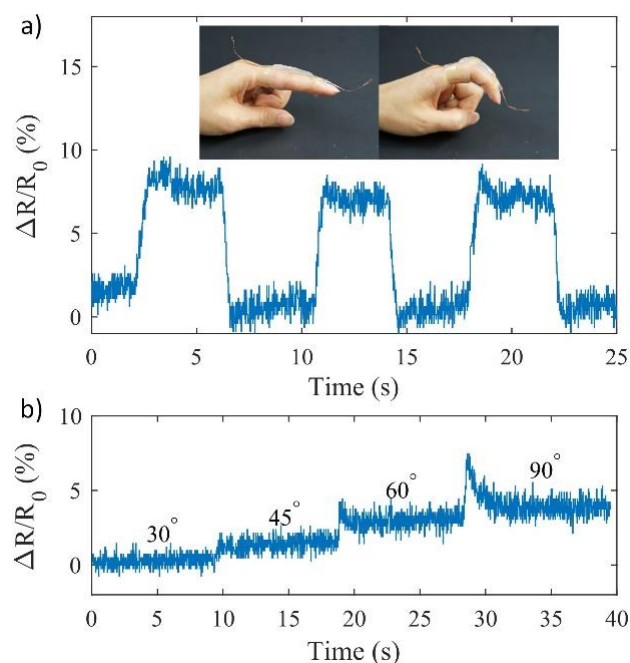


Figure 5-10 Case studies of the soft strain sensor. a) soft strain sensor as a monitor of finger bending by resistance change compared to its original length resistance. b) finger bended to 30°, 45°, 60° and 90°.

The finger bending and relaxing test results are shown in Figure 5-10(a). When the finger was bent from a relaxed straight state, the resistance of the soft strain sensor changed by approximately 10%. When the finger was relaxed, the resistance of the soft strain sensor increased slightly over time. And when the finger was bending, the resistance of the soft strain sensor reached a peak and then decreased over time.

At the same measuring configuration, Figure 5-10 (b) record the resistance changes of the soft strain sensor when the finger was bent to 30°, 45°, 60° and 90°, holding for 10 seconds. As the results are shown in Figure 5-10 (b), the resistance of the proposed soft strain sensor raised when the bending angle of the finger increased. But the resistance would decrease when the finger held the position and angle of bending.

### 5.3.2 Monitoring soft tentacle movement

The soft sensor was then applied to a soft pneumatic tentacle. The two ends of the soft sensor were taped to the tentacle with double tapes (Scotch Permanent Double-Sided Tape, 3M). And the pneumatic tentacle was hanging in mid-air by the connected air tube. The pneumatic tentacle was operated to bend through a programmed pneumatic pressure system with constant air pressure increment control at a constant inflating speed of 0.05 psi/sec (0.01 psi of pressure step precision). As the tentacle was inflated to 2.5 psi and bent gradually to a degree, the sensor was strained. The tentacle held for 10 seconds when it was inflated to the end. The measurement circuit measured the resistance, and the changes were recorded by myRIO, as shown in Figure 5-11.

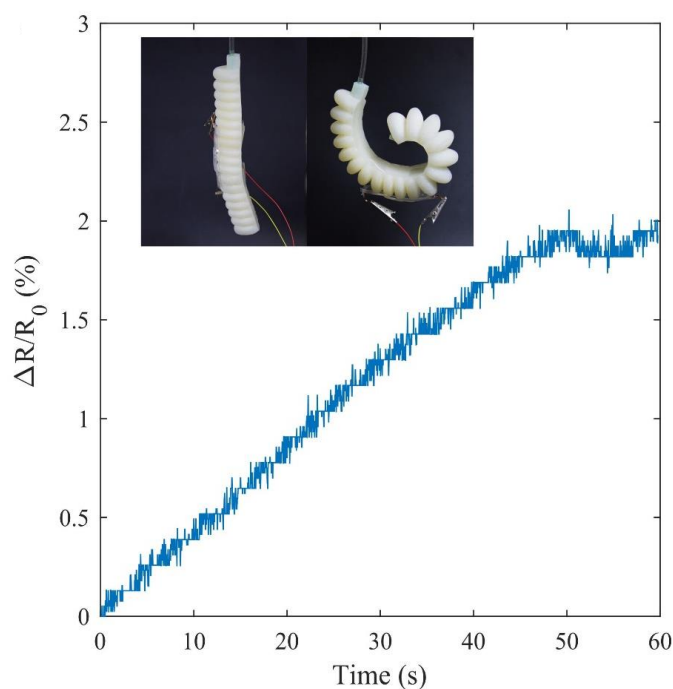


Figure 5-11 Soft strain sensor applied to sensing the bending of a pneumatic actuator. The pneumatic actuator was inflated to bend and then hold.

As the results suggest, the soft strain sensor's electrical resistance kept increasing when the pneumatic actuator was bending to stretch the installed soft strain sensors. The maximum resistance change was 1.9% appearing at the endpoint of the

---

bend of a pneumatic actuator. The resistance increases of the tested soft sensor showed linearity when the pneumatic actuator is bending at a constant speed. The resistance of soft sensors showed a decline and a return afterwards when the pneumatic actuator was holding still.

## 5.4 Discussion and Summary

Existing soft sensors had paved outstanding performance for soft strain sensors in terms of stretchability, softness and durability. However, several aspects can be further developed of existing soft sensors, 1) compared to soft sensors filled with nanowire and conductive liquid, a fully elastomeric soft sensor will enable linearity in strain measurement, 2) transparent encapsulation of hydrogel sensor can bring a fully transparent soft sensor extending applications to occasions requiring optically clarity, 3) integration of strain sensor with softness, stretchability, elasticity, durability and transparency has not been proposed yet.

A fully elastomeric soft strain sensor was designed to address the above gaps in existing research. The bonding of PDMS and hydrogel provided a robust hybrid with high mechanical performance, including linear elasticity, high deformation and low stiffness. The encapsulation of PDMS also assisted hydrogel for high water retention, allowing the conductive hydrogel to maintain electrical and mechanical properties. The integrated soft strain sensor made by hydrogel-PDMS hybrids was applied to monitoring joint movement and soft robot. The applications showed the potential of a fully elastomeric strain sensor in softness, stretchability, elasticity, durability and transparency.

In hydrogel fabrication, glass plates were used as part of the fabrication mould. In the beginning, transparent acrylic plates were applied as a mould, but the hydrogel

---

pre-solution failed to cure under the same period of UV exposure as the glass plates mould. This effect may be because the acrylic plates absorbed part of the UV, which cause a lack of radical energy in the hydrogel pre-solution. A higher temperature was observed when using transparent acrylic plates than the glass plates. The usage of glass plates will, to some degree, affect the complicity of the mould because of the low manufacturing ability of glass. When fabricating a more complex structure, the glass mould is less applicable. Thus, materials that suit the UV fabrication of hydrogel should be investigated.

In the electrical characterisation of the soft strain sensor, an increase in electrical resistance was observed when the measuring circuit started to work. At the same time, no strain was applied to the soft sensor. This resistance increase may be due to the reaction of copper electrodes and NaCl solution in hydrogel under electrical current. Copper atoms were excited and combined with free chloride ions. When the generated copper chloride exceeded its solubility, it started to crystallise. At the end of the test, green powders appeared on the hydrogel. The decrease of free chloride ions would cause a rise in the electrical resistance of hydrogel. A solution for this problem would be altering the copper electrodes with platinum or gold electrodes.

In summary, this chapter presented a fully elastomeric soft strain sensor with high performance in softness, stretchability, elasticity, durability and transparency. A sensor structure was first designed with a PDMS layer encapsulating the conductive hydrogel for anti-dehydration. Water retention and peeling test were conducted to validate the robust bond between hydrogel and PDMS. The sensor fabrication method using UV initiation was then studied. Cycling load-unload tests then characterised the produced soft strain sensor. At last, the proposed fully elastomeric soft sensor was applied to finger bending and soft tentacle movement monitoring.

# **Chapter 6**

## **Case Study: Soft Tactile Sensor and Soft 2D Strain Sensor**

The previous chapter presents a fully soft strain sensor by conductive hydrogels and PDMS encapsulation. This chapter further explores the applications of soft sensors made of conductive hydrogels and hydrogel-PDMS hybrids. This chapter presents two case studies, including a multi-electrodes soft tactile sensor and a 2D soft strain sensor.

## 6.1 Case Study 1: Soft Tactile Sensor

This case study examines the application of multi-electrode detection to conductive hydrogels sensing. By applying multi-electrode detection, the sensor can simultaneously detect both magnification and position of the stimulus. In this case, the hydrogel sensor can localise both the pressure and location of the touch.

The objectives of the case study are:

**Objective 1** – *Demonstrate the pressure sensing ability of the conductive hydrogel through the resistive sensing method.*

**Objective 2** – *Explore the effect and enhancement of multi-electrode detection to the conductive hydrogel.*

### 6.1.1 Materials and design

A 25×25×1 mm hydrogel film by standard hydrogel recipe is prepared. The hydrogel sample is connected to 8 electrodes. The eight electrodes are scanned in sequence to measure the electrical resistance between the two electrodes.

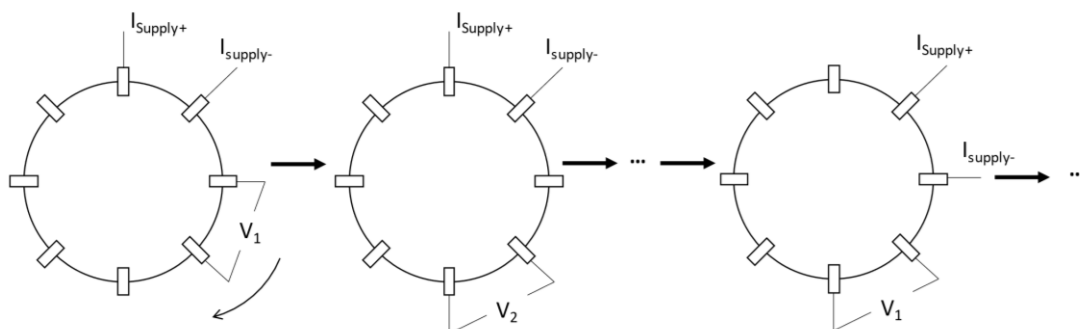


Figure 6-1 Schematic of the sequential scan. In each scan, two neighbouring electrodes are first served as exciting electrodes. A constant current is output through the two exciting electrodes.

As shown in Figure 6-1, two neighbouring electrodes are first served as exciting electrodes in each scan. A constant current is output through the two exciting electrodes.

The rest six electrodes consist of 5 pairs of neighbouring electrodes. The voltage on each pair of neighbouring electrodes will be recorded. Then, one of the exciting electrodes is switched to the next electrode beside the previous exciting electrodes. The newly selected electrode and the other electrode in previous exciting electrodes consist of a new pair of exciting electrodes. At the same time, the other six electrodes consist of 5 pairs of neighbouring electrodes as measuring electrodes to record their voltage reading. The switching of exciting electrodes covers half of the total electrodes due to the symmetric layout of the electrodes.

### 6.1.2 Test configuration

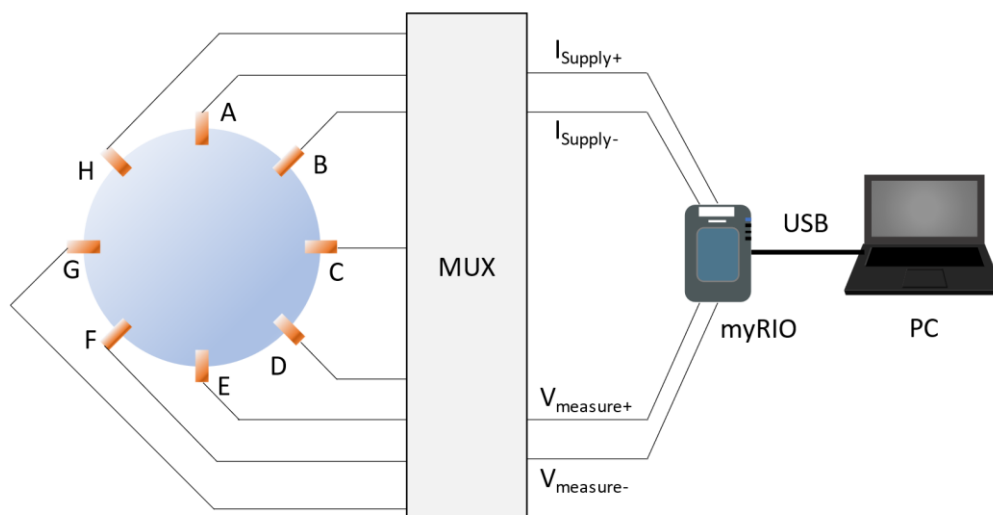


Figure 6-2 Configuration for multi-electrodes sensing. The sensing system consists of 8 electrodes, multiplexers, myRIO and PC.

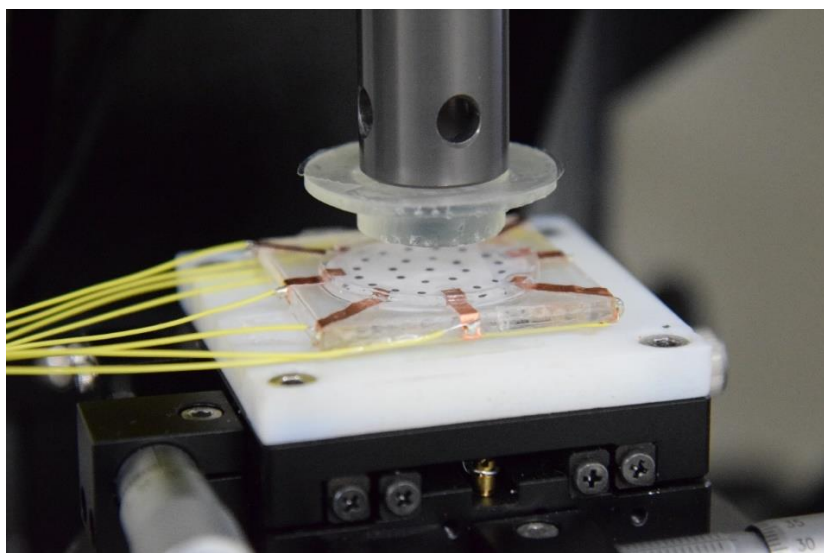


Figure 6-3 Photo for the indentation test. The hydrogel sample was placed on an acrylic plate which was stuck on the X-Y table. The electrodes were stuck on the acrylic plate and under the hydrogel sample.

As shown in Figure 6-2, a multi-electrode sensing system is designed with eight electrodes. Three low-voltage dual 1-of-4 multiplexers (IDT74CBTLV3253, IDT, Santa Clara, CA), connected in series, are applied to the sensing system. The current supply wires and voltage measure wires connect to one end of multiplexers and the myRIO. The myRIO is running in FPGA mode at a 10 kHz sampling rate. There are 4 pairs of exciting electrodes in each scan by 5 measuring electrodes, which is 20 channels in total. In this case, the actual sampling rate is 500 Hz (10 kHz/20). And the data of myRIO is transferred to the PC and stored on the PC.

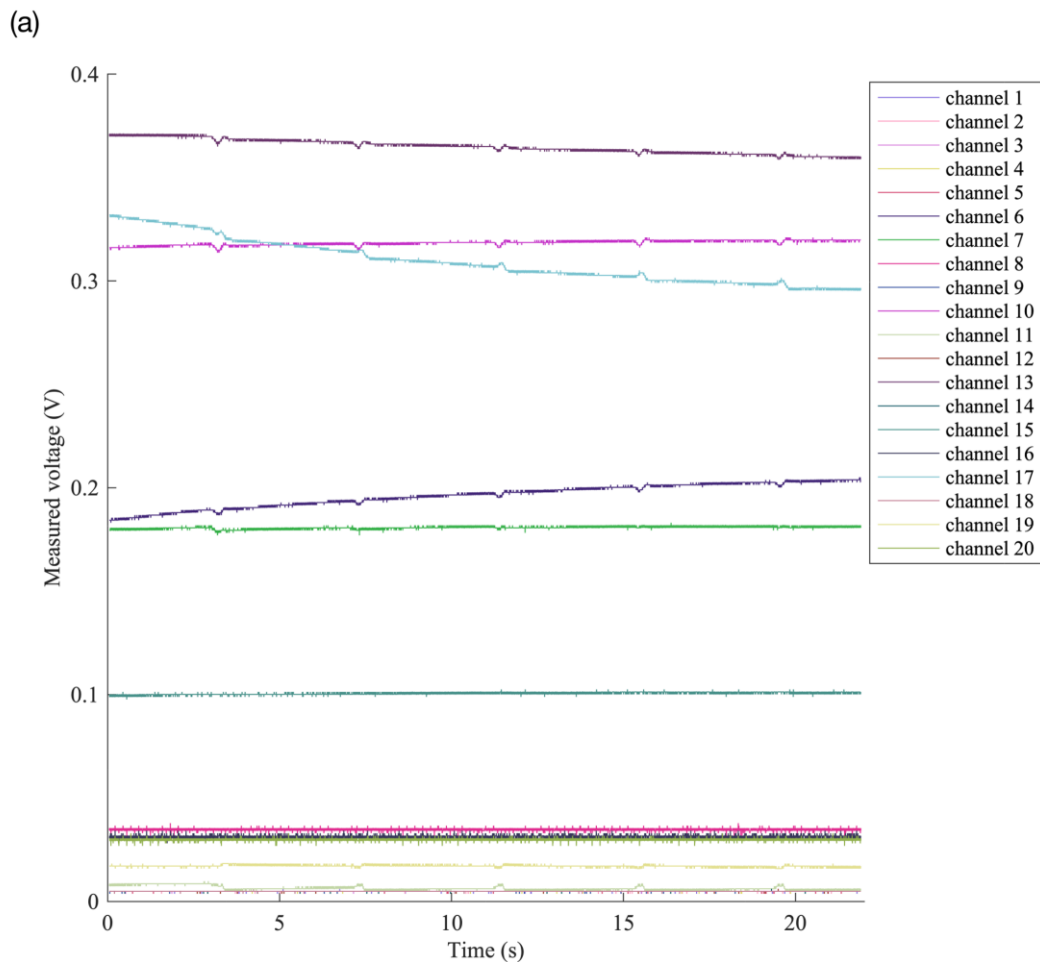
To test the multi-electrode soft sensor, an indenter will be installed on a 50 N load cell connecting to the test bench (Instron 5943, Instron, Norwood, MA, USA).

As shown in Figure 6-3, a 20 mm diameter indenter with a flat head was applied in the test, which was 3D printed (form 3, Formlabs, Somerville, MA, USA). To test the multi-electrode soft sensor, the indenter was installed on a 50 N load cell connected to the test bench (Instron 5943, Instron, Norwood, MA, USA). By adjusting the X-Y table under the sample, the indenter was able to compress a different area of the sensor. Five indentation targets were set up in the experiment, the centre point of the hydrogel

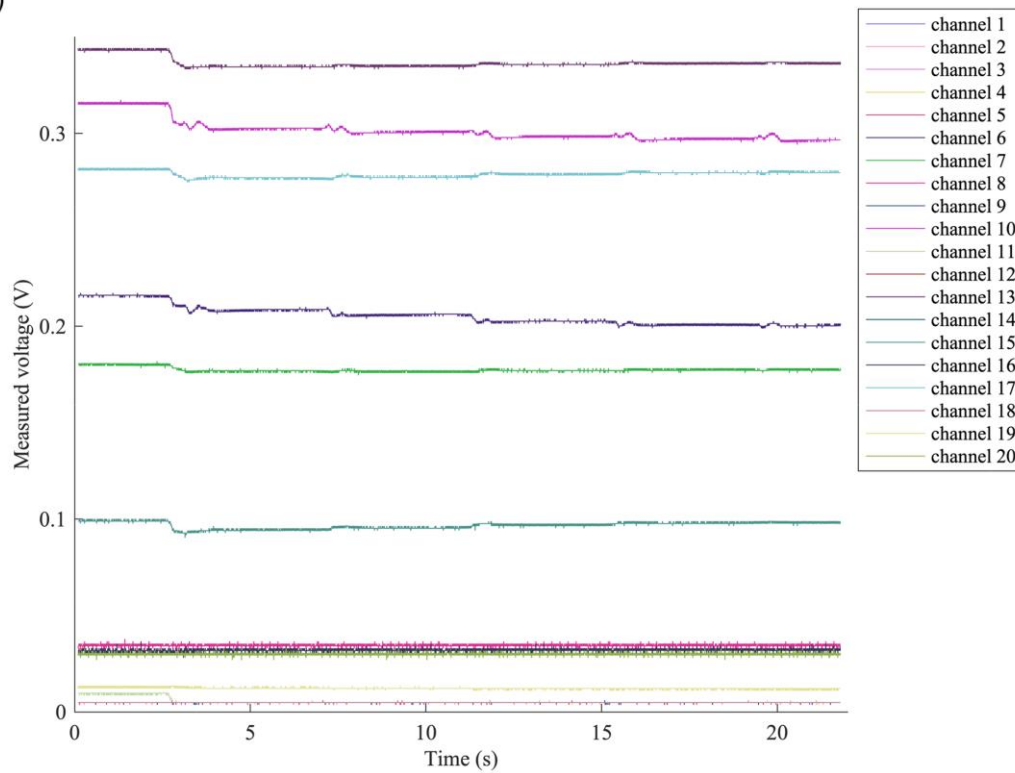
film and four symmetrical points 2mm off centre in the four directions of top, bottom, left and right. In each test, the indenter moved vertically up and down at a speed of 2mm/s and compressed the sample to 0.4 mm in depth.

### 6.1.3 Results

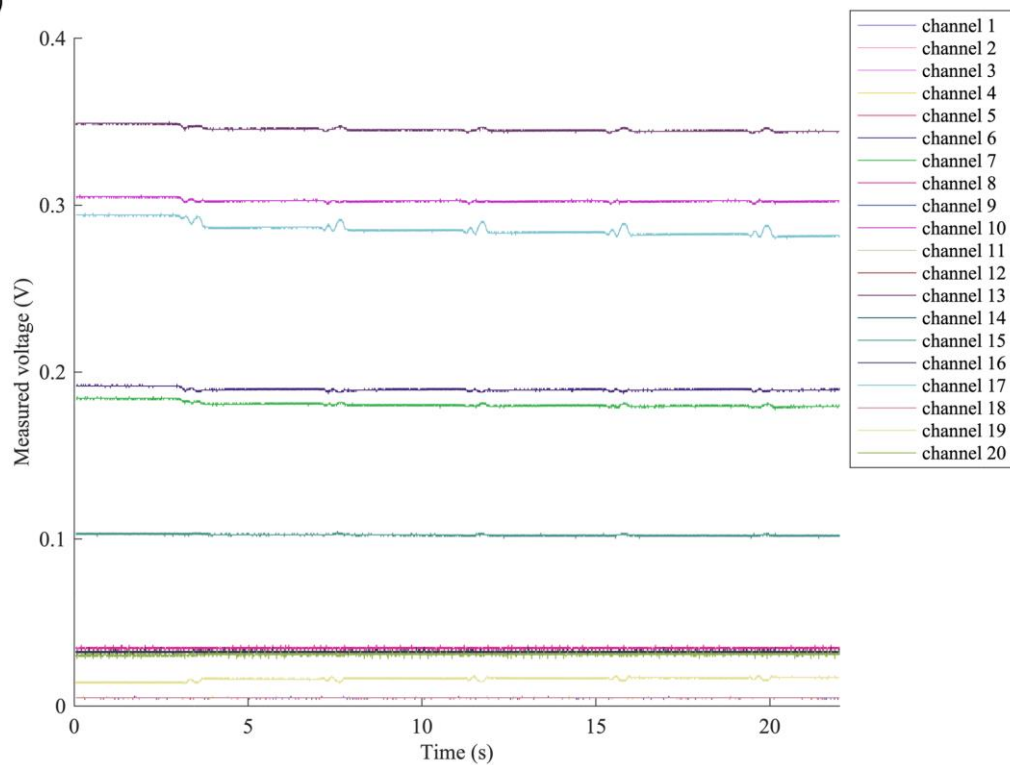
As shown in Figure 6-4, each channel of the multi-electrode sensing system has a different response to the different indentation positions. Shown in the figures, the voltage measurements were divided into several groups of voltage levels from 0 to 0.4 volts.



(b)



(c)



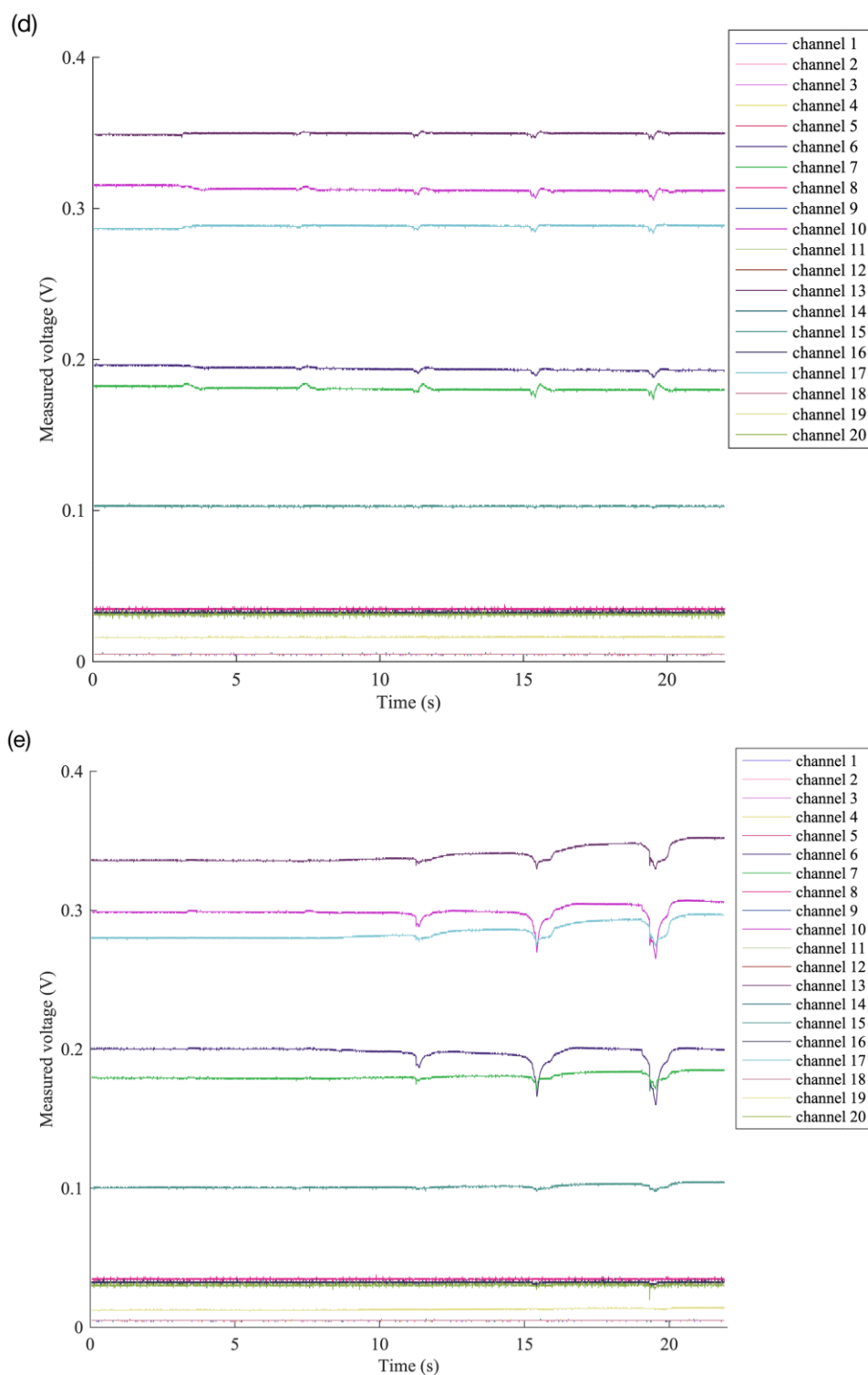


Figure 6-4 Test results for multi-electrode sensing. Each line in the figure represents one channel of measurement. a) The indenter was targeting the centre of the hydrogel. b) The indenter was targeting 2 mm off the centre of the hydrogel in the direction of the top. c) The indenter was targeting 2 mm off the centre of the hydrogel in the direction of the left d) The indenter was targeting 2 mm off the centre of the hydrogel in the direction of the bottom, and e) The indenter was targeting 2 mm off the centre of the hydrogel in the direction of right.

Figure 6-4(a) shows that the measured voltage had minor fluctuations responding to the indentation because the indentation was in the centre and close to every exciting electrode. On the contrary, as shown in Figure 6-4(e), there were the most significant fluctuations of the measured voltages because the position of indentation was on the left, and all the exciting electrodes were located on the right.

Considering the magnitude of the fluctuation of each channel and its position, the indentation can be located in a 2D plane. The magnitude of the fluctuation is described by,

$$f = \frac{\Delta V}{V_0} \quad (6 - 1)$$

where  $\Delta V$  is the gained voltage responding to the indentation and  $V_0$  is the initial voltage without indentation.

As previously described, the larger the distance from exciting electrodes, the larger the fluctuation. To simplify the calculation, let the fluctuation be proportional to the distance,

$$f \propto s \quad (6 - 2)$$

where  $s$  stands for the distance from the indentation position to the exciting electrodes. In the ideal situation, the data of the fluctuation  $f$  cannot be perfectly measured due to errors. The measured fluctuation  $f_m$  can be expressed as,

$$f_m \propto s_m \quad (6 - 3)$$

where  $s_m$  is the distance from the indentation position to the exciting electrodes calculated by measured data.

Let  $\mathbf{x}$  be the position for indentation, the possible position for indentation should be the minimum of the sum of the distance from  $\mathbf{x}$  to every circle with radius  $s_m$ ,

$$\min \sum_n^4 \sqrt{(\mathbf{x}^2 - s_{mn}^2)} \quad (6 - 4)$$

where  $n$  stands for the number of the exciting electrodes.

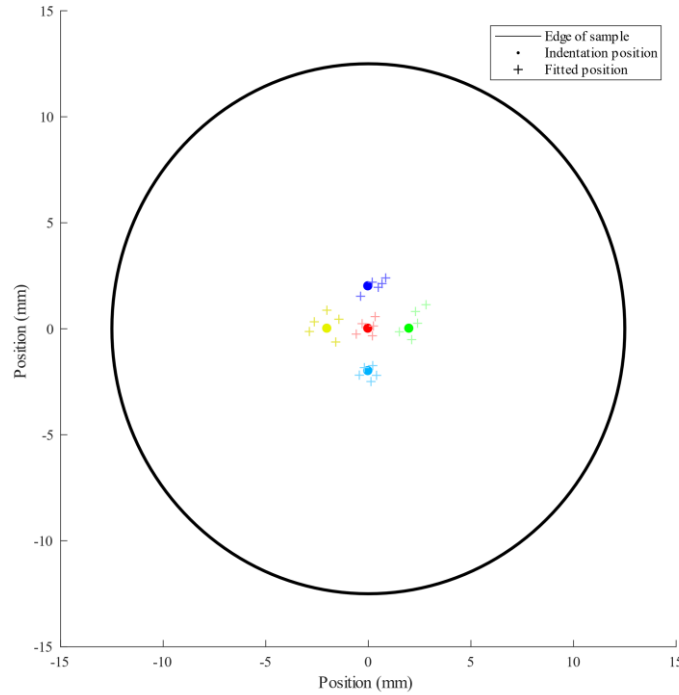


Figure 6-5 Fitted position of indentation. The outer circle represents the edge of the tested hydrogel sample. The coloured dot stands for the real indentation centre in the test. And coloured crosses are the fitting position for 5 runs of indentation in each position.

According to Equation (6-4), the test data of measured voltage can be used to fit the indentation position. The fitted results are shown in Figure 6-5. The results show that the multi-electrodes sensing for hydrogel can locate the indentation position for the 2D plane. Based on the size of the hydrogel sample, the locating error  $e$  of indentation is calculated by,

$$e = \frac{\sqrt{\mathbf{p}^2 - \mathbf{p}_f^2}}{d} \quad (6-5)$$

where  $\mathbf{p}$  is the real position of indentation,  $\mathbf{p}_f$  is the fitted position of indentation and  $d$  is the diameter of the hydrogel sample.

By Equation (6-5), the average locating error for the multi-electrodes sensing system is 1.54% with a standard deviation of 0.13%.

---

### 6.1.4 Discussion

This section presented a soft tactile sensor made of conductive hydrogels. A multi-electrode sensing system was applied to detect the resistance change. The multiple resistance changes were then post-processed to locate the indentation position on the sensor. The sensor achieved a precision of 1.54% average locating error with a standard deviation of 0.13%.

In the test, the measured voltage on each channel were related to the physical distance between the exciting electrodes and the measuring electrodes. A shorter distance showed a less current loss from the exciting electrodes and made a higher measured voltage. And the fluctuations of measured voltage responding to the indentation on the hydrogel were related to the distance between the location of indentation and exciting electrodes. Larger distance appeared to have larger fluctuations.

For each exciting electrode, the indentation position should be on the circle with radius  $s$ . And every circle should be intersected at one point, which is the indentation position. But  $s$  is not available in realistic tests, the circles with radius  $s_m$  cannot be intersected at one point.

There are five channels of measured voltages in the test set for a pair of excitation electrodes. Each channel of measured voltage has measurement error, and some channel has non-detectable change due to the resolution of ADC. The  $f_m$  for each channel would be the average of the measured voltage variations of the 5 channels.

---

## 6.2 Case Study 2: Soft 2D Strain Sensor

This case study presents a 2D soft strain sensor by extending the rectangular soft strain sensor in Chapter 4 to a 2D planar structure. The final product is an array of soft strain sensors. 9 electrodes are located at the centre and edge of the PDMS film, 4 of which are activation electrodes and 5 of which are detection electrodes. The 4 activation electrodes are located at the midpoints of the 4 edges, and the 5 detection electrodes are located at the centre and 4 corners of the PDMS film. The hydrogel acts as a single soft strain sensing unit between each activation electrode and detection electrode. By sequentially measuring the electrical resistance change in the strain sensing units, the 2D strain change in the whole PDMS film are obtained.

The objectives of the case study are:

**Objective 1** – *Demonstrate a complex configuration of conductive hydrogel embedded in the fully elastomeric soft sensor to achieve bidimensional strain sensing.*

**Objective 2** – *Demonstrate the potential of hydrogel-PDMS hybrids to apply in complex structures and the reliability of related fabrication methods.*

### 6.2.1 Fabrication

As shown in Figure 6-6, a 30×30×1mm PDMS film with 0.2mm grooves was firstly fabricated by a 3D print mould. The mould had a 1mm groove for casting the sensor's body. And there were protruding patterns in the 1mm groove to create 0.2mm grooves in the sensor. The PDMS pre-solution of the standard recipe was injected into the groove of the 3D printed mould. The PDMS film was cured at room temperature for 48

h. Then the PDMS film was peeled off the 3D printed mould. The grooves on the PDMS film were treated with benzophenone according to the procedures in Chapter 4. Later the PDMS film was filled with hydrogel pre-solution of the standard recipe and covered by a glass plate to cure in the UV chamber.

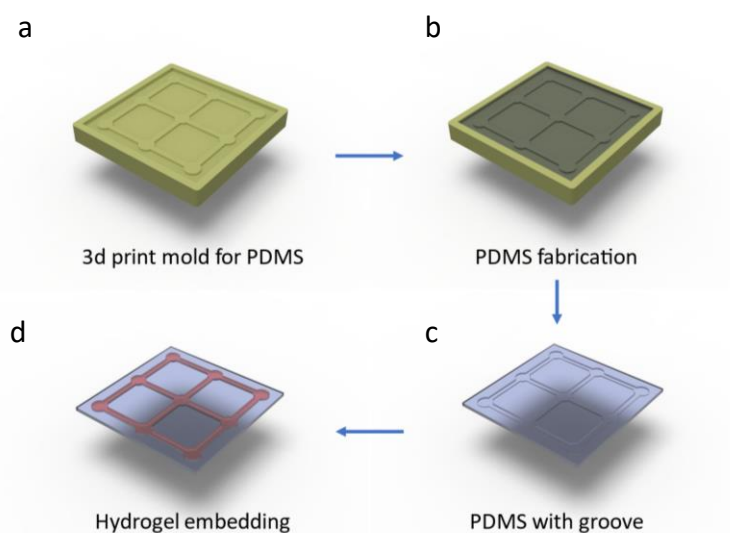


Figure 6-6 Fabrication of sensor array. a) a 3D printed mould was prepared for PDMS casting. b), c) a PDMS film with the groove was fabricated using the mould. d) conductive hydrogel was embedded into the groove.

## 6.2.2 Pull test

The sensor is tested by an INSTRON 5943 (Instron, Norwood, MA, USA) universal testing system in the pull test. The sensor is fixed on an acrylic plate clamped by a pair of anti-slippery clamps installed on pneumatic grips (2712-05x, Instron, Norwood, MA, USA). The pneumatic grips are connected to the testing system. Pulling force is obtained by a 50N loadcell and recorded at a sampling rate of 500 Hz. Displacement of pulling and running time is also recorded by the testing system.

The strain sensor array is divided into 12 sensing units according to the 12 beams of hydrogels on the array. A measuring circuit using digital multiplexers is designed to measure and record the 12 sensing units in real-time on the soft strain sensor

array. FPGA on myRIO is applied to extend its data communication and record speed. The electronic schematic is shown in Figure 6-7. A low-voltage dual 1-of-4 multiplexer (IDT74CBTLV3253, IDT, Santa Clara, CA) is used to connect to the 4 activation electrodes. The 4 channels are independently controlled by the myRIO digital signal output. Another two same-model multiplexers are applied to control the 5 detection electrodes. One uses 4 channels to control the on/off of 4 corner detection electrodes. And another one uses one channel to control the on/off of the centre detection electrodes and uses one channel to switch the multiplexer connecting to 4 corner detection electrodes.

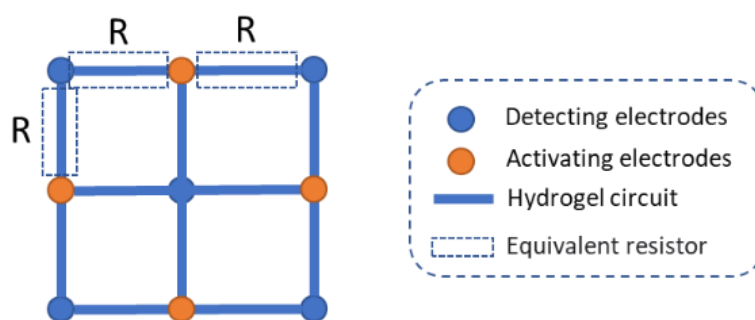


Figure 6-7 schematic of electrodes distribution for the sensor array. Each beam of the hydrogel circuit is an equivalent resistor. Detecting and activating electrodes are set at the joint of beams.

During the pull tests, magnets are applied to ensure the conductivity between the electrodes and the conductive hydrogel. A pair of magnets are clamped to the top of the electrode and the back of the sensor, which is PDMS film. The magnetic clamps provide good stability and adaptability when the sensor is stretched.

There were four cyclic pull tests conducted with two installation methods of sensors and two displacements, as shown in Figure 6-8. The sensor was firstly clamped on two diagonal corners and pulled diagonally for 2mm and 4mm displacement. And then, the sensor was clamped vertically on the top and bottom edges and pulled parallelly for 2mm and 4mm displacement. The testing system ran the pull test at 2

mm/s. For each installation and displacement, there were 5 rounds of hold-pull tests. The sensor was held for 5 seconds and then pulled to destination displacement and held for another 5 seconds. After the holding, the sensor was returned to the initial position at the same speed. The installation of the sensor is shown in Figure 6-9.

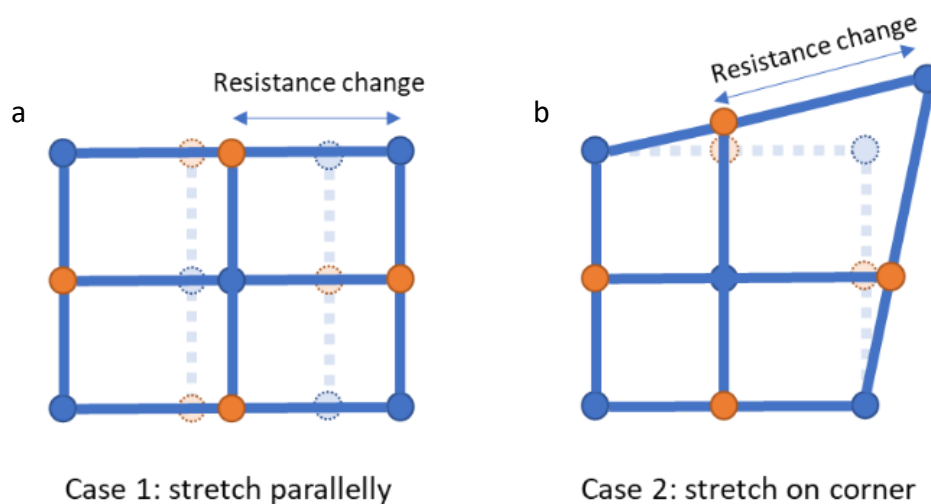


Figure 6-8 Schematic of pull test on soft strain sensor array. a) the sensor was stretched parallelly, and the beams of the sensor extended equally. b) the sensor was stretched diagonally, and the beams of the sensor extended unequally but symmetrically.

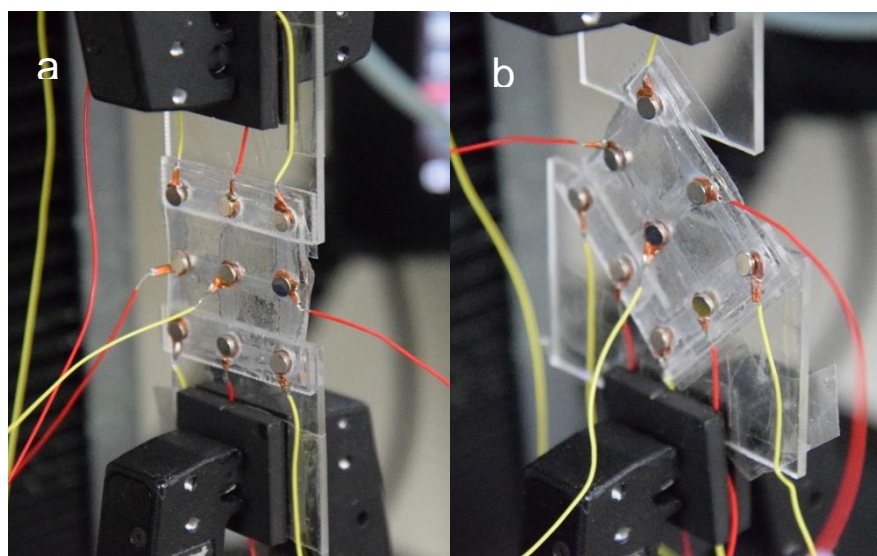


Figure 6-9 Installation of sensor sample. The sensor sample was stuck on the acrylic plate clamped by pneumatic grips. Red wires stand for the exciting electrodes, and yellow wires stand for the measuring electrodes. a) pull test on vertical direction. b) Pull the test in the diagonal direction.

### 6.2.3 Results

The test results of pull tests on the strain sensor array in different directions and strains are presented in Figure 6-10 to Figure 6-13. The results first show the displacement of the pull test as a reference for the test progress. The resistance changes of each part of the sensor are then presented in groups according to the change patterns. And sections with different change patterns are also compared. Finally, a visual graph of resistance changes is plotted to show the overall effect on the strain sensor array.

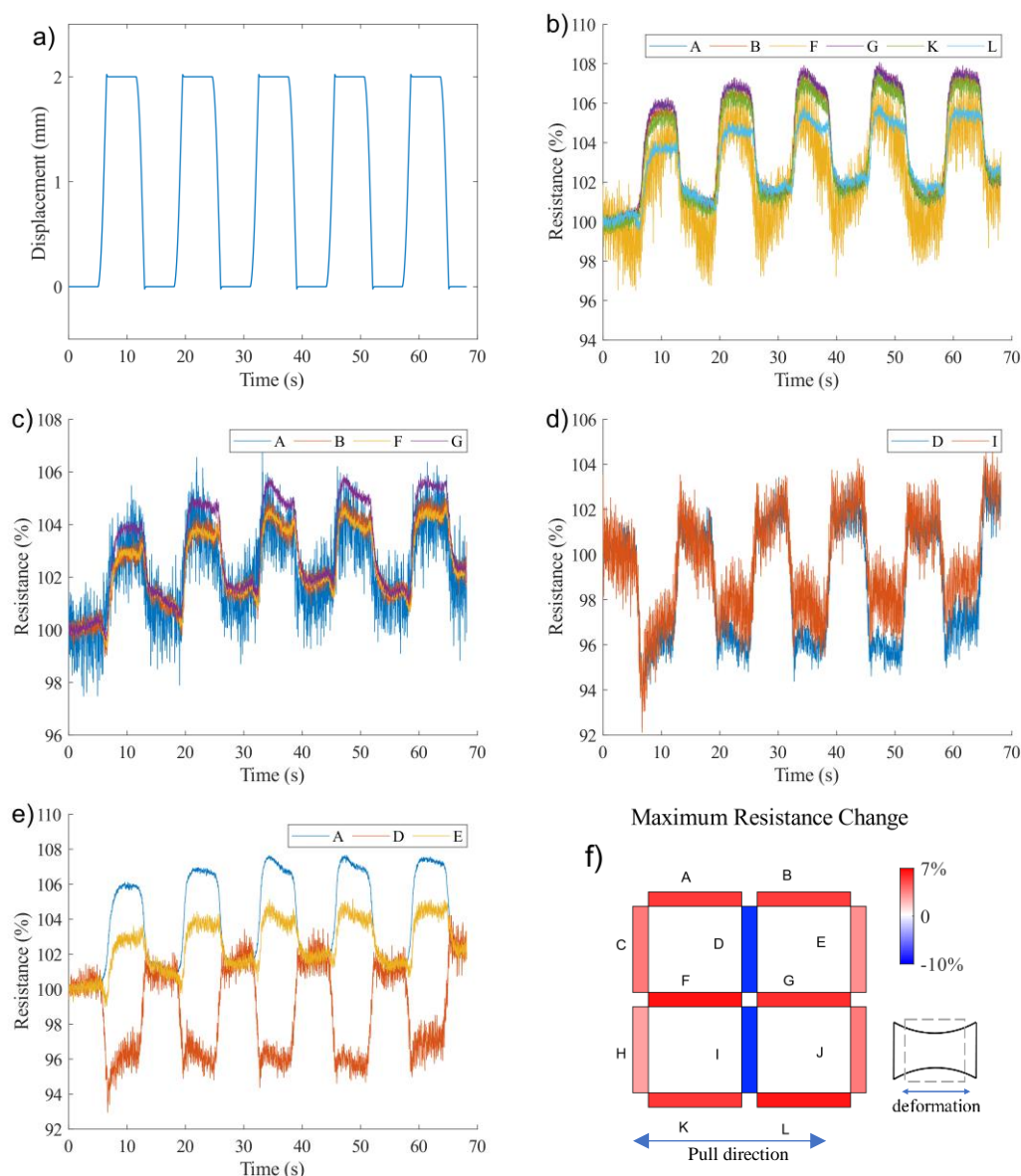


Figure 6-10 Resistance changes during the 2 mm parallel pull test. The sensor array can be divided into 12 beams of hydrogel strain sensors. a) Displacement vs time in the pull test. b) Six beams were parallel

to the pull direction. The resistance of the six parallel beams raised to 107% of the initial resistance. c) Four beams were located at the edges of the sensor array and were vertical to the pull direction. The resistance of the four vertical beams raised to 103% of the initial resistance. d) Two beams were located at the centre of the sensor array and were vertical to the pull direction. The two beams showed negative changes in resistance to 90% of the initial resistance. e) Comparison of three different resistance change patterns. f) Visualization of the resistance change. The shape of deformation is schematic but mathematically constructable.

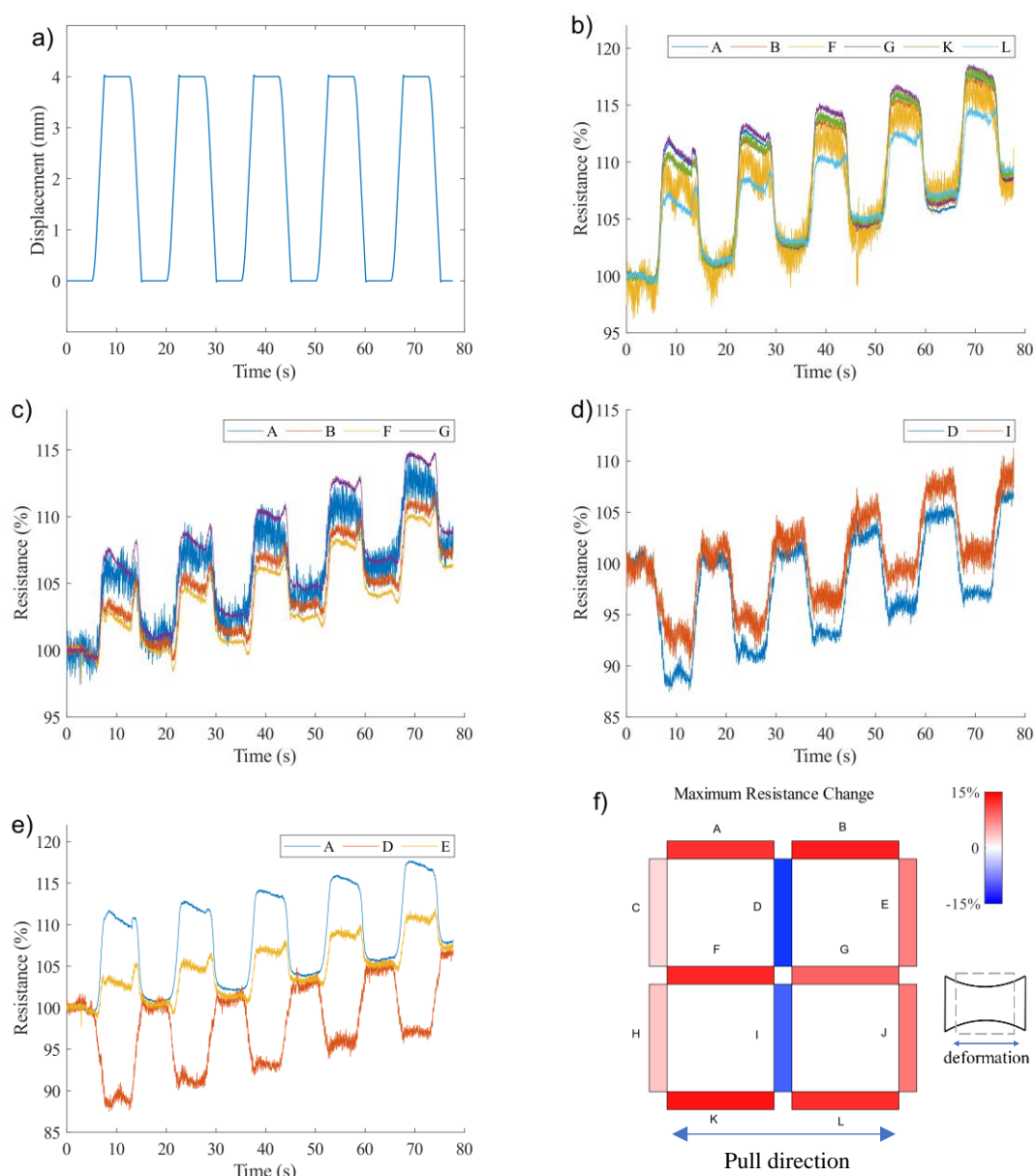


Figure 6-11 Resistance changes during the 4 mm parallel pull test. The sensor array can be divided into 12 beams of hydrogel strain sensors. a) Displacement vs time in the pull test. b) Six beams were parallel to the pull direction. The resistance of the six parallel beams raised to 113% of the initial resistance. c) Four beams were located at the edges of the sensor array and were vertical to the pull direction. The resistance of the four vertical beams raised to 105% of the initial resistance. d) Two beams were located at the centre of the sensor array and were vertical to the pull direction. The two beams showed negative

---

changes in resistance to 85% of the initial resistance. e) Comparison of three different resistance change patterns. f) Visualization of the resistance change. The shape of deformation is schematic but mathematically constructable.

For the parallel pull test, there are three patterns of resistance changes in the sensor array, as shown in Figure 6-10(e) and Figure 6-11(e).

The six beams of hydrogels that are parallel to the pull direction have the largest resistance changes, up to 107% and 113%, respectively, for 2mm and 4mm displacement, compared to the initial resistance, as shown in Figure 6-10(b) and Figure 6-11(b). The most significant resistance changes match the largest strain in the same direction.

The resistance of the four beams at the edges of the sensor array also have increased up to 103% and 105%, respectively, for 2mm and 4mm displacement, compared to the initial resistance, as shown in Figure 6-10(c) and Figure 6-11(c). Since the resistance are measured on long-axis, the relatively smaller resistance changes indicate these beams of the hydrogel are not strained in their long-axis direction.

The rest two beams located in the centre have a dropdown to 90% and 85%, respectively, for 2mm and 4mm displacement, compared to the initial resistance when the sensor array is pulled vertically to the long axis of the beams, as shown in Figure 6-10(d) and Figure 6-11(d). The dropdowns in resistance indicate negative strains in the long-axis direction of the two beams in the centre. These negative strains match the effect when a rectangular elastomer is pulled.

The resistance changes are visualised in coloured bars in Figure 6-10(f) and Figure 6-11(f). Comparing the 2 mm and 4 mm displacement pull tests, the larger strain brings larger resistance changes.

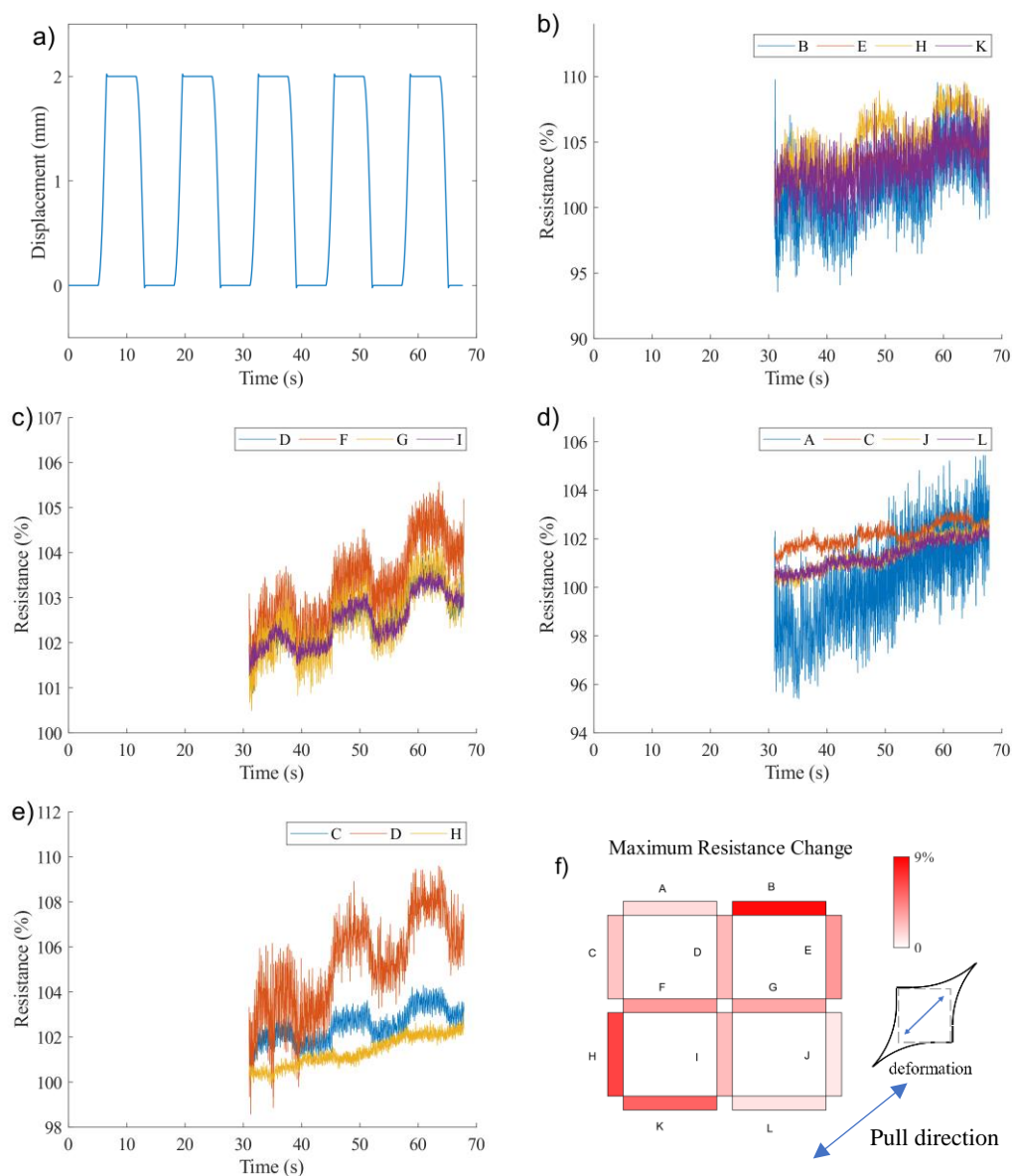


Figure 6-12 Resistance changes during the 2 mm diagonal pull test. The sensor array can be divided into 12 beams of hydrogel strain sensors. The resistance data from 0s to 31s are invalid in this test. a) Displacement vs time in the pull test. b) Four beams were located at the fixing corners of the diagonal pull tests. The resistance of the four parallel beams raised to 109% of the initial resistance. c) Four beams located at the centre of the sensor array. The resistance of the four vertical beams raised to 101% of the initial resistance. d) Four beams were located at the corner of the sensor array and far away from the fixing corners of the diagonal pull tests. The four beams showed changes in resistance to 103% of the initial resistance. e) Comparison of three different resistance change patterns. f) Visualisation of the resistance change.

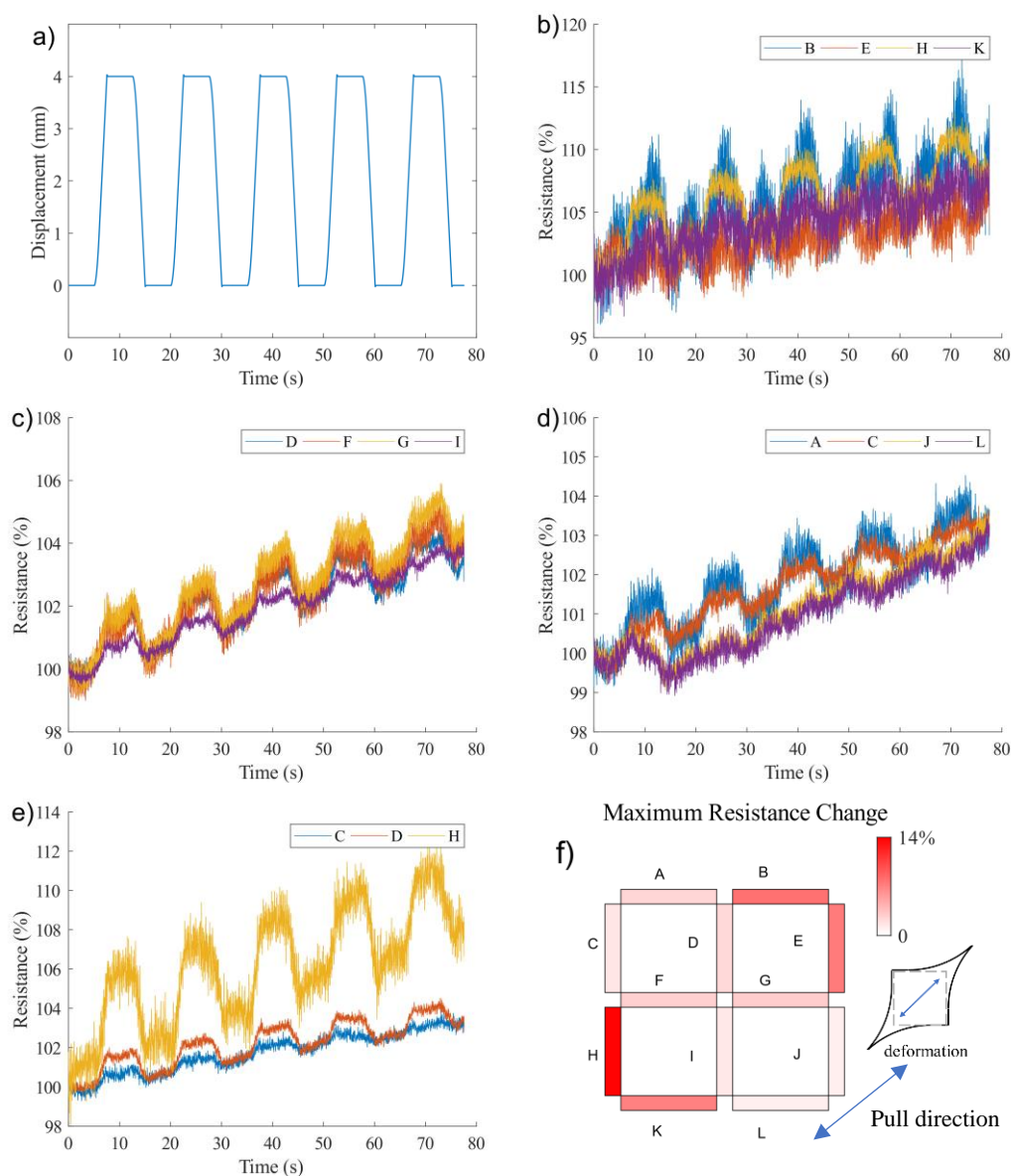


Figure 6-13 Resistance changes during the 4 mm diagonal pull test. The sensor array can be divided into 12 beams of hydrogel strain sensors. a) Displacement vs time in the pull test. b) Four beams were at the corners of the sensor array and at the ends of parallel diagonal. The resistance of the four parallel beams raised to 114% of the initial resistance. c) Four beams were located at the centre of the sensor array. The resistance of the four vertical beams raised to 101% of the initial resistance. d) Four beams are located at the corners of the sensor array and the ends of the vertical diagonal. The four beams showed changes in resistance to 102% of the initial resistance. e) Comparison of three different resistance change patterns. f) Visualisation of the resistance change.

Similar to the parallel pull tests, there are three patterns of resistance changes for the sensor array in the diagonal pull tests, as shown in Figure 6-12(e) and Figure 6-13(e).

---

The four beams of hydrogels which are at the corners of the sensor array and the ends of the parallel diagonal have the largest resistance changes, up to 109% and 114%, respectively, for 2mm and 4mm displacement, compared to the initial resistance, as shown as in Figure 6-12(b) and Figure 6-13(b).

The four beams of hydrogels which are at the centre of the sensor array have the smallest resistance changes up to 101% and 101%, respectively, for 2mm and 4mm displacement, compared to the initial resistance, as shown in Figure 6-12(b) and Figure 6-13(b).

The four beams of hydrogels which are at the corners of the sensor array and at the ends of the parallel diagonal have resistance changes up to 102% and 102%, respectively, for 2mm and 4mm displacement, compared to the initial resistance, as shown as in Figure 6-12(c) and Figure 6-13(c).

Figure 6-12(f) and Figure 6-13(f) showed the resistance changes of 12 beams of the sensor array. In the observation of the pull test, when the square elastomeric sensor array was pulled in the diagonal direction, the sensor array had the most significant deformation in the parallel diagonal, most minor deformation in the vertical diagonal and moderate deformation in the centre. In this case, the resistance changes of 12 beams of the sensor array are synchronous to the strain changes when the sensor array is pulled in the tests. By drawing the 12 beams with different lengths, the resistance changes of the sensor array can rebuild the outlines of the strain of the sensor array in the pull tests.

## **6.2.4 Discussion**

In this section, a soft 2D strain sensor was presented for multi-directional strain sensing. The sensor was built from the hydrogel-PDMS hybrid presented in Chapter 5. The PDMS layer provided insulation for the conductive layer working on the potential

---

conductor, such as human skin. The hydrogels were designed as several resistive beams and distributed in different directions to obtain bidimensional strain sensing.

In the current form of sensors, the hydrogel was exposed to the air for easy installation of exciting and detecting electrodes. However, the conductive hydrogel faced the risk of dehydration that would affect both electrical and mechanical properties. The fabrication of the soft strain sensor can be improved by the PDMS encapsulation methods presented in Chapter 5. In that case, the electrodes should be entirely redesigned to ensure stable excitation and detection.

In the pull test, the exciting and detecting electrodes were clamped and installed by pairs of magnets. Instead of applying glue or clipper to fix the electrodes, which may change the stiffness or shape of the hydrogel, the clamp of magnets minimised the effect on the conductive hydrogel. The electrodes and their installation on conductive hydrogels remained for further study.

The pull test results showed that the 2D strain sensor had high sensing resolution, up to 4%/mm of resistance change. The resistance change can be easily and rapidly separated, in which case the data processing of the sensor can be implemented by a low power mobile computing chip. This allows possible stand-alone devices to be developed.

## **6.3 Summary**

In this chapter, two case studies on soft sensors are presented through the techniques developed in Chapters 4 and 5. The first case study explores the potential of applying multi-electrode detection on conductive hydrogels, making soft-touch sensors possible. This case study uses basic and primitive conductive hydrogel films during complex

---

detection and sensing configurations. The complete setup is suitable for the mass production of printed integrated circuits. The second case study presents a two-dimensional soft strain sensor by extending the rectangular soft strain sensor from Chapter 5 to a two-dimensional planar structure. Both case studies extend the use of conductive hydrogel and hydrogel-PDMS bonding techniques. This study shows the potential of 3D printing hydrogel circuits on surface-modified PDMS films to build complex sensor arrays through conductive hydrogels.

# Chapter 7

## Discussion and Conclusion

This thesis has built a framework to utilise ionic conductive hydrogels for soft sensors, addressing the effect of variant formulation on the mechanical and electrical properties, enabling tuneable conductive hydrogel for applications. The fabrication using UV gives a rapid and straightforward method for conductive hydrogels. The research on hydrogel-PDMS hybrid solves hydrogel dehydration and makes robust use of conductive hydrogel for soft sensors. The applications presented in this thesis demonstrate the potential of conductive hydrogels used as soft sensors.

---

## 7.1 General Discussion

The fully elastomeric soft sensors presented in the thesis enabled a highly flexible, stretchable and transparent sensor. The techniques of design, fabricating, and characterising the hydrogel-PDMS hybrid also have potential in applying bio-mimic, medical, healthcare, and wearable devices. The following sections describe and discuss technical details not covered in the previous chapters and some findings that have meaningful implications for future research work.

### 7.1.1 Materials and fabrication

In previous research [47], the acrylamide-bisacrylamide hydrogel was conventional initiated by free radical initiator Ammonium Persulfate and accelerated by N,N,N',N'-tetramethyl ethylenediamine (TEMED). Due to the oxidation effect of ammonium persulfate (APS)[174, 175], the fabrication process required a non-oxygen chamber, such as a nitrogen chamber. Otherwise, the side effect of APS oxidation will lead to incomplete polymerisation. In this case, the fabrication needs to be finished within a short period, which complicates the fabrication process.

As a substitutive initiator, Irgacure 2959 is stable in oxygen conditions and has low toxicity in low saturation. In non-light-isolation conditions, Irgacure 2959 has a low initiating rate which ensures relative long-term storage of pre-mixed UV-polymerised hydrogel solution. A low saturation of 0.1% w/v Irgacure 2959 was used to consider reaction speed and toxicity.

The soft materials of polyacrylamide (PAAm) used in this thesis are selected by a UV initiating polymerisation method. This method advances in fewer components and higher stability in oxygen conditions and has low toxicity in low saturation. These

features improve the biocompatibility and fabricability of proposed fully elastomeric soft sensors. The mechanical and electric properties of fabricated conductive hydrogels were varied from the conventional Ammonium Persulfate (APS), and N,N,N',N'-tetramethyl ethylenediamine (TEMED) initiated fabrication method. In this case, variant recipes of hydrogel were fabricated and tested to locate the suitable one for soft sensors.

The casting mould used in the fabrication of hydrogels were carefully processed. The mould was consisted of two glass plates sandwiching laser cutting acrylic plates in the middle. The bottom and top plates were glasses because of higher surface energy, and hydrophilicity of mould would help the polymerisation of hydrogel under UV exposure. The hydrogel pre-solution was hard to start the polymerisation on the acrylic plate by tests. As the middle frames of the mould, acrylic plates, were laser cut with groove, there were errors in verticality on the edge of the groove. And the errors would sum up to create a tilting vertical surface. The tilting samples of hydrogel would affect the mechanical properties test.

In the encapsulation of hydrogel and PDMS, glass plates were also used as part of the fabrication mould. On this occasion, the hydrogel pre-solution should polymerise to bond surface-modified PDMS and hydrogel precursors. While applying the acrylic plate to clutch the PDMS and hydrogel precursors, the hydrogel pre-solution would not polymerise even without contacting to the acrylic plate. This effect may be because the acrylic plates absorbed part of the UV, which cause a lack of radical energy in the hydrogel pre-solution. A higher temperature was observed when using transparent acrylic plates than the glass plates. The usage of glass plates will, by some degree, affect the complicity of the mould because of the low manufacturing ability of glass. When

---

fabricating more a complex structure, the glass mould is less applicable. Thus, materials that suit the UV fabrication of hydrogel should be investigated.

### **7.1.2 Experiments**

There are two common failures of the tensile test for conductive hydrogels—the slipperiness of the hydrogel strip samples and the early break of the hydrogel samples. In the failing cases of the slippery hydrogel tensile test, there was a dropping in stress when the slipperiness started as a slippery curve. And in the failing cases of the early break of the hydrogels, the samples were obviously broken when the strain was less than the average strain of break. Both failures would largely affect the accuracy of the mechanical properties. The solutions for both cases were emphasising the clamp of the hydrogel samples. The samples were clamped by a pair of pneumatic claws with designed non-slippery conductive clamps in the presented test configurations. The pressure of pneumatic claws was crucial. High pressure would conduct mechanical damage to the hydrogel samples and cause an early break. Low pressure would cause the slipperiness of hydrogel samples during the tensile test. A 10 psi pressure for the pneumatic claws was selected after the optimisation test. Besides, the non-slippery conductive clamps were designed. There was a copper film cover on the clamp as electrodes to contact the conductive hydrogels. The copper film should be thin and flexible to prevent damage on the much softer hydrogel sample. Also, there should be soft edge when the edge of the copper film tends to curve to avoid any sharpness. In addition, the copper film was top stamped with dense cross patterns to increase non-slippery ability.

In the electrical characterisation of the soft strain sensor, an increase in electrical resistance was observed when the measuring circuit started to work while no strain was applied to the soft sensor. This resistance increase may be due to the reaction of copper

---

electrodes and NaCl solution in hydrogel under electrical current. Copper atoms were excited and combined with free chloride ions. When the generated copper chloride exceeded its solubility, it started to crystallise. At the end of the test, green powders have appeared on the hydrogel. The decrease of free chloride ions would cause the rise of the electrical resistance of hydrogel. A solution for this problem would be altering the copper electrodes with platinum or gold electrodes.

## **7.2 Contribution and assessment of research objectives**

This thesis has presented a methodology to produce a high-performance fully elastomeric soft strain sensor. The soft strain sensor is fully and highly stretchable with enhanced durability performance and practicability with PDMS encapsulation.

The thesis contributes to digging out a suitable soft material, tuning and characterising the properties of a soft material by testifying different formulations of conductive polyacrylamide hydrogels using UV exposed polymerisation and presented considerable tested data on the mechanical and electrical properties of conductive polyacrylamide hydrogels that contribute to the future research.

This thesis has also proposed new designs of fully elastomeric soft sensors with good compliance, flexibility, sensitivity, and durability. The related fabricating and manufacturing techniques were proved to be able to expand to more applications such as 2D soft strain sensor array and soft tactile sensor.

Section 1.3 described a list of objectives for the thesis. This section examines how each of the objectives has been addressed in the research.

- 1) To fully investigate the literature and state-of-the-art research on soft sensors to locate under-researched areas and address potential techniques.*

---

A wide and deep literature review was investigated to address the development and recent progress on the design, material, fabrication, validation and application of soft sensors. This informative review located the gaps as well as promising solutions to build a solid base for developing techniques in the thesis.

2) *To design a conceptual soft sensor and address the approaches to the concept in aspects of materials, fabrications and experiments.*

The concept of a fully elastomeric soft sensor using a hydrogel-PDMS hybrid was presented, including design, materials and applications. Requirements for mechanical and electrical performance had been defined. And approaches in fabrications and validations have been proposed to achieve the described fully elastomeric soft sensor.

3) *To develop a characterisation method to understand the mechanical and electrical properties of selected soft materials.*

A test configuration to characterise the mechanical and electrical properties of hydrogels was set up. The effect of each component of the PAAm hydrogel was quantified and understood by this test configuration.

4) *To develop the hybrid material techniques to improve the stability and durability of selected soft materials.*

A hydrogel-PDMS hybrid was fabricated and tested. The produced hybrids showed capable anti-dehydration and robust bond, verified by the peel test and the water retention test. The stability and durability of hydrogel were ensured by the encapsulation of the PDMS elastomer layer.

5) *To fabricate, evaluate and demonstrate a fully elastomeric soft sensor through the developed design, material and experimental techniques.*

---

A fully elastic soft strain sensor was fabricated using a hydrogel-PDMS hybrid material and UV light radiation. The proposed sensor was validated by a series of tensile tests, showing high sensitivity and high stretchability. The application of the sensor in monitoring finger bending and soft tentacle bending demonstrates the effectiveness of the sensor.

6) *To demonstrate the potential of the developed sensing techniques by conducting case studies in different applications.*

Two case studies are presented, including a multi-electrodes soft tactile sensor and a 2D soft strain sensor. The multi-electrodes soft tactile sensor proved the potential of the proposed conductive hydrogel applied as a resistive tactile sensor and the feasibility to apply multi-electrodes detection in the soft sensor. The 2D soft strain sensor expanded the soft sensor to a complex structure and configuration to achieve bidimensional strain sensing.

## 7.3 Outlook

The applications in Chapter 4 have shown the validity of the proposed soft strain sensor in advantages of adaptivity and stretchability. In the case of monitoring the bending finger joint, the soft sensor firmly sensed different angles of finger bending. And in the case of sensing the actuation of a soft pneumatic tentacle, the soft sensor is able to track the motion of the tentacle. In Chapter 6, the techniques on the conductive hydrogel sensor are expanded to a multi-electrode sensor and sensor array. The case studies prove the potential of such conductive hydrogel as capable sensing materials.

Future work on the soft sensors focuses on the soft circuits, including soft electrodes and integration with soft robots. The limitation of this research is that the

---

soft strain sensor is still using rigid copper electrodes due to the lack of research on soft electrodes. Conductive hydrogels also act as a suitable material for soft electrodes, but the research is still inadequate. Soft circuits especially soft electrodes must be studied to fully utilise soft sensors in soft robotics systems. In this research, soft sensors are independently working along with soft actuators. To better serve soft robots' sensing needs, soft sensors tend to be integrated into the system. This integration should be conducted in the design process of soft robots to plan the usage of soft sensors and embed the soft sensors in the manufacturing procedures of soft robots. Further studies on how to determine the parameters of soft strain sensors are also needed to understand the influence of different sensor shape under different applications.

Recent research work has drawn directions for soft strain sensors. Self-powered soft sensors emerge as more integrated sensors without an external power supply. Those soft sensors utilise the triboelectricity effect to sense and generate electricity simultaneously [176-179]. The techniques of conductive hydrogels and PDMS bonding also fit this mechanism and have the potential for sensing application via triboelectricity. Soft sensors are also suitable for wearable sensors due to their biocompatibility, softness and stretchability. Hydrogels based wearable sensors are an important ongoing technique which is widely studied [59, 131, 180]. Due to its high stretchability, durability, and optical transparency, the soft sensor proposed in this thesis is also promising in its application as a wearable sensor.

## **7.4 Conclusion**

This thesis proposed a fully elastomeric soft strain sensor with high stretchability up to 724% strain, low stiffness down to 1.37 kPa. The soft strain sensor also achieved high water retention, optical clearance and fully elasticity. This study has addressed the

---

objectives proposed in Chapter 1. A fully elastomeric soft sensor was presented to tackle the gaps in soft sensors and adapt to the sensing needs of soft robots. Existing methods for soft sensors toward tactile and strain sensing were detailed investigated in Chapter 2. Requirements were defined in Chapter 3 with qualified concept design and accessible approaches. Fabrication methods and variant formulations of conductive hydrogels were closely studied in Chapter 4 to build the base of soft sensors with conductive hydrogels. The design, fabrication and characterisation of the fully elastomeric soft sensors were presented in Chapter 5. The usage of PDMS coating on hydrogel extended the durability and practicality of conductive hydrogels. Case studies have proven the potential and advantages of proposed fully elastomeric soft sensors in application in Chapter 6.

In Chapter 2, the development of soft robotics and soft sensors were investigated in depth. The gaps in applying soft sensors for soft robots were located that existing soft sensors were lack of high-performance materials and adaptive design of sensors. In this scene, current soft materials were also researched to compare their advantages and drawbacks. Hydrogels were selected as a promising representative material to be further reviewed in aspects of materials, fabrication methods and soft sensors based on the conductive hydrogel. The focus is locked on the fabrication methods of soft materials in order to present a capable soft sensor.

Chapter 4 presented an ionic conductive hydrogel advanced in high stretchability, low stiffness, high optical transparency, and good electrical conductivity. To achieve better mechanical and electrical performance, the research started with the formulation of hydrogels with polyacrylamide. Ratios of each component in the hydrogel formulation were researched to evaluate the effect of those factors on final hydrogel products. Tensile and compression tests of variant formulations were

---

conducted to characterise the mechanical and electrical properties of conductive hydrogels under tensile or compressive strain. Ratios of monomers, crosslinkers and ionic solutions affect the mechanical properties of hydrogel most in aspects of tensile stress and maximum strain limit. The concentration of ions was proven to domain the electrical resistance of conductive hydrogels. By adjusting the ratios of components in the conductive hydrogel formulation, the conductive hydrogel can be toned in mechanical and electrical properties corresponding to different applications.

Chapter 5 proposed a fully elastomeric and transparent soft strain sensor based on the study of ionic conductive hydrogel. The soft strain sensor was designed by encapsulating an ionic conductive hydrogel in PDMS modified by benzophenone. PDMS was applied to wrap the hydrogel and decrease the hydrogel's dehydration, extending the conductive hydrogel's durability. Both the hydrogel and PDMS have high optical transparency and elasticity. The hydrogel-PDMS bond was examined on the bonding mechanism and cooperating materials. The hydrogel-PDMS hybrid was proven to decrease water loss by a water retention test. And bonding strength of the hydrogel-PDMS bond was verified by a peel test on a hydrogel-PDMS hybrid. The fabrication of a soft strain sensor encapsulated by PDMS was detailed described. The soft strain sensor was characterised in tensile tests on real-time changes of mechanical and electrical properties. Changes in electrical resistance had a good fit with the changes in tensile strain. The soft strain sensors exhibited potential in applications of movement monitors for human joints or soft actuators.

In Chapter 6, two case studies on conductive hydrogel sensors were conducted, including a multi-electrodes soft tactile sensor and a 2D soft strain sensor. The first case study explored the use of multi-electrode detection in conductive hydrogels sensing. By applying multi-electrode detection, the sensor can simultaneously detect both the

---

magnification and location of the stimulus. The hydrogel sensor was tested as capable to locate both stress and location of the tactile. The second case study presented a 2D soft strain sensor by extending the rectangular soft strain sensor in Chapter 4 to a 2D planar structure. The final product was an array of soft strain sensors. 9 electrodes were used to activate and detect the sensing signal. Between each activation electrode and detection electrode, the hydrogel acted as a single soft strain sensing unit. By sequentially measuring the electrical resistance change in the strain sensing units, the 2D strain change in the whole PDMS film were obtained.

---

## Reference

- [1] S. Kim, C. Laschi, and B. Trimmer, "Soft robotics: a bioinspired evolution in robotics," *Trends in Biotechnology*, vol. 31, no. 5, pp. 287-294, 2013/05/01/ 2013.
- [2] B. Mosadegh *et al.*, "Pneumatic Networks for Soft Robotics that Actuate Rapidly," *Advanced Functional Materials*, vol. 24, no. 15, pp. 2163-2170, 2014/04/01 2014.
- [3] C. Laschi, B. Mazzolai, and M. Cianchetti, "Soft robotics: Technologies and systems pushing the boundaries of robot abilities," *Science Robotics*, vol. 1, no. 1, p. eaah3690, 2016.
- [4] D. Trivedi, C. D. Rahn, W. M. Kier, and I. D. Walker, "Soft robotics: Biological inspiration, state of the art, and future research," *Applied Bionics and Biomechanics*, vol. 5, no. 3, pp. 99-117, 2008/12/16 2008.
- [5] M. Cianchetti, C. Laschi, A. Menciasci, and P. Dario, "Biomedical applications of soft robotics," *Nature Reviews Materials*, vol. 3, no. 6, pp. 143-153, 2018/06/01 2018.
- [6] D. Rus and M. T. Tolley, "Design, fabrication and control of soft robots," *Nature*, vol. 521, no. 7553, pp. 467-75, May 28 2015.
- [7] M. Carmel, "Soft Robotics: A Perspective—Current Trends and Prospects for the Future," *Soft Robotics*, vol. 1, no. 1, pp. 5-11, 2014.
- [8] A. Albu-Schaffer *et al.*, "Soft robotics," *IEEE Robotics & Automation Magazine*, vol. 15, no. 3, pp. 20-30, 2008.
- [9] R. Deimel and O. Brock, "A novel type of compliant and underactuated robotic hand for dexterous grasping," *The International Journal of Robotics Research*, vol. 35, no. 1-3, pp. 161-185, 2016/01/01 2015.
- [10] C. Majidi, R. F. Shepherd, R. K. Kramer, G. M. Whitesides, and R. J. Wood, "Influence of surface traction on soft robot undulation," *The International Journal of Robotics Research*, vol. 32, no. 13, pp. 1577-1584, 2013/11/01 2013.
- [11] C. Paul, "Morphological computation: A basis for the analysis of morphology and control requirements," *Robotics and Autonomous Systems*, vol. 54, no. 8, pp. 619-630, 2006/08/31/ 2006.
- [12] K. Suzumori, S. Iikura, and H. Tanaka, "Applying a flexible microactuator to robotic mechanisms," *IEEE Control Systems*, vol. 12, no. 1, pp. 21-27, 1992.
- [13] K. Suzumori, T. Maeda, H. Wantabe, and T. Hisada, "Fiberless flexible microactuator designed by finite-element method," *IEEE/ASME Transactions on Mechatronics*, vol. 2, no. 4, pp. 281-286, 1997.

- 
- [14] K. Suzumori and S. Asaad, "A novel pneumatic rubber actuator for mobile robot bases," in *Intelligent Robots and Systems '96, IROS 96, Proceedings of the 1996 IEEE/RSJ International Conference on*, 4-8 Nov 1996 1996, vol. 2, pp. 1001-1006 vol.2.
- [15] K. Suzumori, K. Hori, and T. Miyagawa, "A direct-drive pneumatic stepping motor for robots: designs for pipe-inspection microrobots and for human-care robots," in *Proceedings. 1998 IEEE International Conference on Robotics and Automation (Cat. No.98CH36146)*, 16-20 May 1998 1998, vol. 4, pp. 3047-3052 vol.4.
- [16] K. Suzumori, S. Endo, T. Kanda, N. Kato, and H. Suzuki, "A Bending Pneumatic Rubber Actuator Realizing Soft-bodied Manta Swimming Robot," in *Proceedings 2007 IEEE International Conference on Robotics and Automation*, 10-14 April 2007 2007, pp. 4975-4980.
- [17] M. A. Robertson and J. Paik, "New soft robots really suck: Vacuum-powered systems empower diverse capabilities," *Science Robotics*, vol. 2, no. 9, p. eaan6357, 2017.
- [18] M. Wehner *et al.*, "An integrated design and fabrication strategy for entirely soft, autonomous robots," *Nature*, vol. 536, no. 7617, pp. 451-5, Aug 25 2016.
- [19] N. Kellaris, V. Gopaluni Venkata, G. M. Smith, S. K. Mitchell, and C. Keplinger, "Peano-HASEL actuators: Muscle-mimetic, electrohydraulic transducers that linearly contract on activation," *Science Robotics*, vol. 3, no. 14, p. eaar3276, 2018-01-05 2018.
- [20] E. T. Roche *et al.*, "Soft robotic sleeve supports heart function," *Sci Transl Med*, vol. 9, no. 373, Jan 18 2017.
- [21] C. J. Payne *et al.*, "Soft robotic ventricular assist device with septal bracing for therapy of heart failure," *Science Robotics*, vol. 2, no. 12, p. 6736, 2017.
- [22] M. Mirvakili Seyed, D. Sim, W. Hunter Ian, and R. Langer, "Actuation of untethered pneumatic artificial muscles and soft robots using magnetically induced liquid-to-gas phase transitions," *Science Robotics*, vol. 5, no. 41, p. eaaz4239, 2020/04/15 2020.
- [23] A. Hamidi and Y. Tadesse, "3D printing of very soft elastomer and sacrificial carbohydrate glass/elastomer structures for robotic applications," *Materials & Design*, vol. 187, p. 108324, 2020/02/01/ 2020.
- [24] M. A. Skylar-Scott, J. Mueller, C. W. Visser, and J. A. Lewis, "Voxelated soft matter via multimaterial multinozzle 3D printing," *Nature*, vol. 575, no. 7782, pp. 330-335, 2019/11/01 2019.
- [25] S. Salmanipour, O. Youssefi, and E. D. Diller, "Design of Multi-Degrees-of-Freedom Microrobots Driven by Homogeneous Quasi-Static Magnetic Fields," *IEEE Transactions on Robotics*, vol. 37, no. 1, pp. 246-256, 2021.
- [26] H. Niu *et al.*, "MagWorm: A Biomimetic Magnet Embedded Worm-Like Soft Robot," *Soft Robotics*, vol. 8, no. 5, pp. 507-518, 2021/10/01 2020.
- [27] S. R. Goudu, I. C. Yasa, X. Hu, H. Ceylan, W. Hu, and M. Sitti, "Biodegradable Untethered Magnetic Hydrogel Milli-Grippers," *Advanced Functional Materials*, vol. 30, no. 50, p. 2004975, 2020/12/01 2020.
- [28] G. Li *et al.*, "Self-powered soft robot in the Mariana Trench," *Nature*, vol. 591, no. 7848, pp. 66-71, 2021/03/01 2021.
- [29] X. Ji *et al.*, "Untethered Feel-Through Haptics Using 18- $\mu$ m Thick Dielectric Elastomer Actuators," *Advanced Functional Materials*, vol. 31, no. 39, p. 2006639, 2021/09/01 2021.

- 
- [30] B. Aksoy and H. Shea, "Reconfigurable and Latchable Shape-Morphing Dielectric Elastomers Based on Local Stiffness Modulation," *Advanced Functional Materials*, vol. 30, no. 27, p. 2001597, 2020/07/01 2020.
- [31] H. Yousef, M. Boukallel, and K. Althoefer, "Tactile sensing for dexterous in-hand manipulation in robotics—A review," *Sensors and Actuators A: Physical*, vol. 167, no. 2, pp. 171-187, 2011/06/01/ 2011.
- [32] R. S. Dahiya, G. Metta, M. Valle, and G. Sandini, "Tactile Sensing—From Humans to Humanoids," *IEEE Transactions on Robotics*, vol. 26, no. 1, pp. 1-20, 2010.
- [33] T. Assaf, C. Roke, J. Rossiter, T. Pipe, and C. Melhuish, "Seeing by Touch: Evaluation of a Soft Biologically-Inspired Artificial Fingertip in Real-Time Active Touch," *Sensors*, vol. 14, no. 2, p. 2561, 2014.
- [34] Y. L. Park, B. R. Chen, and R. J. Wood, "Design and Fabrication of Soft Artificial Skin Using Embedded Microchannels and Liquid Conductors," *IEEE Sensors Journal*, vol. 12, no. 8, pp. 2711-2718, 2012.
- [35] S. Stassi, V. Cauda, G. Canavese, and C. F. Pirri, "Flexible Tactile Sensing Based on Piezoresistive Composites: A Review," *Sensors*, vol. 14, no. 3, pp. 5296-5332, 2014.
- [36] H. S. Lee *et al.*, "Design analysis and fabrication of arrayed tactile display based on dielectric elastomer actuator," *Sensors and Actuators A: Physical*, vol. 205, pp. 191-198, 2014.
- [37] A. Ahmed and K. Jürgen, "Magnetic Nanocomposite Cilia Tactile Sensor," *Advanced Materials*, vol. 27, no. 47, pp. 7888-7892, 2015.
- [38] D. Chen and Q. Pei, "Electronic Muscles and Skins: A Review of Soft Sensors and Actuators," *Chemical Reviews*, vol. 117, no. 17, pp. 11239-11268, 2017/09/13 2017.
- [39] K. Zhang, J. Zhang, F. Wang, and D. Kong, "Stretchable and Superwetttable Colorimetric Sensing Patch for Epidermal Collection and Analysis of Sweat," *ACS Sensors*, vol. 6, no. 6, pp. 2261-2269, 2021/06/25 2021.
- [40] M. Ramuz, B. C. K. Tee, J. B. H. Tok, and Z. Bao, "Transparent, Optical, Pressure-Sensitive Artificial Skin for Large-Area Stretchable Electronics," *Advanced Materials*, vol. 24, no. 24, pp. 3223-3227, 2012/06/26 2012.
- [41] S. Yao and Y. Zhu, "Wearable multifunctional sensors using printed stretchable conductors made of silver nanowires," *Nanoscale*, vol. 6, no. 4, pp. 2345-2352, 2014.
- [42] R. K. Kramer, C. Majidi, and R. J. Wood, "Wearable tactile keypad with stretchable artificial skin," in *2011 IEEE International Conference on Robotics and Automation*, 9-13 May 2011 2011, pp. 1103-1107.
- [43] J. Shintake, Y. Piskarev, S. H. Jeong, and D. Floreano, "Ultrastretchable Strain Sensors Using Carbon Black-Filled Elastomer Composites and Comparison of Capacitive Versus Resistive Sensors," *Advanced Materials Technologies*, vol. 3, no. 3, p. 1700284, 2018/03/01 2018.
- [44] M. D. Mitchell, F. E. Hurley, and C. D. Onal, "Fast Probabilistic 3-D Curvature Proprioception with a Magnetic Soft Sensor," in *2021 IEEE 17th International Conference on Automation Science and Engineering (CASE)*, 23-27 Aug. 2021 2021, pp. 215-220.
- [45] Y. Ohmura, Y. Kuniyoshi, and A. Nagakubo, "Conformable and scalable tactile sensor skin for curved surfaces," in *Proceedings 2006 IEEE International Conference on Robotics and Automation, 2006. ICRA 2006.*, 15-19 May 2006 2006, pp. 1348-1353.

- 
- [46] F. L. Hammond, R. K. Kramer, Q. Wan, R. D. Howe, and R. J. Wood, "Soft tactile sensor arrays for micromanipulation," in *2012 IEEE/RSJ International Conference on Intelligent Robots and Systems*, 7-12 Oct. 2012 2012, pp. 25-32.
- [47] J. Y. Sun, C. Keplinger, G. M. Whitesides, and Z. Suo, "Ionic skin," *Adv Mater*, vol. 26, no. 45, pp. 7608-14, Dec 3 2014.
- [48] S. Y. Kim *et al.*, "Highly Sensitive and Multimodal All-Carbon Skin Sensors Capable of Simultaneously Detecting Tactile and Biological Stimuli," *Advanced Materials*, vol. 27, no. 28, pp. 4178-4185, 2018.
- [49] J. J. Clark, "A magnetic field based compliance matching sensor for high resolution, high compliance tactile sensing," in *Proceedings. 1988 IEEE International Conference on Robotics and Automation*, 24-29 Apr 1988 1988, pp. 772-777 vol.2.
- [50] T. Paulino *et al.*, "Low-cost 3-axis soft tactile sensors for the human-friendly robot Vizzy," in *2017 IEEE International Conference on Robotics and Automation (ICRA)*, May 29 2017-June 3 2017 2017, pp. 966-971.
- [51] L. Jamone, L. Natale, G. Metta, and G. Sandini, "Highly Sensitive Soft Tactile Sensors for an Anthropomorphic Robotic Hand," *IEEE Sensors Journal*, vol. 15, no. 8, pp. 4226-4233, 2015.
- [52] M. Goka, H. Nakamoto, and S. Takenawa, "A magnetic type tactile sensor by GMR elements and inductors," in *2010 IEEE/RSJ International Conference on Intelligent Robots and Systems*, 18-22 Oct. 2010 2010, pp. 885-890.
- [53] C. Ledermann, S. Wirges, D. Oertel, M. Mende, and H. Woern, "Tactile sensor on a magnetic basis using novel 3D Hall sensor - First prototypes and results," in *2013 IEEE 17th International Conference on Intelligent Engineering Systems (INES)*, 19-21 June 2013 2013, pp. 55-60.
- [54] S. Youssefian, N. Rahbar, and E. Torres-Jara, "Contact Behavior of Soft Spherical Tactile Sensors," *IEEE Sensors Journal*, vol. 14, no. 5, pp. 1435-1442, 2014.
- [55] N. Ni and L. Zhang, "Dielectric Elastomer Sensors," in *Elastomers: intech*, 2017.
- [56] J.-B. Chossat, H.-S. Shin, Y.-L. Park, and V. Duchaine, "Soft Tactile Skin Using an Embedded Ionic Liquid and Tomographic Imaging," *Journal of Mechanisms and Robotics*, vol. 7, no. 2, p. 021008, 2015.
- [57] H. Lee, D. Kwon, H. Cho, I. Park, and J. Kim, "Soft Nanocomposite Based Multi-point, Multi-directional Strain Mapping Sensor Using Anisotropic Electrical Impedance Tomography," *Scientific Reports*, vol. 7, p. 39837, 2017-01-25 2017.
- [58] E. Roh, B. U. Hwang, D. Kim, B. Y. Kim, and N. E. Lee, "Stretchable, Transparent, Ultrasensitive, and Patchable Strain Sensor for Human-Machine Interfaces Comprising a Nanohybrid of Carbon Nanotubes and Conductive Elastomers," *ACS Nano*, vol. 9, no. 6, pp. 6252-61, Jun 23 2015.
- [59] J. Hughes and F. Iida, "Multi-Functional Soft Strain Sensors for Wearable Physiological Monitoring," *Sensors*, vol. 18, no. 11, p. 3822, 2018.
- [60] G. Cai, J. Wang, K. Qian, J. Chen, S. Li, and P. S. Lee, "Extremely Stretchable Strain Sensors Based on Conductive Self-Healing Dynamic Cross-Links Hydrogels for Human-Motion Detection," *Advanced Science*, vol. 4, no. 2, p. 1600190, 2017.
- [61] J. T. Muth *et al.*, "Embedded 3D printing of strain sensors within highly stretchable elastomers," *Adv Mater*, vol. 26, no. 36, pp. 6307-12, Sep 2014.

- 
- [62] D. J. Cohen, D. Mitra, K. Peterson, and M. M. Maharbiz, "A Highly Elastic, Capacitive Strain Gauge Based on Percolating Nanotube Networks," *Nano Letters*, vol. 12, no. 4, pp. 1821-1825, 2012/04/11 2012.
- [63] Y. Wang *et al.*, "Wearable and Highly Sensitive Graphene Strain Sensors for Human Motion Monitoring," *Advanced Functional Materials*, vol. 24, no. 29, pp. 4666-4670, 2014/08/01 2014.
- [64] U.-H. Shin, D.-W. Jeong, S.-M. Park, S.-H. Kim, H. W. Lee, and J.-M. Kim, "Highly stretchable conductors and piezocapacitive strain gauges based on simple contact-transfer patterning of carbon nanotube forests," *Carbon*, vol. 80, pp. 396-404, 2014/12/01/ 2014.
- [65] J.-H. Kong, N.-S. Jang, S.-H. Kim, and J.-M. Kim, "Simple and rapid micropatterning of conductive carbon composites and its application to elastic strain sensors," *Carbon*, vol. 77, pp. 199-207, 2014/10/01/ 2014.
- [66] Y. Wang *et al.*, "Super-Elastic Graphene Ripples for Flexible Strain Sensors," *ACS Nano*, vol. 5, no. 5, pp. 3645-3650, 2011/05/24 2011.
- [67] S. Luo and T. Liu, "Structure–property–processing relationships of single-wall carbon nanotube thin film piezoresistive sensors," *Carbon*, vol. 59, pp. 315-324, 2013/08/01/ 2013.
- [68] S. Tadakaluru, W. Thongsuwan, and P. Singjai, "Stretchable and flexible high-strain sensors made using carbon nanotubes and graphite films on natural rubber," *Sensors (Basel)*, vol. 14, no. 1, pp. 868-76, Jan 6 2014.
- [69] C. Yan *et al.*, "Highly Stretchable Piezoresistive Graphene–Nanocellulose Nanopaper for Strain Sensors," *Advanced Materials*, vol. 26, no. 13, pp. 2022-2027, 2014/04/01 2014.
- [70] L. Cai *et al.*, "Super-stretchable, Transparent Carbon Nanotube-Based Capacitive Strain Sensors for Human Motion Detection," *Scientific Reports*, vol. 3, no. 1, p. 3048, 2013/10/25 2013.
- [71] T. Yamada *et al.*, "A stretchable carbon nanotube strain sensor for human-motion detection," *Nature Nanotechnology*, vol. 6, no. 5, pp. 296-301, 2011/05/01 2011.
- [72] Y. Park, B. Chen, and R. J. Wood, "Design and Fabrication of Soft Artificial Skin Using Embedded Microchannels and Liquid Conductors," *IEEE Sensors Journal*, vol. 12, no. 8, pp. 2711-2718, 2012.
- [73] C. Yeom, K. Chen, D. Kiriya, Z. Yu, G. Cho, and A. Javey, "Large-Area Compliant Tactile Sensors Using Printed Carbon Nanotube Active-Matrix Backplanes," *Advanced Materials*, vol. 27, no. 9, pp. 1561-1566, 2015/03/01 2015.
- [74] Y. Lin *et al.*, "Drawing liquid metal wires at room temperature," *Extreme Mechanics Letters*, vol. 7, pp. 55-63, 2016/06/01/ 2016.
- [75] M. R. Khan, J. Bell, and M. D. Dickey, "Localized Instabilities of Liquid Metal Films via In-Plane Recapillarity," *Advanced Materials Interfaces*, vol. 3, no. 23, 2016.
- [76] C. W. Park *et al.*, "Photolithography-Based Patterning of Liquid Metal Interconnects for Monolithically Integrated Stretchable Circuits," *ACS Applied Materials & Interfaces*, vol. 8, no. 24, pp. 15459-15465, 2016/06/22 2016.
- [77] G. Li, X. Wu, and D. W. Lee, "A galinstan-based inkjet printing system for highly stretchable electronics with self-healing capability," *Lab Chip*, vol. 16, no. 8, pp. 1366-73, Apr 21 2016.

- 
- [78] M. Vatani, M. Vatani, and J. W. Choi, "Multi-layer stretchable pressure sensors using ionic liquids and carbon nanotubes," *Applied Physics Letters*, vol. 108, no. 6, p. 061908, 2016/02/08 2016.
- [79] T. Helps and J. Rossiter, "Proprioceptive Flexible Fluidic Actuators Using Conductive Working Fluids," *Soft Robotics*, vol. 5, no. 2, pp. 175-189, 2018/04/01 2017.
- [80] H.-S. Shin, J. Ryu, C. Majidi, and Y.-L. Park, "Enhanced performance of microfluidic soft pressure sensors with embedded solid microspheres," *Journal of Micromechanics and Microengineering*, vol. 26, no. 2, p. 025011, 2016/01/08 2016.
- [81] J. Chossat, T. Yiwei, V. Duchaine, and Y. Park, "Wearable soft artificial skin for hand motion detection with embedded microfluidic strain sensing," in *2015 IEEE International Conference on Robotics and Automation (ICRA)*, 26-30 May 2015 2015, pp. 2568-2573.
- [82] S. G. Yoon, H.-J. Koo, and S. T. Chang, "Highly Stretchable and Transparent Microfluidic Strain Sensors for Monitoring Human Body Motions," *ACS Applied Materials & Interfaces*, vol. 7, no. 49, pp. 27562-27570, 2015/12/16 2015.
- [83] H. Nulwala, A. Mirjafari, and X. Zhou, "Ionic liquids and poly(ionic liquid)s for 3D printing – A focused mini-review," *European Polymer Journal*, vol. 108, pp. 390-398, 2018/11/01/ 2018.
- [84] J.-B. Chossat, H.-S. Shin, Y.-L. Park, and V. Duchaine, "Soft Tactile Skin Using an Embedded Ionic Liquid and Tomographic Imaging," *Journal of Mechanisms and Robotics*, vol. 7, no. 2, 2015.
- [85] S. Russo, T. Ranzani, H. Liu, S. Nefti-Meziani, K. Althoefer, and A. Menciassi, "Soft and Stretchable Sensor Using Biocompatible Electrodes and Liquid for Medical Applications," *Soft Robotics*, vol. 2, no. 4, pp. 146-154, 2015/12/01 2015.
- [86] F. Xu and Y. Zhu, "Highly conductive and stretchable silver nanowire conductors," *Adv Mater*, vol. 24, no. 37, pp. 5117-22, Sep 25 2012.
- [87] M. Hempel, D. Nezich, J. Kong, and M. Hofmann, "A Novel Class of Strain Gauges Based on Layered Percolative Films of 2D Materials," *Nano Letters*, vol. 12, no. 11, pp. 5714-5718, 2012/11/14 2012.
- [88] S.-H. Bae, Y. Lee, B. K. Sharma, H.-J. Lee, J.-H. Kim, and J.-H. Ahn, "Graphene-based transparent strain sensor," *Carbon*, vol. 51, pp. 236-242, 2013/01/01/ 2013.
- [89] T. N. Abraham, D. Ratna, S. Siengchin, and J. Karger-Kocsis, "Rheological and thermal properties of poly(ethylene oxide)/multiwall carbon nanotube composites," *Journal of Applied Polymer Science*, vol. 110, no. 4, pp. 2094-2101, 2008/11/15 2008.
- [90] M. Behl and A. Lendlein, "Shape-memory polymers," *Materials Today*, vol. 10, no. 4, pp. 20-28, 2007/04/01/ 2007.
- [91] R. Langer and D. A. Tirrell, "Designing materials for biology and medicine," *Nature*, vol. 428, p. 487, 04/01/online 2004.
- [92] E. W. H. Jager, E. Smela, and O. Inganäs, "Microfabricating Conjugated Polymer Actuators," *Science*, vol. 290, no. 5496, pp. 1540-1545, 2000.
- [93] M. Armand, F. Endres, D. R. MacFarlane, H. Ohno, and B. Scrosati, "Ionic-liquid materials for the electrochemical challenges of the future," *Nature Materials*, vol. 8, p. 621, 07/24/online 2009.

- 
- [94] T. F. Otero, J. G. Martinez, and J. Arias-Pardilla, "Biomimetic electrochemistry from conducting polymers. A review: Artificial muscles, smart membranes, smart drug delivery and computer/neuron interfaces," *Electrochimica Acta*, vol. 84, pp. 112-128, 2012/12/01/ 2012.
- [95] W. Zheng *et al.*, "Artificial Muscles Based on Polypyrrole/Carbon Nanotube Laminates," *Advanced Materials*, vol. 23, no. 26, pp. 2966-2970, 2011/07/12 2011.
- [96] D. Pugal, K. Jung, A. Aabloo, and J. Kim Kwang, "Ionic polymer-metal composite mechano-electrical transduction: review and perspectives," *Polymer International*, vol. 59, no. 3, pp. 279-289, 2010/03/01 2010.
- [97] P. J. Glazer, M. van Erp, A. Embrechts, S. G. Lemay, and E. Mendes, "Role of pH gradients in the actuation of electro-responsive polyelectrolyte gels," *Soft Matter*, vol. 8, no. 16, pp. 4421-4426, 2012.
- [98] F. Carpi, S. Bauer, and D. De Rossi, "Stretching Dielectric Elastomer Performance," *Science*, vol. 330, no. 6012, pp. 1759-1761, 2010.
- [99] R. Pelrine, R. Kornbluh, Q. Pei, and J. Joseph, "High-Speed Electrically Actuated Elastomers with Strain Greater Than 100%," *Science*, vol. 287, no. 5454, pp. 836-839, 2000.
- [100] Q. M. Zhang, V. Bharti, and X. Zhao, "Giant Electrostriction and Relaxor Ferroelectric Behavior in Electron-Irradiated Poly(vinylidene fluoride-trifluoroethylene) Copolymer," *Science*, vol. 280, no. 5372, pp. 2101-2104, 1998.
- [101] J. Foroughi *et al.*, "Torsional Carbon Nanotube Artificial Muscles," *Science*, 2011.
- [102] R. Kornbluh, R. Pelrine, J. Eckerle, and J. Joseph, "Electrostrictive polymer artificial muscle actuators," in *Proceedings. 1998 IEEE International Conference on Robotics and Automation*, 16-20 May 1998 1998, vol. 3, pp. 2147-2154 vol.3.
- [103] M. Zhenyi, J. I. Scheinbeim, J. W. Lee, and B. A. Newman, "High field electrostrictive response of polymers," *Journal of Polymer Science Part B: Polymer Physics*, vol. 32, no. 16, pp. 2721-2731, 1994/12/01 1994.
- [104] R. P. R. Kornbluh, and J. Joseph, "Elastomeric dielectric artificial muscle actuators for small robots," in *3rd IASTED International Conference on Robotics and Manufacturing*, Cancun, Mexico, 1995,
- [105] D. D. R. Federico Carpi, Roy Kornbluh, Ronald Pelrine and Peter Sommer-Larsen *Dielectric elastomers as electromechanical transducers*. Elsevier, 2007.
- [106] A. Fassler and C. Majidi, "Soft-matter capacitors and inductors for hyperelastic strain sensing and stretchable electronics," *Smart Materials and Structures*, vol. 22, no. 5, p. 055023, 2013.
- [107] P. Roberts, D. D. Damian, W. Shan, T. Lu, and C. Majidi, "Soft-matter capacitive sensor for measuring shear and pressure deformation," in *2013 IEEE International Conference on Robotics and Automation*, 6-10 May 2013 2013, pp. 3529-3534.
- [108] J. C. Lötters, W. Olthuis, P. H. Veltink, and P. Bergveld, "The mechanical properties of the rubber elastic polymer polydimethylsiloxane for sensor applications," *Journal of Micromechanics and Microengineering*, vol. 7, no. 3, p. 145, 1997.
- [109] S. C. B. Mannsfeld *et al.*, "Highly sensitive flexible pressure sensors with microstructured rubber dielectric layers," *Nature Materials*, vol. 9, p. 859, 09/12/online 2010.

- 
- [110] M. Kaltenbrunner *et al.*, "An ultra-lightweight design for imperceptible plastic electronics," *Nature*, vol. 499, p. 458, 07/24/online 2013.
- [111] X. Pu *et al.*, "Ultrastretchable, transparent triboelectric nanogenerator as electronic skin for biomechanical energy harvesting and tactile sensing," *Science Advances*, vol. 3, no. 5, 2017.
- [112] S. Cheng and Z. Wu, "A Microfluidic, Reversibly Stretchable, Large-Area Wireless Strain Sensor," *Advanced Functional Materials*, vol. 21, no. 12, pp. 2282-2290, 2011/06/21 2011.
- [113] C. Majidi, R. Kramer, and R. J. Wood, "A non-differential elastomer curvature sensor for softer-than-skin electronics," *Smart Materials and Structures*, vol. 20, no. 10, p. 105017, 2011.
- [114] R. D. Ponce Wong, J. D. Posner, and V. J. Santos, "Flexible microfluidic normal force sensor skin for tactile feedback," *Sensors and Actuators A: Physical*, vol. 179, pp. 62-69, 2012/06/01/ 2012.
- [115] P. Yong-Lae, M. Carmel, K. Rebecca, B. Phillipe, and J. W. Robert, "Hyperelastic pressure sensing with a liquid-embedded elastomer," *Journal of Micromechanics and Microengineering*, vol. 20, no. 12, p. 125029, 2010.
- [116] B. C. K. Tee, C. Wang, R. Allen, and Z. Bao, "An electrically and mechanically self-healing composite with pressure- and flexion-sensitive properties for electronic skin applications," *Nature Nanotechnology*, vol. 7, p. 825, 11/11/online 2012.
- [117] Y. Kim So, S. Park, W. Park Han, H. Park Do, Y. Jeong, and H. Kim Do, "Highly Sensitive and Multimodal All-Carbon Skin Sensors Capable of Simultaneously Detecting Tactile and Biological Stimuli," *Advanced Materials*, vol. 27, no. 28, pp. 4178-4185, 2015/07/01 2015.
- [118] K. Inpil, J. S. Mark, H. K. Jay, S. Vesselin, and S. Donglu, "A carbon nanotube strain sensor for structural health monitoring," *Smart Materials and Structures*, vol. 15, no. 3, p. 737, 2006.
- [119] M. Shimojo, A. Namiki, M. Ishikawa, R. Makino, and K. Mabuchi, "A tactile sensor sheet using pressure conductive rubber with electrical-wires stitched method," *IEEE Sensors Journal*, vol. 4, no. 5, pp. 589-596, 2004.
- [120] P. Le Floch *et al.*, "Wearable and Washable Conductors for Active Textiles," *ACS Appl Mater Interfaces*, vol. 9, no. 30, pp. 25542-25552, Aug 2 2017.
- [121] S. E. Root *et al.*, "Ionotactile Stimulation: Nonvolatile Ionic Gels for Human-Machine Interfaces," January 19, 2018 2018.
- [122] N. Yuan *et al.*, "Dual Physically Cross-Linked Double Network Hydrogels with High Mechanical Strength, Fatigue Resistance, Notch-Insensitivity, and Self-Healing Properties," November 30, 2016 2016.
- [123] K. Tian *et al.*, "3D Printing of Transparent and Conductive Heterogeneous Hydrogel-Elastomer Systems," *Adv Mater*, vol. 29, no. 10, Mar 2017.
- [124] M. S. Sarwar, Y. Dobashi, C. Preston, J. K. M. Wyss, S. Mirabbasi, and J. D. W. Madden, "Bend, stretch, and touch: Locating a finger on an actively deformed transparent sensor array," *Science Advances*, vol. 3, no. 3, p. e1602200, 2017.
- [125] C.-C. Kim, H.-H. Lee, K. H. Oh, and J.-Y. Sun, "Highly stretchable, transparent ionic touch panel," *Science*, vol. 353, no. 6300, pp. 682-687, 2016.
- [126] J. Y. Sun *et al.*, "Highly stretchable and tough hydrogels," *Nature*, vol. 489, no. 7414, pp. 133-6, Sep 6 2012.

- 
- [127] C. Keplinger, J. Y. Sun, C. C. Foo, P. Rothmund, G. M. Whitesides, and Z. Suo, "Stretchable, transparent, ionic conductors," *Science*, vol. 341, no. 6149, pp. 984-7, Aug 30 2013.
- [128] A. Frutiger *et al.*, "Capacitive soft strain sensors via multicore-shell fiber printing," *Adv Mater*, vol. 27, no. 15, pp. 2440-6, Apr 17 2015.
- [129] C. Larson *et al.*, "Highly stretchable electroluminescent skin for optical signaling and tactile sensing," *Science*, vol. 351, no. 6277, pp. 1071-4, Mar 4 2016.
- [130] Z. Wang *et al.*, "Dually Synergetic Network Hydrogels with Integrated Mechanical Stretchability, Thermal Responsiveness, and Electrical Conductivity for Strain Sensors and Temperature Alertors," *ACS Appl Mater Interfaces*, vol. 10, no. 16, pp. 14045-14054, Apr 25 2018.
- [131] Y. Gao, F. Jia, and G. Gao, "Transparent and conductive amino acid-tackified hydrogels as wearable strain sensors," *Chemical Engineering Journal*, vol. 375, 2019.
- [132] S. Martínez-Crespiera *et al.*, "Fabrication of silicon oxycarbide-based microcomponents via photolithographic and soft lithography approaches," *Sensors and Actuators A: Physical*, vol. 169, no. 1, pp. 242-249, 2011/09/10/ 2011.
- [133] X. Liu, Y.-L. Li, and F. Hou, "Fabrication of SiOC Ceramic Microparts and Patterned Structures from Polysiloxanes via Liquid Cast and Pyrolysis," *Journal of the American Ceramic Society*, vol. 92, no. 1, pp. 49-53, 2009.
- [134] J. Grossenbacher, M. R. Gullo, R. Grandjean, T. Kiefer, and J. Brugger, "Sub micrometer ceramic structures fabricated by molding a polymer-derived ceramic," *Microelectronic Engineering*, vol. 97, pp. 272-275, 2012/09/01/ 2012.
- [135] B. E. Schubert and D. Floreano, "Variable stiffness material based on rigid low-melting-point-alloy microstructures embedded in soft poly(dimethylsiloxane) (PDMS)," *RSC Advances*, vol. 3, no. 46, 2013.
- [136] "Multi-Axis Soft Sensors Based on Dielectric Elastomer," *Soft Robotics*, vol. 3, no. 1, pp. 3-12, 2016.
- [137] H. Cho, H. Lee, Y. Kim, and J. Kim, "Design of an optical soft sensor for measuring fingertip force and contact recognition: IJCAS," *International Journal of Control, Automation, and Systems*, vol. 15, no. 1, pp. 16-24, Feb 2017 2017.
- [138] T. Fujii, "PDMS-based microfluidic devices for biomedical applications," *Microelectronic Engineering*, vol. 61-62, pp. 907-914, 2002/07/01/ 2002.
- [139] J. Zhou, A. V. Ellis, and N. H. Voelcker, "Recent developments in PDMS surface modification for microfluidic devices," *ELECTROPHORESIS*, vol. 31, no. 1, pp. 2-16, 2010.
- [140] S. K. Sia and G. M. Whitesides, "Microfluidic devices fabricated in Poly(dimethylsiloxane) for biological studies," *ELECTROPHORESIS*, vol. 24, no. 21, pp. 3563-3576, 2003.
- [141] I.-K. Hong and S. Lee, "Cure kinetics and modeling the reaction of silicone rubber," *Journal of Industrial and Engineering Chemistry*, vol. 19, no. 1, pp. 42-47, 2013.
- [142] Z. Liao, M. Hossain, X. Yao, R. Navaratne, and G. Chagnon, "A comprehensive thermo-viscoelastic experimental investigation of Ecoflex polymer," *Polymer Testing*, vol. 86, 2020.

- 
- [143] F. Chambon and H. H. Winter, "Stopping of crosslinking reaction in a PDMS polymer at the gel point," *Polymer Bulletin*, vol. 13, no. 6, pp. 499-503, 1985/06/01 1985.
- [144] R. T. Johnson Jr., R. M. Biefeld, and J. A. Sayre, "High-temperature electrical conductivity and thermal decomposition of Sylgard® 184 and mixtures containing hollow microspherical fillers," *Polymer Engineering & Science*, vol. 24, no. 6, pp. 435-441, 1984.
- [145] G. C. Lisensky *et al.*, "Replication and Compression of Surface Structures with Polydimethylsiloxane Elastomer," *Journal of Chemical Education*, vol. 76, no. 4, p. 537, 1999/04/01 1999.
- [146] H.-B. Liu, H.-Q. Gong, N. Ramalingam, Y. Jiang, C.-C. Dai, and K. M. Hui, "Micro air bubble formation and its control during polymerase chain reaction (PCR) in polydimethylsiloxane (PDMS) microreactors," *Journal of Micromechanics and Microengineering*, vol. 17, no. 10, pp. 2055-2064, 2007/09/07 2007.
- [147] S.-H. Kim, S. Lee, D. Ahn, and J. Y. Park, "PDMS double casting method enabled by plasma treatment and alcohol passivation," *Sensors and Actuators B: Chemical*, vol. 293, pp. 115-121, 2019/08/15/ 2019.
- [148] S. C. H. Thian, J. Y. H. Fuh, Y. S. Wong, H. T. Loh, P. W. Gian, and Y. Tang, "Fabrication of microfluidic channel utilizing silicone rubber with vacuum casting," *Microsystem Technologies*, vol. 14, no. 8, pp. 1125-1135, 2008.
- [149] S. Venkatachalam and D. Hourlier, "Heat treatment of commercial Polydimethylsiloxane PDMS precursors: Part I. Towards conversion of patternable soft gels into hard ceramics," *Ceramics International*, vol. 45, no. 5, pp. 6255-6262, 2019/04/01/ 2019.
- [150] M. Gallo and R. G. Rinaldi, "The effect of pre-curing UV-irradiation on the crosslinking of silicone rubber," *Journal of Applied Polymer Science*, vol. 138, no. 6, p. 49807, 2021.
- [151] L. Xue, Y. Zhang, Y. Zuo, S. Diao, J. Zhang, and S. Feng, "Preparation and characterization of novel UV-curing silicone rubber via thiol-ene reaction," *Materials Letters*, vol. 106, pp. 425-427, 2013/09/01/ 2013.
- [152] Y. Zuo, J. Cao, and S. Feng, "Sunlight-Induced Cross-Linked Luminescent Films Based on Polysiloxanes and d-Limonene via Thiol-ene "Click" Chemistry," *Advanced Functional Materials*, vol. 25, no. 18, pp. 2754-2762, 2015.
- [153] Y. Li *et al.*, "Fast preparation of mechanically stable superhydrophobic surface by UV cross-linking of coating onto oxygen-inhibited layer of substrate," *Chemical Engineering Journal*, vol. 338, pp. 440-449, 2018/04/15/ 2018.
- [154] M. N. Temnikov *et al.*, "Simple and fast method for producing flexible superhydrophobic aerogels by direct formation of thiol-ene networks in scCO<sub>2</sub>," *Polymer*, vol. 138, pp. 255-266, 2018/02/28/ 2018.
- [155] M. M. Ozmen, Q. Fu, J. Kim, and G. G. Qiao, "A rapid and facile preparation of novel macroporous silicone-based cryogels via photo-induced thiol-ene click chemistry," *Chem Commun (Camb)*, vol. 51, no. 98, pp. 17479-82, Dec 21 2015.
- [156] J. Holländer, R. Hakala, J. Suominen, N. Moritz, J. Yliruusi, and N. Sandler, "3D printed UV light cured polydimethylsiloxane devices for drug delivery," *International Journal of Pharmaceutics*, vol. 544, no. 2, pp. 433-442, 2018/06/15/ 2018.

- [157] Z. Liu *et al.*, "Self-healing, reprocessing and 3D printing of transparent and hydrolysis-resistant silicone elastomers," *Chemical Engineering Journal*, vol. 387, p. 124142, 2020/05/01/ 2020.
- [158] Y. Su, H. Lin, S. Zhang, Z. Yang, and T. Yuan, "One-Step Synthesis of Novel Renewable Vegetable Oil-Based Acrylate Prepolymers and Their Application in UV-Curable Coatings," *Polymers*, vol. 12, no. 5, p. 1165, 2020.
- [159] S. S. Rahman, M. Arshad, A. Qureshi, and A. Ullah, "Fabrication of a Self-Healing, 3D Printable, and Reprocessable Biobased Elastomer," *ACS Applied Materials & Interfaces*, vol. 12, no. 46, pp. 51927-51939, 2020/11/18 2020.
- [160] H. Xiang *et al.*, "UV-curable, 3D printable and biocompatible silicone elastomers," *Progress in Organic Coatings*, vol. 137, p. 105372, 2019/12/01/ 2019.
- [161] S. E. A. H. Landrock, *Adhesives Technology Handbook*. William Andrew, 2014.
- [162] D. Hegemann, H. Brunner, and C. Oehr, "Plasma treatment of polymers for surface and adhesion improvement," *Nuclear Instruments and Methods in Physics Research Section B: Beam Interactions with Materials and Atoms*, vol. 208, pp. 281-286, 2003/08/01/ 2003.
- [163] K. Efimenko, W. E. Wallace, and J. Genzer, "Surface Modification of Sylgard-184 Poly(dimethyl siloxane) Networks by Ultraviolet and Ultraviolet/Ozone Treatment," *Journal of Colloid and Interface Science*, vol. 254, no. 2, pp. 306-315, 2002/10/15/ 2002.
- [164] D. Bodas and C. Khan-Malek, "Hydrophilization and hydrophobic recovery of PDMS by oxygen plasma and chemical treatment—An SEM investigation," *Sensors and Actuators B: Chemical*, vol. 123, no. 1, pp. 368-373, 2007/04/10/ 2007.
- [165] C. Yang and Z. Suo, "Hydrogel ionotronics," *Nature Reviews Materials*, vol. 3, no. 6, pp. 125-142, 2018/06/01 2018.
- [166] H. Yuk, T. Zhang, G. A. Parada, X. Liu, and X. Zhao, "Skin-inspired hydrogel-elastomer hybrids with robust interfaces and functional microstructures," *Nature Communications*, vol. 7, p. 12028, 06/27/online 2016.
- [167] C. S. Simmons, A. J. S. Ribeiro, and B. L. Pruitt, "Formation of composite polyacrylamide and silicone substrates for independent control of stiffness and strain," *Lab Chip*, vol. 13, no. 4, pp. 646-649, 2013.
- [168] Y. Wang, H. H. Lai, M. Bachman, C. E. Sims, G. P. Li, and N. L. Allbritton, "Covalent micropatterning of poly(dimethylsiloxane) by photografting through a mask," *Analytical chemistry*, vol. 77, no. 23, pp. 7539-46, Dec 1 2005.
- [169] Q. Liu, G. Nian, C. Yang, S. Qu, and Z. Suo, "Bonding dissimilar polymer networks in various manufacturing processes," *Nat Commun*, vol. 9, no. 1, p. 846, Feb 27 2018.
- [170] H. Yuk, B. Lu, and X. Zhao, "Hydrogel bioelectronics," *Chem Soc Rev*, vol. 48, no. 6, pp. 1642-1667, Mar 18 2019.
- [171] J. Y. Oh, S. Kim, H.-K. Baik, and U. Jeong, "Conducting Polymer Dough for Deformable Electronics," *Advanced Materials*, vol. 28, no. 22, pp. 4455-4461, 2016/06/01 2016.
- [172] D. J. Lipomi, J. A. Lee, M. Vosgueritchian, B. C. K. Tee, J. A. Bolander, and Z. Bao, "Electronic Properties of Transparent Conductive Films of PEDOT:PSS on Stretchable Substrates," *Chemistry of Materials*, vol. 24, no. 2, pp. 373-382, 2012/01/24 2012.

- 
- [173] X. Liu *et al.*, "Stretchable living materials and devices with hydrogel–elastomer hybrids hosting programmed cells," *Proceedings of the National Academy of Sciences*, vol. 114, no. 9, pp. 2200-2205, 2017/02/28 2017.
- [174] H. Jiang, Y. Wu, B. Han, and Y. Zhang, "Effect of oxidation time on the properties of cellulose nanocrystals from hybrid poplar residues using the ammonium persulfate," *Carbohydrate Polymers*, vol. 174, pp. 291-298, 2017/10/15/ 2017.
- [175] M. M. Bashar, H. Zhu, S. Yamamoto, and M. Mitsuishi, "Highly carboxylated and crystalline cellulose nanocrystals from jute fiber by facile ammonium persulfate oxidation," *Cellulose*, vol. 26, no. 6, pp. 3671-3684, 2019/04/01 2019.
- [176] Y. Zhou *et al.*, "Biocompatible and Flexible Hydrogel Diode-Based Mechanical Energy Harvesting," *Advanced Materials Technologies*, vol. 2, no. 9, 2017.
- [177] W. Xu, L.-B. Huang, M.-C. Wong, L. Chen, G. Bai, and J. Hao, "Environmentally Friendly Hydrogel-Based Triboelectric Nanogenerators for Versatile Energy Harvesting and Self-Powered Sensors," *Advanced Energy Materials*, vol. 7, no. 1, 2017.
- [178] J. Liu *et al.*, "Highly Conductive Hydrogel Polymer Fibers toward Promising Wearable Thermoelectric Energy Harvesting," *ACS Appl Mater Interfaces*, vol. 10, no. 50, pp. 44033-44040, Dec 19 2018.
- [179] K. Dong *et al.*, "A Highly Stretchable and Washable All-Yarn-Based Self-Charging Knitting Power Textile Composed of Fiber Triboelectric Nanogenerators and Supercapacitors," *ACS Nano*, vol. 11, no. 9, pp. 9490-9499, Sep 26 2017.
- [180] Y.-J. Liu, W.-T. Cao, M.-G. Ma, and P. Wan, "Ultrasensitive Wearable Soft Strain Sensors of Conductive, Self-healing, and Elastic Hydrogels with Synergistic "Soft and Hard" Hybrid Networks," *ACS Applied Materials & Interfaces*, vol. 9, no. 30, pp. 25559-25570, 2017/08/02 2017.